

ALMA MATER STUDIORUM

University of Bologna

DEI - Department of Electrical, Electronic and Information
Engineering - Guglielmo Marconi

PhD in Bioengineering

**From inverted pendulum to N-link chain:
inertial sensors-based assessment of
movement kinematics and dynamics for
functional evaluation and rehabilitation**

Thesis submitted for the degree of
PhD in Bioengineering (09/G2, ING-INF/06)
XXV Cycle

Candidate:	Eng. Valeria Fuschillo
PhD Coordinator:	Prof. Angelo Cappello
Supervisor:	Prof. Angelo Cappello
Co-Supervisor:	Prof. Lorenzo Chiari
Examiners:	Prof. Guido Avanzolini Prof. Kamiar Aminian

Thesis defense: 12th April, 2013

*"On bended knee is no way to be free,
lifting up an empty cup, I ask silently
that all my destinations will accept the one that's me
so I can breath..."*

(Eddie Vedder - Guaranteed)

Prologue

Despite several clinical tests that have been developed to qualitatively describe complex motor tasks by functional testing, these methods often depend on subjective interpretation, which make the assessment results inconsistent and have limited accuracy in recall. Although their predictive value is undeniable, cutoff values for clinical use merely correspond with clearly visible instability or reduced ambulation. For these reasons, the validity of such assessment essentially depends on clinicians' experience and training. Results might not have the precision needed to objectively assess the effect of the rehabilitative intervention or the decline over time in patients. A more detailed characterization is required to fully capture the various aspects of motor control and performance during complex movements of lower and upper limbs. The need for objective, cost-effective and clinically applicable methods, as well as methods that possess a high sensitivity and specificity, is hence clear. Instrumented tests would enable quantitative assessment of performance on a subject-specific basis, overcoming the limitations due to the lack of objectiveness related to individual judgment, and possibly disclosing subtle alterations that are not clearly visible to the observer.

Postural motion measurements at additional locations, such as lower and upper limbs and trunk, may be necessary in order to obtain information about the inter-segmental coordination during different functional tests involved in clinical practice. With these considerations in mind, this Thesis aims: i) to suggest a novel quantitative assessment tool for the kinematics and dynamics evaluation of a multi-link kine-

matic chain during several functional motor tasks (i.e. squat, sit-to-stand, postural sway), using one single-axis accelerometer (SAA) per segment, ii) to present a novel quantitative technique for the upper limb joint kinematics estimation, considering a 3-link kinematic chain during the Fugl-Meyer Motor Assessment and using one inertial measurement unit (IMU) per segment. Traditional movement analysis systems, such as stereo-photogrammetry and force plates, were used for validation only.

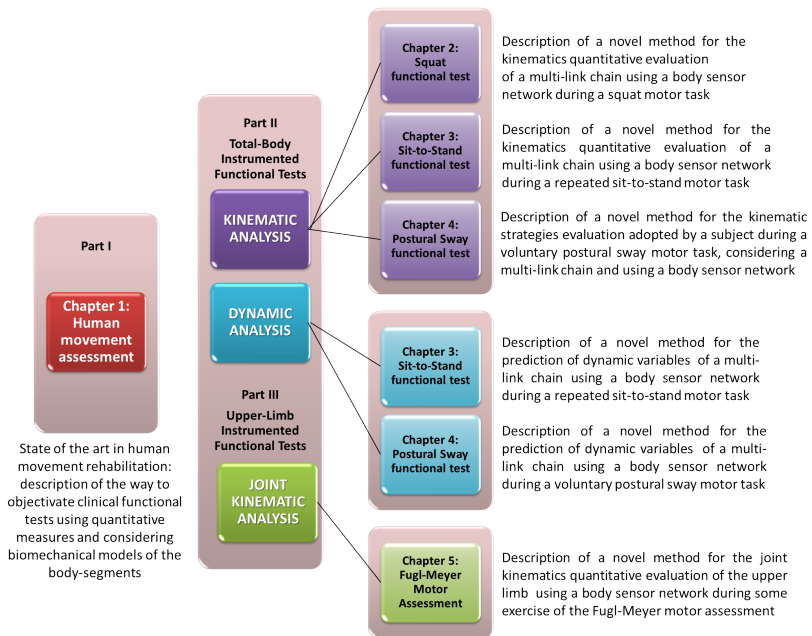
With regard to the first aim of this Thesis, kinematics and dynamics prediction techniques are based on the use of one SAA per segment. A preliminary calibration allows the estimation of sensors position and orientation and segment lengths. These parameters are then used to predict the N -link chain kinematics during a squat motor task, applying a bi-directional low pass filter to the SAA outputs. Results demonstrated the usability of the method, showing errors lower than 1° for the considered body-segments and suggesting the opportunity to evaluate compensatory postural strategies in different functional tasks in a easy and portable way. Dynamics prediction method is based on the estimation of the subject-specific anthropometric parameters during the sit-to-stand functional test. Considering the relationships between kinematic and kinetic variables, dynamics of a N -link model is well-known. Results confirmed the accuracy of the technique, showing errors on predicted center of pressure equal to about 2cm during the sit-to-stand test and 6mm during the postural sway test, using one SAA per segment only. During sit-to-stand, also error on ankle joint moment, about 10Nm, demonstrated the the usability of this instrumented test in the clinical practice.

Regarding to the second aim of this Thesis, the upper limb joint kinematics estimation method, based on the use of one IMU per segment takes advantage by the application of a sensors fusion algorithm based on an extended Kalman Filter to estimate segment orientations. A preliminary IMU technical systems of reference alignment procedure, using accelerometers and gyroscopes data only, allows the definition of

a common global system of reference, neglecting the use of any magnetometers in the experimental set-up, which are typically affected by disturbances due to the presence of iron in both clinical and domestic environments. Shoulder and elbow joint angles are estimated after a functional calibration of body-segment anatomical axes, showing mean errors lower than 4° and confirming the accuracy of the technique.

The suggested methods could have several positive feedbacks from clinical practice. In this perspective, the use of objective biomechanical measurements in the context of the rehabilitation, provided by inertial sensor-based technique, may help clinicians to: i) objectively track changes in motor ability, ii) provide timely feedback about the effectiveness of administered rehabilitation interventions, iii) enable intervention strategies to be modified or changed if found to be ineffective, and iv) speed up the experimental sessions when several subjects are asked to perform different functional tests.

Thesis at a Glance



List of Publications and Awards

International Peer-Reviewed Journals

1. BAGALÀ F, FUSCHILLO VL, CHIARI L, CAPPELLO A (2012)
Calibrated 2D angular kinematics by single-axis accelerometers: from inverted pendulum to N-link chain, IEEE Sensors Journal, 12(3): 479-486.
2. FUSCHILLO VL, BAGALÀ F, CHIARI L, CAPPELLO A (2012)
Accelerometry -based dynamics prediction for balance monitoring, Medical & Biological Engineering and Computing, 50(9): 925-936.

Conference Proceedings published on International Journals

1. BAGALÀ F, FUSCHILLO VL, CHIARI L, CAPPELLO A (2009)
2D Kinematics estimation of postural sway using single-axis accelerometers, Proceedings of SIAMOC 2009, October 1-3, Alghero, Italy, Gait & Posture, 30(Suppl.1): S59.
2. FUSCHILLO VL, BAGALÀ F, CHIARI L, CAPPELLO A (2009)
Anthropometric parameters and CoP and CoP prediction using single-axis accelerometers and force plate, Proceedings of SIAMOC 2009, October 1-3, Alghero, Italy, Gait & Posture, 30(Suppl.1): S5-S6.

3. BAGALÀ F, FUSCHILLO VL, CHIARI L, CAPPELLO A (2009) *Net joint moments prediction during balance using single-axis accelerometers*, Proceedings of SIAMOC 2009, October 1-3, Alghero, Italy, Gait & Posture, 30(Suppl.1): S6-S7.
4. FUSCHILLO VL, CHIARI L, CAPPELLO A (2011) *Kinematic strategy evaluation by single-axis accelerometers during voluntary oscillations*, Proceedings of SIAMOC 2011, September 28 - October 1, Bosisio Parini, Italy, Gait & Posture, 35(Suppl.1): S19-S20.

National Conferences Proceedings

1. BAGALÀ F, FUSCHILLO VL, CHIARI L, CAPPELLO A (2010) *Single-axis accelerometer kinematics estimation of an inverted pendulum balance model*, Proceedings of GNB 2010, July 8-10, Torino, Italy - BOLOGNA, Patron, 2010, pp. 175-176.
2. FUSCHILLO VL, BAGALÀ F, CHIARI L, CAPPELLO A (2010) *Single-axis accelerometer anthropometry estimation of an inverted pendulum balance model*, Proceedings of GNB 2010, July 8-10, Torino, Italy - BOLOGNA, Patron, 2010, pp. 219-220.
3. FUSCHILLO VL, BAGALÀ F, CHIARI L, CAPPELLO A (2010) *Single-axis accelerometer CoP, CoM and T prediction in an inverted pendulum model*, Proceedings of GNB 2010, July 8-10, Torino, Italy - BOLOGNA, Patron, 2010, pp. 221-22.
4. FUSCHILLO VL, BAGALÀ F, CHIARI L, CAPPELLO A (2012) *Net joint moments accelerometers-based prediction during sit-to-stand*, Proceedings of GNB 2012, June 26-29, Roma, Italy (in press).
5. BAGALÀ F, FUSCHILLO VL, CHIARI L, CAPPELLO A (2012) *Accelerometers -based telescopic inverted pendulum model for the analysis of sit-to-stand*, Proceedings of GNB 2012, June 26-29, Roma, Italy (in press).

Awards

1. Best contribution to the methodologies for the professional practices, Third Congress of the National Group of Bioengineering, Roma, Italy, 2012: FUSCHILLO VL, BAGALÀ F, CHIARI L, CAPPELLO A, *Net joint moments accelerometers-based prediction during sit-to-stand.*

Contents

Prologue	v
Thesis at a Glance	ix
List of Publications	xi
1 Human movement assessment	1
1.1 Human motion analysis in rehabilitation	1
1.2 Inertial sensors	4
1.3 Inertial sensor- and model-based instrumentation of func- tional tests	7
1.4 Outline of the Thesis	14
2 Angular kinematics evaluation during the <i>Squat</i> func- tional test	17
2.1 Introduction	18
2.2 Methods and Materials	20
2.2.1 Inverted Pendulum Model	20
2.2.2 Multi-link Model	24
2.3 Results	30
2.3.1 Mechanical Inverted Pendulum Kinematics	30
2.3.2 Multi-link Kinematics	31
2.4 Discussion	33

3	Dynamics evaluation during the <i>repeated Sit-to-Stand</i> functional test	37
3.1	Introduction	38
3.2	Methods and Materials	41
3.2.1	Experimental Set-Up	41
3.2.2	N -link Biomechanical Model	42
3.2.3	Subject-specific Body-Segment Parameters Estimation	44
3.2.4	Dynamics Prediction	45
3.2.5	Quasi-Real-Time Prediction	48
3.3	Results	49
3.4	Discussion	54
4	Kinematic strategies and dynamics evaluation during the <i>voluntary Postural Sway</i> functional tests	59
4.1	Introduction	61
4.2	Methods and Materials	66
4.2.1	Experimental Set-Up	66
4.2.2	Kinematic Strategies Evaluation	66
4.2.3	Dynamics Prediction	69
4.3	Results	70
4.3.1	Kinematic Strategies Evaluation	70
4.3.2	Dynamics Prediction	72
4.4	Discussion	75
5	Joint kinematics evaluation during the <i>Fugl-Meyer Motor Assessment</i> for the upper extremity	81
5.1	Introduction	82
5.2	Methods and Materials	94
5.2.1	2D real-time multi-link model kinematics	94
5.2.2	3D upper limb joint kinematics	100
5.3	Results	118
5.3.1	2D real-time multi-link kinematics	118
5.3.2	3D upper limb kinematics	120

5.4 Discussion	129
Epilogue	137
List of Figures	140
List of Tables	144
Bibliography	147

Chapter 1

Human movement assessment

1.1 Human motion analysis in rehabilitation

Many different disciplines use motion analysis systems to capture movement and posture of the human body. Basic scientists seek a better understanding of the mechanisms that are used to translate muscular contractions about articulating joints into functional accomplishment.

In the contemporary medicine the patient is the starting and ending point of a circular path (see Figure 1.1). Clinicians are directly in contact with the patient, but at the same time instrumentation as support to the diagnosis and/or the therapy is adopted. Instrumental human motion analysis can be adopted by the practitioners in order to allow them to mostly concentrate on the therapy decision-making process and to improve the knowledge about a specific biological system. In fact, without the use of instrumental analysis, for example in the

case of the musculo-skeletal system, physicians are not able to deeply examine the biological systems from the anatomical and physiological points of view only.

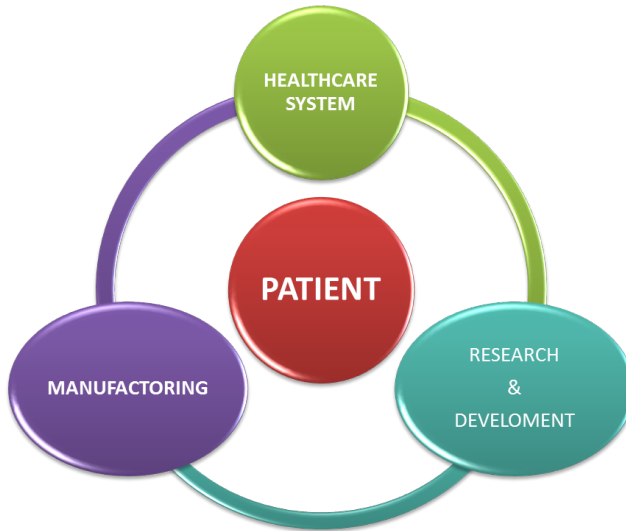


Figure 1.1: Schematic representation of the circular path describing contemporary medicine

Research initiative to define the effectiveness of rehabilitation have seen a steady growth over the past decade. This growth has, for the most part, been precipitated by advances in our understanding of mechanism of neuroplasticity and the exciting possibility for sensorimotor rehabilitation to exploit this hitherto unrecognized potential. The evidence of neuroplasticity in the adult brain has offered new hope to those treating patients with long-term disability and underlines the increasing interest in finding new and more effective ways to maximize this potential. The field of rehabilitation research seen an exponential escalation over the past twenty years. One reason for the increase in the number of researchers is the realization and recognition that rehabilitation is an interdisciplinary undertaking. In addition to those with professional rehabilitation backgrounds, investigators representing dif-

ferent fields and including engineering, physiology, neuroscience, and medicine, now identify themselves with rehabilitation [111].

An active collaboration between bioengineers and clinicians is necessary in order to provide the engineer with the right information about the clinical question to solve and, from the other side, to provide the practitioner with the necessary knowledge about the optimal way of using the technology. The application of instrumental motion analysis on the rehabilitation field is based on several aspects, like the instrumentation adopted, the mathematical models, the algorithms, the data processing. The combination of these elements determines the complexity of the analysis system and at the same time its validity.

The characteristics of a motion analysis system have to be close to the ones in clinical settings. For example the time required for performing a clinical examination using a motion analysis system has to be similar to the one spent during a normal routine examination or, even, the time required for the motion analysis system must be less than that, when the system is adopted as additional instrument together with clinical evaluation scales.

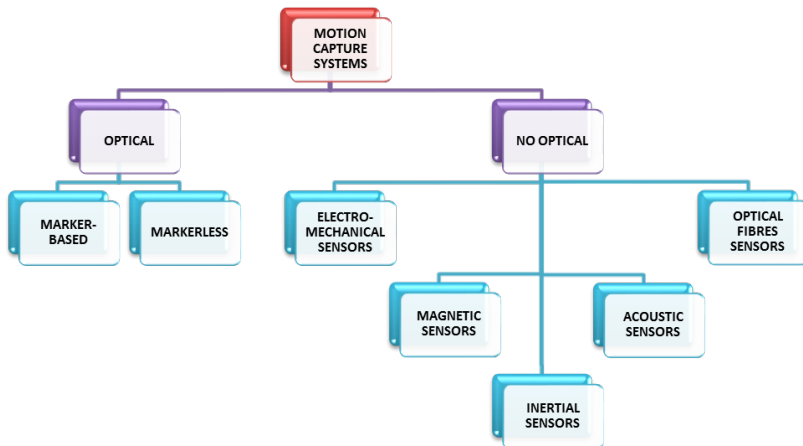


Figure 1.2: Classification of the common motion capture systems

Commercial optical systems (see Figure 1.2) are often considered as a "gold standard" in human motion analysis. Although these systems provide accurate position information (errors $\approx 1\text{mm}$), there are some important limitations. The most important factors are the high costs and the limited measurement volume. The use of a specialized laboratory with fixed equipment impedes many applications, as monitoring of daily life activities or assessment of workload in ergonomic studies. Recently, the health care system trend toward early discharge to monitor and train patients in their own environment. This has promoted a large development of non-invasive, portable and wearable systems. The advent of Micro-Electro-Mechanical Systems (MEMS) technology allowed systems based on inertial and magnetic sensors to be introduced in the biomechanical community, thanks to their low costs, sizes, and power consumption, overcoming some of the limitation related to commercial optical systems, allowing the motion analysis outside the laboratory.

1.2 Inertial sensors

Inertial sensors use the property of bodies to maintain constant translational and rotational velocity, unless disturbed by forces and torques, respectively. The vestibular system, located in the inner ear, is a biological 3D inertial sensor. It can sense the angular motion as well as the linear acceleration of the ear, allowing to maintain balance and to stabilize eye positions relative to the environment. MEMS units are usually placed on each body-segment to be tracked.

The accelerometer is a sensor which converts a linear acceleration into an electrical signal by a known relationship. A single-axis accelerometer (SAA) consists of a mass, suspended by a spring in a housing (see Figure 1.3). Springs, within their linear region, are governed by a physical principle known as Hooke's law. Hooke's law states that a spring will exhibit a restoring force which is proportional to the amount it has been expanded or compressed. Specifically, $\mathbf{F} = K_s \mathbf{x}_0$, where K_s is the constant of proportionality between displacement \mathbf{x}_0 and force \mathbf{F} .

The other important physical principle is that of Newton's second law of motion, which states that a force operating on a mass M , which is accelerated with an acceleration \mathbf{a} , will exhibit a force with magnitude $\mathbf{F} = M\mathbf{a}$. This force causes the mass to either compress or expand the spring under the constraint that $\mathbf{F} = M\mathbf{a} = K_s\mathbf{x}_0$. Hence an acceleration \mathbf{a} will cause the mass M to be displaced by $\mathbf{x}_0 = \frac{M\mathbf{a}}{K_s}$, or, if we observe a displacement equal to \mathbf{x}_0 , we know the mass has undergone an acceleration equal to $\mathbf{a} = \frac{K_s\mathbf{x}_0}{M}$. In this way, the problem of measuring acceleration has been turned into one of measuring the displacement of a mass connected to a spring, which is converted into an electrical signal by the sensor. In order to measure multiple axes of acceleration, this system needs to be duplicated along each of the required axes. Various MEMS geometries are available, of which the most interesting uses the capacity effect for measure mass displacements.

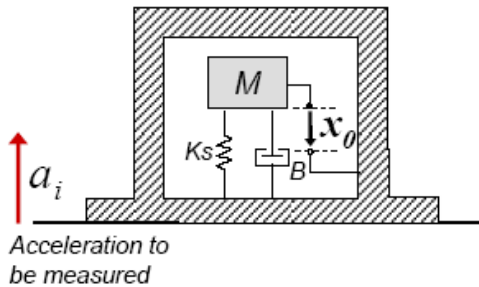


Figure 1.3: A single-axis accelerometer consisting of a mass suspended by a spring

The gyroscope is a sensor which converts an angular velocity into an electrical signal by a known relationship. There are two broad categories: mechanical gyroscopes and optical gyroscope. The first mechanical gyroscope was built by Foucault in 1852, as a gimbaled wheel that stayed fixed in the space due to angular momentum, while the platform rotated around it (see Figure 1.4a). Mechanical gyroscopes operate on the basis of conservation of angular momentum by sensing the change

in direction of an angular moment. According to Newton's second law, the angular moment of a body will remain unchanged unless it is acted upon by a torque. The fundamental equation describing the behavior of the gyroscope is $\boldsymbol{\tau} = \frac{d\mathbf{L}}{dt} = \frac{d(I\boldsymbol{\omega})}{dt} = I\boldsymbol{\alpha}$, where the vectors $\boldsymbol{\tau}$ and \mathbf{L} are, respectively, the torque on the gyroscope and its angular moment, the scalar I is its moment of inertia, the vector $\boldsymbol{\omega}$ is its angular velocity, and the vector $\boldsymbol{\alpha}$ is its angular acceleration. Gimballed and laser gyroscopes are not suitable for human motion analysis due to their large size and high costs. Over the last few years, micro-machined inertial sensors have become more available. Vibrating mass gyroscopes are small, inexpensive, and have low power requirements, making them ideal for human movement analysis. A vibrating element (vibrating resonator), when rotated, is subjected to the Coriolis effect that causes secondary vibration orthogonal to the original vibrating direction. By sensing the secondary vibration, the rate of turn can be measured (see Figure 1.4b).

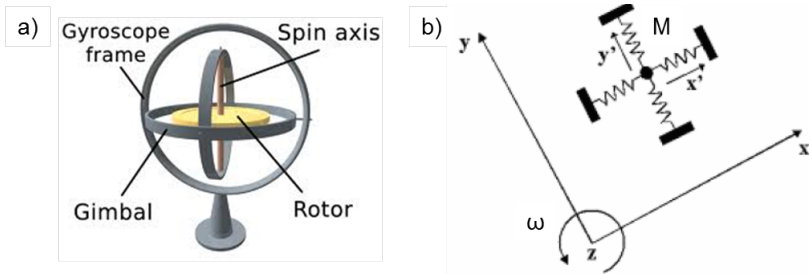


Figure 1.4: a) A conventional spinning wheel gyroscope, b) a vibrating mass gyroscope consisting in a mass subjected to the Coriolis effect

The Coriolis force is given by $\mathbf{F}_c = -2M(\boldsymbol{\omega} \wedge \mathbf{v})$, where M is the mass, the vector \mathbf{v} is the momentary velocity of the mass relative to the moving object to which it is attached, and the vector $\boldsymbol{\omega}$ is the angular velocity of that object. Various MEMS geometries are available, of which many use the piezo-electric effect for vibration exert and detection.

1.3 Inertial sensor- and model-based instrumentation of functional tests

The ability to observe and interpret measurements of human movement has been the primary factors limiting growth of the rehabilitation field. Future advancements in the study of human movement should be discussed in the context of new technology and ways that this new technology can be applied to the evaluation of musculoskeletal disease and injury [2].

Over the last several centuries, there have been several fundamental advancements that have made a substantial impact on our understanding of the process of human movement. As instruments have been developed to enhance our ability to observe human movement, models have been used to develop information that cannot be directly observed. Typically, models are an abstraction in the form of a physical construction governed by principles of physics and mathematics. Models of biomechanical systems provide the basis for the seeking of truth through application of physical laws. Borelli (1608–1679) [20] was among the first to apply physical laws to the analysis of the locomotion of animals. Borelli, in his classic work *De Motu Animalum* (1680), recognized that complex biological structures could be reduced to simplified constructs that facilitated the estimation of forces and patterns of movement. Borelli's work has been fundamental to the development of biomechanical models and the study of human movement. In modern times, the prediction of intersegmental forces and moments has been extremely valuable in improving our understanding of the musculoskeletal system. The information from these studies should be applied to fundamental clinical studies, and the same methodology should be used for both the lower and the upper joints.

Skilled motor ability is based on the learner acquiring classes of elemental motor behaviors, such as muscle or movement synergies, and learning how to apply them in different combinations to accomplish the desired motor task [144]. At the moment, clinical scales are usually

administered to evaluate motor performance during several functional tests, based on visual observation of joint angle motion to describe alterations in coordination and movement pattern.

Despite several clinical tests that have been developed to qualitatively describe complex motor tasks by functional testing, these methods often depend on subjective interpretation, which make the assessment results inconsistent and have limited accuracy in recall [132]. Although their predictive value is undeniable, cutoff values for clinical use merely correspond with clearly visible instability or reduced ambulation. For these reasons, the validity of such assessment essentially depends on clinicians' experience and training. Results might not have the precision needed to objectively assess the effect of the rehabilitative intervention or the decline over time in patients. A more detailed characterization is required to fully capture the various aspects of motor control and performance during complex movements of lower and upper limbs. The need for objective, cost-effective and clinically applicable methods, as well as methods that possess a high sensitivity and specificity, is hence clear. Instrumented tests would enable quantitative assessment of performance on a subject-specific basis, overcoming the limitations due to the lack of objectiveness related to individual judgment, and possibly disclosing subtle alterations that are not clearly visible to the observer.

By way of example, elderly patients may use different compensatory strategies to achieve successful transition, such as a deviation from normal motion. Deviations are due to several types of motion irregularities, among which sway is the most frequently encountered. Sway consists in repetitive, quick changes in motion orientation due to a temporary loss of balance or to insufficient strength in lower limbs. The subtle deviation from normal motion could not be seen by the clinician who is administering typical functional tests. These considerations suggest that further quantitative investigations of postural transition with other additional parameters have the potential to provide important predictive information about the status of the sensorimotor system of the

patient.

Actually, traditional clinical balance tests, as the *Romberg Test* [96], the *Berg Balance Scale* [140], the *Balance Evaluation System Test* [85], are dependent on subjective scores related to the motor task accomplishment, while traditional FP-based [157, 184] or active balance system-based [187] methods, focused on CoP displacement and neglected the biomechanics of the single body-segments [164]. Furthermore, other static and dynamic balance test widely used to assess patient's mobility abilities (e.g. traditional community walk tests, as the *Walking Distance*, the *Walking Speed*, the *Functional Ambulation*, the *Fugl-Meyer Motor Assessment* [61], the *Tinetti Test* [185]) are based on visual observation of motion. The relative balance improvement or deterioration of a subject, during static or postural transitions tests, can be of interest in several case of the clinical setting:

- neurodegenerative disorder that leads to a progressive decline in motor function (e.g. Parkinson disease [122, 150], diabetic neuropathies [189], cerebellar diseases [49]),
- deficit in postural control [54, 115, 165],
- impairments after stroke [106, 130],
- risk of falls evaluation that might cause bone fractures [21, 51, 73, 121, 177, 220],
- sport medicine pathologies [169],
- reductions in lower-extremity strength [26, 37],
- rehabilitation programs for the postural training on ankle, knee and hip joint after a traumatic event [83],
- gerontology studies for the aging and balance relationship [103, 120, 154, 211].

Only in recent years, functional tests as the *Timed Up and Go* and the *Sit-to-Stand* or *Stand-To-Sit*, have been marked by advances in

technology, specifically, in wearable, small, light-weight body-fixed sensors. The *Timed Up and Go* (TUG) is a well-known clinical test of mobility. In older adults and in other populations such as patients with Parkinson’s disease or stroke, longer TUG times have been associated with impaired mobility and an increased risk of fall [12, 142, 159]. TUG duration is also sensitive to therapeutic interventions, for example in patients with Parkinson’s disease [7, 16]. The predecessor of the TUG was the *Up and Go Test*, introduced by Mathias *et al.* in 1986 [125]. In this version, multiple components of the test are scored by an observer. However, to enhance widespread usability and diminish the subjective nature of scoring, Podsiadlo and Richardson introduced the timed version of the test [159]. In this popular version, the single outcome of the test is its duration: the time it takes to stand up from a chair, walk 3 m, turn around, return, and sit down again. Despite enhancing the objectivity of the test, this timed version does not capture subtle differences in test performance. Since Mathias introduced the *Up and Go Test* more than two decades ago, published studies which have instrumented the TUG or portions of it using wearable devices have reported intriguing and promising results. For example, Marschollek *et al.* [124] placed a tri-axial accelerometer on the lower back to assess group differences in the TUG between fallers and non-fallers in the geriatric population. They investigated acceleration parameters related to the walking portion of the TUG, rather than to the *Sit-to-Stand* or *Stand-To-Sit* components. Similarly, Gillian *et al.* [70] examined differences in the walking portion of the TUG in healthy older adult and patients with cognitive impairment. Ganea *et al.* [67] used an inertial sensor on the lower trunk comprised of 1 gyroscope and 2 accelerometers to assess the dynamic complexity (estimated by the fractal dimensions of an acceleration–angular velocity plot) of the *Sit-to-Stand* movement in frail elderly subjects. Using a gyroscope, Najafi *et al.* [142] evaluated the performance of the *Sit-to-Stand* and *Stand-To-Sit* tasks of two groups of elderly subjects (with and without fall risk) by applying wavelet transform methods and calculating shifting duration related pa-

rameters. Similarly, Bidargaddi *et al.* [18] developed a wavelet-based algorithm for detecting and calculating the durations of *Sit-to-Stand* and *Stand-To-Sit* transitions from the signal vector magnitude of a measured acceleration signal. The algorithm was tested on waist worn accelerometer data collected from young subjects as well as geriatric patients. In a small, pilot study, Giansanti *et al.* [69] used a sensor unit which included 3 mono-axial accelerometers and 3 rate gyroscopes on 5 control subjects and 3 early Parkinson’s disease patients who performed the *Sit-to-Stand* in 3 different chair height conditions. They derived peak acceleration and timing parameters and were able to discriminate between the different *Sit-to-Stand* conditions. The existing literature suggests that quantification of the TUG may be beneficial. However, to our knowledge, body-fixed sensors devices have not yet been applied to systematically assess the TUG transitions in patients with PD. Weiss *et al.* [200] demonstrated, in a recent study, the potential of using an accelerometer to measure TUG and the *Sit-to-Stand* transitions performance in order to detect and quantify subtle differences in mobility and function, not be readily quantified by simple visual analysis, to identify Parkinson’s disease, to document disease progression, and to assess the response and benefits to different therapeutic interventions. Palmerini *et al.* [150] presented an accelerometer-based approach to quantify postural impairments in Parkinson’s disease, easier than the conventional protocol with force plates, which are more expensive and non-portable, focusing on the early-mild stage of the disease, where accelerometers have already proved their usefulness in detecting impaired anticipatory postural adjustments [123] and deficits in gait and turning [215]. Although all these methods take advantage by the use of wearable devices in order to obtain quantitative measures of mobility performance, they neglect the assumption of a biomechanical model to describe the physical laws that are typical of human body-segments movements.

The lack of objective measures of clinical tests is also clear, for instance, in the context of typical functional evaluation of hemiparetic upper limb in patient following stroke. Assuming that neurological in-

jury leads to the loss of skilled motor behavior, motor relearning would depend on the reacquisition of such elemental motor patterns (*recovery*) or, in the absence of reacquisition, adaptation of remaining (*compensation*) or integration of alternative (*substitution*) motor elements. Motor scales that assess impairments (Body Functions/Structure level, see Figure 1.5) rather than disability (Activity level, see Figure 1.5) cannot make the distinction between the recovery of elemental motor patterns, present before the injury, or the motor compensation resulting from the adaptation of remaining motor elements, and cannot provide an appreciation of the movement quality [99, 111].

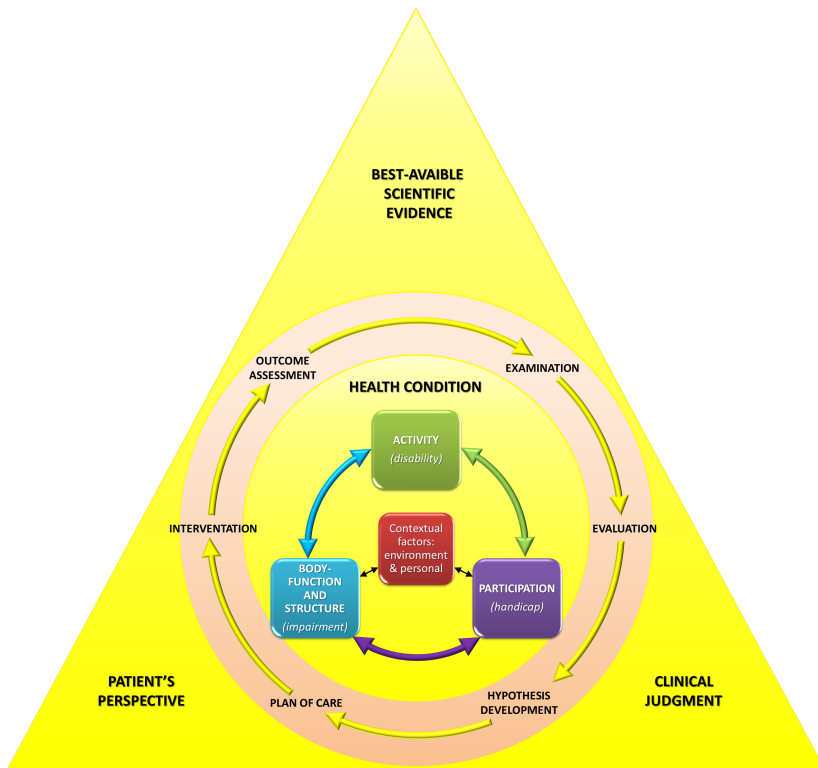


Figure 1.5: Integrated model of the rehabilitation cycle incorporating the World Health Organization’s International Classification of Functioning, Disability and Health (WHO-ICF) model. Image is adapted from [172]

This lack concerns about the extent to which rehabilitative interventions provide improvements in reduction of impairment among the patients. Indeed, motor compensation in the upper limb can include the use of movement patters that incorporate trunk displacement and rotation, scapular elevation, shoulder abduction and internal/external rotation [109, 166]. The use of increased trunk movement to assist arm and hand transport [32, 190], and to aid in hand positioning/orientation for grasping [135], are example of adaptive compensatory strategies. The degree of motor compensations is also related to the severity of the hemiparesis, conditioning the appropriate interventions.

At the Body Function/Structure level, the emphasis is on the quality of movement regardless of movement outcome or task accomplishment. Recovery at this level would be characterized by the reappearance of movement patterns and by a decrease in spasticity or by a reduction in trunk displacement during a reaching or pointing movement. Adaptive compensation at this level would be characterized by the appearance of alternative movement patterns during the accomplishment of a task. Substitutive compensation would reflect the use of different effectors to replace lost motor elements. Numerous valid and reliable clinical scales measure impairments at this level. Scales such as the *Modified Ashworth Scale* [19] and the *Composite Spasticity Index* [108] document the presence or absence of resistance to passive range of motion associated with spasticity. The motor deficit may be quantified in terms of range of active joint motion and muscle strength as the ability of the patient to perform movements of individual joints of group of adjacent joints. Scales such as the *Fugl-Meyer Assessment Scale* [61], the *Chedoke-McMaster Stroke Scale* [74] and the *Reaching Performance Scale* [110] measure upper limb impairment at the Body Function/Structure level. Although these scales may offer the clinicians an appreciation of impairments, more detailed kinematic analysis of motor patterns during the performance of functional tasks would provide even more relevant information about movement patterns and motor compensation.

At the Activity level, recovery requires that the task is performed using the same end effectors and joints of the movement patterns typically used by non-disabled individuals. Compensation often takes the form of substitution and would be noted if the patients were able to accomplish the task using alternative joints or end effectors. Most evaluation at the Activity level neither specify how the task is accomplished nor which compensatory movements were used in place of motor patterns observed in non-disabled individuals. Example of scales that measure function and not motor patterns are the *Barthel Index* [86], the *Box and Block Test* [126], the *Frenchay Arm Test* [195], the *Jebsen Taylor Hand Function Test* [90], the *Motricity Index* [197], the *Action Research Arm Test* [214], the *TEMPA Test* [44]. Difficulties arise in interpretation of studies that use such functional tests to indicate recovery because scores on these tests may improve either when the intervention results in improvements in motor patterns or in increasing compensation, and the distinction between them is not made. An example of a relative new scale that attempts to incorporate both measures of task success as well as movement quality during task accomplishment is the the *Wolf Motor Function Test* [209].

In this perspective, the use of objective biomechanical measurements in the context of the rehabilitation, provided by inertial sensor-based technique, may help clinicians: i) to objectively track changes in motor ability following neurological injury, ii) to provide timely feedback about the effectiveness of administered rehabilitation interventions, iii) to enable intervention strategies to be modified or changed if found to be ineffective, and iv) to speed up the experimental sessions when several subjects are asked to perform different functional tests.

1.4 Outline of the Thesis

In **Chapter 2** a quantitative assessment tool will be provided in order to estimate body sway angles of a 2D multi-link kinematic chain, using a single-axis accelerometer per segment. To evaluate the method,

the algorithm for angular displacement estimation will be tested on a mechanical arm, modeled by an inverted pendulum, and on a subject performing a squat task, considering a 3-link biomechanical model. Reference systems (encoder and stereo-photogrammetric system) will be used to calibrate the sensors position and orientation and to validate results. The presented method may be applied to different balance assessment functional tests and may be used for kinematic chains of any number of link. In Chapter 2 it will be used to objectively evaluate squatting exercises, often performed to characterize the bilateral lower-extremity kinematics, and in the next Chapters to assess sit-to-stand and postural sway angular kinematics, providing the usability of this instrumented functional test in the clinical practice.

In **Chapter 3** a functional subject-specific 2D evaluation tool will be proposed in order to estimate body-segment anthropometric parameters during a repeated sit-to-stand motor task, using a single-axis accelerometer per segment and a force plate. After this preliminary estimation, a quantitative assessment tool will be provided in order to predict the ground reaction forces, the centers of pressure and mass, and the net joint moments of a subject performing a repeated sit-to-stand task, considering a 2D 3-link biomechanical model and using a single-axis accelerometer per segment (force plate will be used for validation only). The method for the instrumentation of the repeated-sit-to-stand functional test, will provide objective kinematic and dynamic informations during postural control, risk of fall, lower-extremity strength, impairment after stroke evaluations. The same method may be applied to evaluate kinematics and dynamics during different functional tests, and may be used for kinematic chains of any number of link.

In **Chapter 4** the quantitative assessment tool to estimate body sway angles (presented in Chapter 2) will be applied to the voluntary postural sway functional test, in order to provide information about the kinematic strategies adopted by a subject during a self-imposed perturbed stance. A single-axis accelerometer per segment will be used (stereo-photogrammetric system will be used for validation only), and

three biomechanical models, from 1- to 3-link, will be evaluated in order to describe as well as possible the sway movement. In addition, the quantitative assessment tool to predict kinematic and dynamic variables (presented in Chapter 3) will be applied to the voluntary postural sway functional test in order to predict the ground reaction forces and the centers of pressure and mass of the subject, considering a 2D 3-link biomechanical model and using a single-axis accelerometer per segment (force plate will be used for validation only). The presented method may be suitable for the response strategy evaluation to unexpected perturbation even if it will be evaluated on a self-induced sway only. An instrumented postural sway functional test will provide objective information to evaluate the balance control in several application of the clinical practice.

In addition to the accelerometers, in **Chapter 5** gyroscopes will be used for the estimation of the upper limb kinematics, considering a 3D 3-link biomechanical model. A sensor consisting of a tri-axes accelerometers and a tri-axes gyroscope will be placed to each body-segment, and a Kalman Filter-based algorithm will be computed in order to estimate the sensors angular kinematics. A new procedure will be introduced in order to align the technical system of reference of all sensors and to obtain a common global system of reference, neglecting the use of any magnetometer in the experimental set-up. Moreover, a quantitative assessment tool will be provided in order to estimate upper limb joint kinematics, considering a functional procedure to define body-segments anatomical axes based on accelerometers and gyroscopes data. Stereophotogrammetric system will be used for validation only. In order to support the usability of this method in the clinical practice, the Fugl-Meyer motor assessment (for the upper extremity) will be performed by the subject. The instrumentation of some of its functional tasks will provide an objective evaluation of motor performance in patients following a stroke, and may be considered also for functional evaluation and rehabilitation after different neurological and orthopedic injuries.

Chapter 2

Angular kinematics evaluation during the *Squat* functional test

Postural motion measurements at additional locations, such as lower and upper limbs and trunk, may be necessary in order to obtain information about the inter-segmental coordination during different functional tests involved in clinical practice. The main aim of this Chapter is to provide a quantitative assessment tool of body sway angles of a multi-link kinematic chain in the sagittal plane, using one single-axis accelerometer (SAA) per segment. A preliminary calibration, using SAAs and a reference system (encoder or stereo-photogrammetry), allows the estimation of sensors position and orientation and segment lengths. These parameters are then used to predict the chain kinematics using the SAAs only. To evaluate the method, the algorithm is first tested on a mechanical arm equipped with a reference encoder. A general method for estimating the kinematics of an x-link chain is also provided. Finally, a three-link biomechanical model is applied to a human subject to estimate the joint angles during squat tasks; a

stereo-photogrammetric system is used for validation. The results are very close to the reference values. Mean descriptive (predictive) root mean squared error (RMSE) is 0.15° (0.16°) for the inverted pendulum, and 0.39° (0.59°) for the shank, 0.82° (1.06°) for the thigh, 0.87° (1.09°) for the HAT (head-arm-trunk) in the three-link model. The mean value of RMSE without calibration is 1.02° for the inverted pendulum, and 11.01° (shank), 11.39° (thigh) and 12.21° (HAT) in the three-link model. These results suggest that, after the calibration procedure, one SAA per segment is enough to estimate 2D joint angles accurately in a kinematic chain of any number of links, providing the usability of this instrumented test in the clinical practice [8].

2.1 Introduction

Several authors have used accelerometers and/or rate gyroscopes to study balance in unperturbed upright stance [94, 127, 136], to estimate the gait kinematic parameters [118, 128], and to evaluate joint angles during specific tasks [35, 41, 53, 58, 112, 168, 182].

In the balance studies, Kamen *et al.* [94] used two Single-Axis Accelerometers (SAAs), taped to the back (at S2 level) and forehead, to quantify postural sway, evaluating the Root Mean Square Error (RMSE) and frequency spectrum of the accelerations in the Anterior-Posterior (AP) direction. Moe-Nilssen [136] used a tri-axial accelerometer placed on the trunk to investigate whether body sway during quiet standing could differentiate between young and elderly healthy subjects in different sensory conditions. In the study of Mayagoitia *et al.* [127], the authors compared the effectiveness of tri-axial accelerometer, placed at the back of the subject, and Force Plate (FP) measurements in distinguishing between different standing conditions. In the gait studies, Mayagoitia *et al.* [128] used four SAAs and one gyroscope per body segment to obtain the kinematics (shank, thigh and knee angles) in the sagittal plane. Their system was validated by an optoelectronic system, and the ratio between the mean RMSEs and the mean peak-to-

peak values was 2-5%. Lyons *et al.* [118] used two SAAs to distinguish between static and dynamic activities and to detect the basic postures of sitting, standing and lying. In the evaluation of the inclination angles of trunk and thigh in posture, the inertial term was neglected. The effect of this decision will be further discussed in the definition of our model. In joint angle evaluation studies, Liu *et al.* [112] used two tri-axial accelerometers to estimate the flexion/extension and abduction/adduction angles of the thigh segment; the RMSE of the thigh segment orientation was between 2.4° and 4.9° during normal gait, comparing accelerometric and Stereo-Photogrammetric (SP) data. Cooper *et al.* [35] estimated knee flexion/extension angles with RMSEs from 0.7° up to 3.4° using two inertial measurement units (i.e., a combination of gyroscopes and accelerometers). Similar results for the 3D knee joint angle measurements were obtained by Favre *et al.* [58] with the same instrumentation. O'Donovan *et al.* [53] found RMSE between 0.5 and 4 degrees for 3D lower limb joint angles estimation during static and dynamic tasks by using tri-axial accelerometers, gyroscopes and magnetometers. Dejnabadi *et al.* [41] showed RMSEs of 1° and 1.6° for shank and thigh segments, respectively, in the sagittal plane using a combination of accelerometers and gyroscopes.

Most of these methods usually require at least two inertial sensors per segment. In contrast, the aim of this study is to develop an alternative method using (only) one SAA per segment aligned with the AP axis of the anatomical reference frame. Off-line evaluation of sagittal plane kinematics is performed through a model-based approach.

To validate the method, three models are used:

- *Inverted pendulum model*: experimental tests using a mechanical arm equipped with an absolute encoder and a SAA.
- *N-link model*: a simulation shows the possible extension of the algorithm to a kinematic chain with N links.
- *Three-link biomechanical model*: an experimental session is conducted with a subject during squat tasks.

A calibration for the inverted pendulum and the 3-link model is provided to give the position and the orientation of the sensors and the anthropometric parameters of the subject (lengths of the shank and the thigh). These parameters are used, together with accelerometric data, to predict the joint angles which are then compared to the encoder outputs (for the inverted pendulum model) or to the SP outputs (for the 3-link biomechanical model).

2.2 Methods and Materials

2.2.1 Inverted Pendulum Model

An inverted pendulum model (1 degree of freedom) is initially analyzed. First, the kinematic equation of the model is shown and the estimation algorithm of the angular sway is provided. Next, in order to validate the method in a simple set-up, a mechanical arm equipped with an absolute encoder and a SAA is used and the sway angle is estimated after a calibration.

Inverted Pendulum Model: the Angle Estimation Method

The SAA is placed at height h from the pivot point P, with the sensitive axis orthogonal to the longitudinal axis of the inverted pendulum (see Figure 2.1a). The accelerometer output $a(t)$ can be expressed, in the continuous-time domain, as the sum of two terms, an inertial contribution depending on the angular acceleration $\ddot{\theta}(t)$, and a gravitational term depending on the sway angle $\theta(t)$:

$$a(t) = h\ddot{\theta}(t) - g \sin \theta(t) \quad (2.1)$$

where g is the gravitational acceleration.

Several authors [97, 118, 127, 128, 136, 203] used an inverted pendulum and a Quasi-Static (QS) model in which the inertial term in Equation (2.1) is neglected, so the accelerometer output can be approximated as $a(t) \approx -g \sin \theta(t)$. This approximation is overcome by

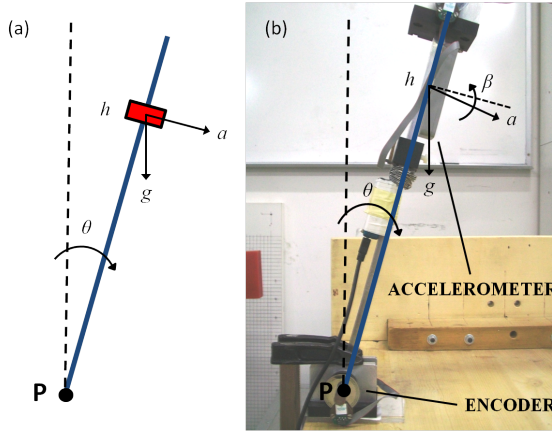


Figure 2.1: a) Inverted Pendulum Model, b) Mechanical Inverted Pendulum

the angular sway estimation algorithm presented in this Chapter, which is based on the dynamic model shown in Equation (2.1). First, Equation (2.1) can be rewritten, in the discrete-time domain, as the sum of a linear (L) and non-linear (NL) term:

$$a(k) = \underbrace{h\ddot{\theta}(k) - g\theta(k)}_{\text{Linear term}} + \underbrace{g(\theta(k) - \sin\theta(k))}_{\text{Corrective non-linear term}} = a_L(k) + a_{NL}(k) \quad k = 1, \dots, n \quad (2.2)$$

where n is the number of samples.

Under the approximation of small angles, ($\sin\theta(k) \approx \theta(k)$), the non-linear term is negligible, Equation (2.2) is linearizable and the linear model transfer function is:

$$H(s) = \frac{\theta(s)}{a(s)} = \frac{1}{hs^2 - g} \quad (2.3)$$

Equation (2.3) clearly shows that the system is unstable, because one of the roots of the denominator is positive. We refrain in this thesis from discussing the inverted pendulum model stabilization and focus instead on the angular sway estimation. This can be solved in

the frequency-domain rewriting Equation (2.3) as the product of two first-order low-pass filters (F_F , forward filter; B_F , backward filter):

$$H(j\omega) = \frac{\theta(j\omega)}{a(j\omega)} = -\frac{1}{g} \underbrace{\frac{1}{1 - \frac{j\omega}{\omega_c}}}_{B_F} \underbrace{\frac{1}{1 + \frac{j\omega}{\omega_c}}}_{F_F} \quad (2.4)$$

$$\omega_c = \sqrt{\frac{g}{h}}$$

The cutoff frequency of the two filters equals the corresponding natural frequency of the system:

$$f_c = \frac{1}{2\pi} \sqrt{\frac{g}{h}} \quad (2.5)$$

which is related to the distance h between the pivot point and the origin of the reference system of the inertial sensor. Equation (2.5) represents the frequency response of a second-order low-pass filter with zero-phase. Therefore, the angular sway can be computed through the *bi-directional* filtering of the accelerometric signal as follows (using the *filtfilt* function in Matlab):

$$\theta(j\omega) = -\frac{1}{g} B_F(j\omega) F_F(j\omega) a(j\omega) \quad (2.6)$$

The corrective non-linear term takes into account the non-linearities due to large angular excursions. The problem of evaluating the non-trivial, large angular displacements in Equation (2.2) is solved using an iterative methods with the following steps:

1. the angle vector $\boldsymbol{\theta} = [\theta(1) \dots \theta(n)]$ is initialized, neglecting the nonlinear and the inertial terms, as $-\mathbf{a}/g$, where $\mathbf{a} = [a(1) \dots a(n)]$ is the accelerometer output.
2. the corrective nonlinear term \mathbf{a}_{NL} is evaluated from Equation (2.2) by substituting the angle vector $\boldsymbol{\theta}$.
3. the linear acceleration vector is estimated as $\mathbf{a}_L = \mathbf{a} - \mathbf{a}_{NL}$ and new samples are added at the beginning and at the end of the vector using the Symmetric Padding technique [178] in order to

neglect the transient effect after filtering. The length of the two extensions has been chosen equal to six times the time constant, $\sqrt{h/g}$, of the filter.

4. the angle vector $\boldsymbol{\theta}$ is estimated by filtering the acceleration \mathbf{a}_L through the bidirectional low-pass filter, and the added extensions are removed.
5. the residual error at step j is estimated as $\mathbf{e}^{(j)} = \boldsymbol{\theta}^{(j)} - \boldsymbol{\theta}^{(j-1)}$.
6. the cost function is evaluated as $f^{(j)} = \mathbf{e}^{(j)} (\mathbf{e}^{(j)})^T$

Iterations 2-6 stopped when $f^{(j)} < \epsilon_0$, where $\epsilon_0 = 10^{-25}$ is the chosen threshold. Usually, the method converges in 10-15 steps.

Mechanical Inverted Pendulum

To test the method, an aluminum rectangular link is used as an inverted pendulum driven by hand to sway with a fixed pivot point. The frequency content of the angular sway is about 2Hz. Five trials are performed. The mechanical arm is equipped with an absolute encoder (Gurley Precision Instrument, mod. 7700, resolution 19 bit) and a tri-axial accelerometer (Dynaport[®] Minimod, McRoberts, range $\pm 2g$, resolution $\pm 1mg$) placed at height $h = 0.31m$ from the pivot point, P (Figure 2.1b). For the present study, only the accelerometer output related to the axis orthogonal to the mechanical arm is acquired at 100Hz sampling rate.

Unlike the ideal condition of the mathematical model, the placement of the sensor on the mechanical link potentially introduces some errors due to the non-orthogonality of the sensitive axis of the SAA to the segment. This effect is even more evident in the human body segments, where the soft tissue between the bone and the skin affects the ideal orthogonality of the SAA sensitive axis. Equation (2.1) is modified by taking into account the projections of the tangential, centripetal and gravity accelerations on the sensitive axis, in order to quantify this

undesired effect, as follows:

$$a(k) = h\ddot{\theta}(k) \cos \beta - h\dot{\theta}^2 \sin \beta - g \sin(\theta(k) - \beta) \quad k = 1, \dots, n \quad (2.7)$$

where the angle β describes the SAA non-orthogonality (see Figure 2.1b).

Preliminary calibration is required to evaluate the two geometric parameters h and β . In the calibration trial the encoder output, $\boldsymbol{\theta}_{enc}$, is used as reference. This algorithm estimates the parameter vector $\mathbf{p} = [h, \beta]$ through a least-squares approach by minimizing the cost function $f^{(j)} = \mathbf{e}^{(j)} (\mathbf{e}^{(j)})^T$, where $\mathbf{e}^{(j)} = \boldsymbol{\theta}_{enc}^{(j)} - \boldsymbol{\theta}^{(j-1)}$ is the residual error at step j . The angle vector $\boldsymbol{\theta}$ is estimated through the iterative algorithm previously described.

In order to test the robustness of the calibration, the two parameters are estimated for each trial and then their mean values are used to predict the angular sway of the inverted pendulum using the SAA; this prediction is compared to the encoder output. Angular RMSE is evaluated both in the calibration and prediction trials. In order to demonstrate the advantage of the angle estimation method with respect to the QS model, the encoder output is compared with the angular sway approximated as $\boldsymbol{\theta} \approx \beta + g \arcsin(\mathbf{a}/g)$, neglecting the inertial terms $\dot{\boldsymbol{\theta}}$ and $\ddot{\boldsymbol{\theta}}$. RMSEs between QS and reference angles are evaluated and the percentage of time in which the QS model is valid is provided. In fact, according to Equation (2.4), if the frequency content of the accelerometer output is below the frequency $f_{max} = f_c \sqrt{e\%/100}$, which implies an angle percentage error less than $e\%$ (e.g., $h = 1\text{m}$, $e\% = 5\%$, $f_{max} = 0.11\text{Hz}$), the QS model approximation is valid; if the frequency content exceeds f_{max} significantly, the accelerometer output, in absolute value, can reach the gravitational acceleration and the QS model provides imaginary angular values.

2.2.2 Multi-link Model

A kinematic chain model (N degrees of freedom) is analyzed. First, the kinematic equations of the model are described and the outputs

of the N accelerometers are simulated. The angular sway of each link is evaluated with the iterative method presented in the Section 2.2.1. The experimental validation of the model is then performed, after a calibration trial in a movement analysis laboratory, on a subject during squat tasks; the human body is assumed to be a 3-link model.

N -link Model

A continuous curve, with a fixed point in the joint ankle, is modeled. The curve can be discretized with any finite number of links, as shown in Figure 2.2. In this first simulation phase, a linear array of $N = 40$ SAAs, equally spaced with $l_i = 2cm (i = 1, \dots, n)$ (Figure 2.2), is assumed. The N angular trends are then simulated by a superposition of sinusoidal functions.

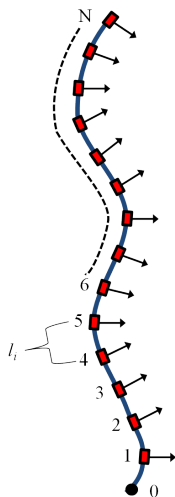


Figure 2.2: Linear array of SAAs

The output of the i -th accelerometer is obtained from Equation (2.2), adding the projection on the measurement axis of the accelerations, a_i^x and a_i^y , at the lower joint. These two contributions can be evaluated considering the second derivative of the lower joint position with

respect to the pivot point (e.g., for the first segment $[l_1 \sin \theta_1, l_1 \cos \theta_1]$, and for the second segment $[l_1 \sin \theta_1 + l_2 \sin \theta_2, l_1 \cos \theta_1 + l_2 \cos \theta_2]$).

Therefore, by simple geometric considerations, the acceleration of the i -th joint will be given by the recursive expressions:

$$\begin{aligned} a_i^x(k) &= a_{i-1}^x(k) + l_{i-1} \left. \frac{d^2[\sin \theta_{i-1}(t)]}{dt^2} \right|_{t=kT} \\ &\approx a_{i-1}^x(k) + l_{i-1} \frac{[\sin \theta_{i-1}(k+1) - 2 \sin \theta_{i-1}(k) + \sin \theta_{i-1}(k-1)]}{T^2} \end{aligned}$$

and

$$\begin{aligned} a_i^y(k) &= a_{i-1}^y(k) + l_{i-1} \left. \frac{d^2[\cos \theta_{i-1}(t)]}{dt^2} \right|_{t=kT} \\ &\approx a_{i-1}^y(k) + l_{i-1} \frac{[\cos \theta_{i-1}(k+1) - 2 \cos \theta_{i-1}(k) + \cos \theta_{i-1}(k-1)]}{T^2} \end{aligned}$$

for $k = 1, \dots, n$ and $i = 1, \dots, N$, where T is the sample time and l_{i-1} is the length of the $(i-1)$ -th segment (it is assumed that $a_0^{x,y} = 0$, $l_0 = 0$).

Therefore, the simulated i -th accelerometer output is expressed as:

$$\begin{aligned} a_i(k) &= h_i \ddot{\theta}_i(k) - g \sin \theta_i(k) + a_i^x(k) \cos \theta_i(k) - a_i^y(k) \sin \theta_i(k) \\ & \quad k = 1, \dots, n \\ & \quad i = 1, \dots, N \end{aligned} \quad (2.8)$$

In order to simulate the accelerometers output, a random Gaussian noise (zero-mean, std=0.01) is added to each of the simulated signals expressed in Equation (2.8). The same iterative method described in Section 2.2.1 allows the evaluation of the time-dependent snake-like profile, by summing and subtracting the linear gravitational contribution $g\theta_i(k)$ in Equation (2.8). In this case, the non-linear term of the acceleration, used in step-2 of the estimation method, is defined as:

$$\begin{aligned} a_{NL,i}(k) &= g\theta_i(k) - g \sin \theta_i(k) + a_i^x(k) \cos \theta_i(k) - a_i^y(k) \sin \theta_i(k) \\ & \quad k = 1, \dots, n \\ & \quad i = 1, \dots, N \end{aligned} \quad (2.9)$$

The estimated profile of the kinematic chain is compared to the simulated profile.

Three-Link Biomechanical Model

In the second experiment, the method is tested on one subject (female, 27 years-old, weight 59kg, height 167cm), who participated after giving her informed consent. In order to estimate the body sway in the sagittal plane during squat tasks [173], a 3-link biomechanical model is introduced.



Figure 2.3: Experimental testing set-up

The feet are supposed to be rigidly connected to the ground; the ankle, knee and hip joints are represented as three hinge joints and the shank (segment 1, length $l_1 = 0.40\text{m}$), the thigh (segment 2, length $l_2 = 0.49\text{m}$) and the Head-Arms-Trunk (HAT, segment 3) are modeled as three rigid segments. The subject is asked to perform a repetition

of squat exercises for 30 seconds with her arms folded, keeping her movement in the AP direction. Four trials are performed. In order to estimate the shank, thigh and HAT angles with respect to the vertical line, three tri-axial accelerometers (Dynaport[®] Minimod, McRoberts, range $\pm 2g$, resolution $\pm 1mg$) are placed at measured heights $h_1 = 0.30m$, $h_2 = 0.29m$, $h_3 = 0.29m$, with respect to the ankle, knee and hip joint, respectively, in order to minimize the skin artifact effect. Each of the three sensors is placed on a rhomboid rigid plate and mounted on the skin at the lateral side of the thigh, shank and HAT by using three hook-and-loop fastener belts, as shown in Figure 2.3. For the present study only the AP accelerometer outputs are acquired at a 100Hz sampling rate.

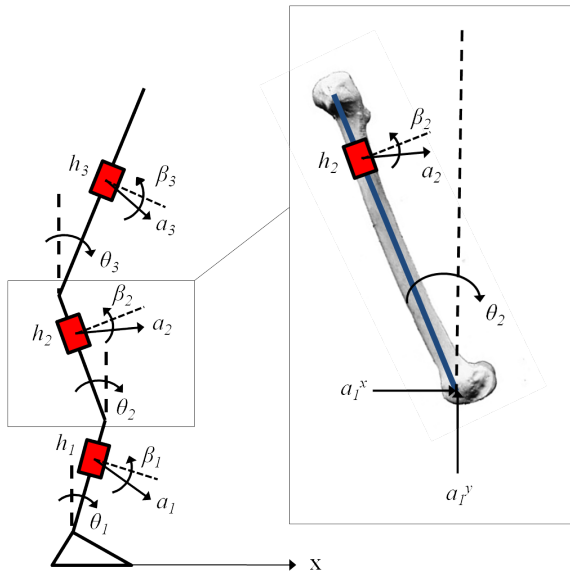


Figure 2.4: Three-link biomechanical model

Four reflective markers are placed on the vertices of each plates, and a SP system (SMART eMOTION, BTS) is used for calibration and validation. SP and accelerometer data are low-pass filtered (zero-phase) at a cut-off frequency of 3Hz. The 12 markers are projected onto

the plane which best approximates the point cloud in the observation interval, and the three reference angles are evaluated through the 2D Singular Value Decomposition (SVD) method [6, 76]. The SP angles are related to the first acquisition frame which defines the cluster model.

As explained in Section 2.2.1, the sensors on the skin surface introduce potential errors, due to non-orthogonality of the measurement axis of the SAAs to the body segment anatomical axis. In order to model this undesired effect, Equation (2.8) is modified by taking into account the projections of the tangential, centripetal, gravity and lower joints acceleration on the measurement axis. The method proposed in this paper provides angles from accelerometric measures with respect to the vertical, rather than from the first acquisition frame as for SP data. In order to take this fact into account, Equation (2.8) is modified as follows:

$$\begin{aligned}
 a_i(k) &= h_i \ddot{\theta}_i(k) \cos \beta_i - h_i \dot{\theta}_i^2(k) \sin \beta_i - g \sin(\theta_i(k) - \beta_i + \theta_{i0}) \quad (2.10) \\
 &+ a_i^x(k) \cos(\theta_i(k) - \beta_i + \theta_{i0}) - a_i^y(k) \sin(\theta_i(k) - \beta_i + \theta_{i0}) \\
 & \qquad \qquad \qquad k = 1, \dots, n \\
 & \qquad \qquad \qquad i = 1, \dots, 3
 \end{aligned}$$

where the angles β_i describe the SAAs non-orthogonality (see Figure 2.4) for each segment, and the angle $\theta_{i0} = -a_{i0}/g$ is related to the first acquisition frame, in which the inertial and non-linear terms are negligible.

The parameters h_i , β_i and l_m ($m = 1, 2$) are estimated by the calibration algorithm using the least-squares minimization, as in Section 2.2.1; the SP angles are used as reference values. The angle vectors $\boldsymbol{\theta}_i = [\theta_i(1) \dots \theta_i(n)]$ are estimated through the iterative algorithm described in Section 2.2.1. In order to test the robustness of the calibration, the 8 parameters are estimated for each trial; the mean values of the parameters are then used to predict the subject's angular sways using the three SAAs. The estimated angles are compared to the SP outputs by evaluating the RMSE.

2.3 Results

2.3.1 Mechanical Inverted Pendulum Kinematics

The calibration algorithm, presented in Section 2.2.1, provides two parameters (mean \pm std): the distance $h = 0.31 \pm 0.00\text{m}$, of the origin of the sensor reference system to the pivot point P (the measured distance equals 0.30m), and an angle $\beta = -1.17 \pm 0.15^\circ$, related to the non-orthogonality of the measurement axis of the SAA to the link. These two parameters are used along with the SAA data to predict the angles which are compared with the encoder angles. Calibration and prediction RMSEs and Peak-to-Peak (P-P) ranges are reported in Table 2.1, along with the results obtained with the QS model and the percentage of time in which it is valid.

Table 2.1: RMSEs and P-P range for the mechanical inverted pendulum

	Trial 1	Trial 2	Trial 3	Trial 4	Trial 5	mean\pmstd
RMSE [°] calibration	0.16	0.18	0.14	0.15	0.12	0.15 \pm 0.02
RMSE [°] prediction	0.17	0.18	0.16	0.15	0.12	0.16 \pm 0.02
RMSE [°] QS model	30.02 (95.2%)	30.08 (91.2%)	25.28 (85.3%)	21.89 (83.5%)	21.15 (85.4%)	25.68 \pm 4.28
P-P range [°]	126.5	117.9	125.4	108.3	151.4	125.9 \pm 16.0

The mean ratio between the RMSEs and the P-P ranges in description and prediction is approximately 0.12%. The mean ratio between the RMSEs and the P-P range obtained without calibration, by neglecting the parameter β and using the measured parameter h , is about 0.82% and the mean value of RMSEs is 1.02°. The use of the calibration parameters therefore allows a less biased estimation. Table I also shows that the mean angular error of the QS model is very high, about 25°, due to the high frequency sways.

2.3.2 Multi-link Kinematics

N -link model kinematics

The linear array of $N = 40$ SAAs, equally spaced with $l_i = 2cm(i = 1, \dots, N)$, is simulated. The snake-like profile for 3 different frames is shown in Figure 2.5, comparing the simulated and estimated profiles: the continuous curve represents the simulated N -link chain, the points of the silhouette are the estimated joint positions, with respect to the pivot point, between two consecutive links. The positions of the joints are evaluated using the estimated angles and segment lengths.

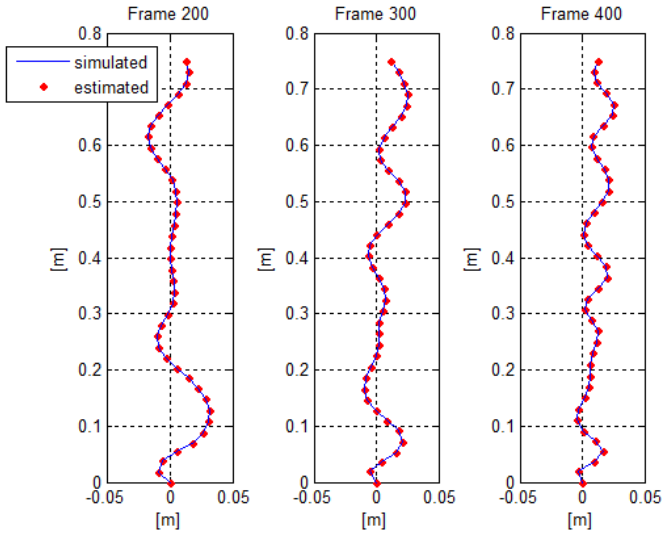


Figure 2.5: Snake-like profile for a 40-link kinematic chain

The angular RMSE between the sway angle of each link and the reference angle is evaluated. The values of the RMSE and P-P range, averaged out the N -link, are (mean \pm std) $0.37\pm 0.16^\circ$ and $70.42\pm 10.19^\circ$, respectively. The Euclidean distance between the joint positions of the estimated and simulated N -link is (mean \pm std) $0.3 \pm 0.1\text{mm}$.

Three-link biomechanical model kinematics

The mean values and standard deviations of the calibration parameters for the 4 trials, estimated by using the accelerometer output and the SP data as reference, are (mean \pm std) $h_1 = 0.31 \pm 0.01\text{m}$, $h_2 = 0.32 \pm 0.00\text{m}$, $h_3 = 0.30 \pm 0.07\text{m}$, $l_1 = 0.51 \pm 0.06$, $l_2 = 0.52 \pm 0.06$ and $\beta_1 = -10.96 \pm 0.21^\circ$, $\beta_2 = -11.83 \pm 0.64^\circ$ and $\beta_3 = -13.17 \pm 0.4^\circ$. These parameters are used to predict angular sway by using the three SAA outputs. The angles obtained are then compared with the SP data. Calibration and prediction RMSEs and P-P ranges are reported in Table 2.2 for shank, thigh and HAT angles, respectively.

Table 2.2: RMSEs and P-P range for the subject during squat tests

	Trial 1	Trial 2	Trial 3	Trial 4	mean\pmstd
RMSE shank [°] calibration	0.34	0.40	0.50	0.85	0.39 \pm 0.08
RMSE shank [°] prediction	0.38	0.47	0.56	0.93	0.59 \pm 0.24
P-P shank range [°]	26.54	24.64	28.11	23.79	25.77 \pm 1.94
RMSE thigh [°] calibration	0.73	0.98	0.86	0.72	0.82 \pm 0.12
RMSE thigh [°] prediction	0.81	1.32	1.16	0.95	1.06 \pm 0.23
P-P thigh range [°]	42.74	59.74	48.30	47.45	49.55 \pm 7.21
RMSE HAT [°] calibration	0.85	0.99	0.81	0.84	0.78 \pm 0.08
RMSE HAT [°] prediction	0.93	1.06	0.97	1.42	1.09 \pm 0.22
P-P HAT range [°]	39.73	56.14	37.30	47.74	42.23 \pm 8.53

The ratios between the mean values of RMSEs and the P-P ranges are 1.5%, 1.7%, 1.9% for shank, thigh and HAT angles, respectively, for the calibration trials, and 2.3%, 2.1%, 2.4% for the prediction trials. The three angular patterns for stereo-photogrammetry and accelerometry data are reported in Figure 2.6 for one prediction trial. The mean RMSEs obtained without calibration, thus neglecting the parameters β_i and using the measured parameters h_i and l_i , are 11.01° , 11.39° and 12.21° for shank, thigh and HAT, respectively.

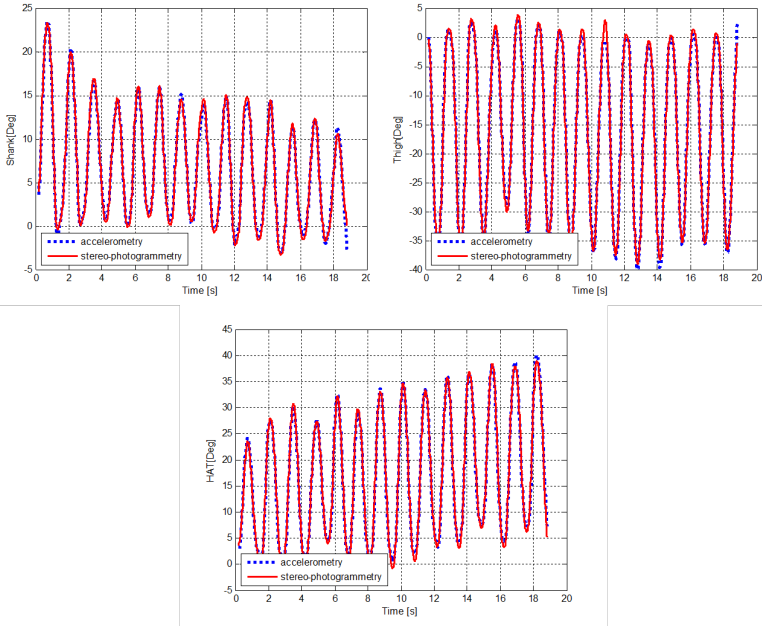


Figure 2.6: Shank, thigh, HAT angular patterns in prediction

2.4 Discussion

This Chapter suggests a novel method based on the use of one SAA per segment, which provides the accurate estimation of 2D joint angles, taking into account the inertial term of the accelerometer output.

Several authors used the QS model to evaluate the angular sway: the procedure of separating the gravitational and inertial components of the accelerometer output has usually been considered very difficult unless multiple accelerometers are used [57, 76, 80, 112, 147]. Our method improves the QS model approximation: the use of the iterative method based on the bidirectional low-pass filter, with a cut-off frequency related to the sensor position with respect to the pivot point, provides RMSEs of approximately 0.1% of the angular range, as shown in Table 2.1. The experimental sessions on the mechanical arm provided a simplified situation in which the method was successfully tested, as

demonstrated by the mean RMSE values of 0.15° with a mean P-P range of 126.1° . This error term partly reflects the encoder resolution (0.036°) and the accelerometer performance limits. As shown in the Methods, the angle evaluation can be extended to an N -link model, providing the possibility of estimating the silhouette of a kinematic chain with any number of links. The results obtained in simulation suggest possible applications in various fields like trunk posture evaluation and swimming, and most importantly to evaluated different strategies response to external stimuli in terms of sway angles.

Additional discussion is required about the subject tests. Description and prediction RMSEs are smaller than those previously reported in the literature. For example, reported shank and thigh angle RMSEs range from 0.7° to 4.1° [35, 53, 112], although these studies analyse 3D joint angle estimation during gait instead of 2D squat tasks. RMSEs of the calculated angular displacements of the three segments (thigh, shank and HAT), as shown in Table 2.2, are larger than those in the inverted pendulum tests, due to several factors:

- *2D errors*: motion is inherently 3D and 2D analysis is an approximation. 2D projection of the markers' coordinates on the best fit plane produces a distortion affecting the SP angles estimation and therefore the validation measures. Consequently, there is not the certainty that SP provides a gold standard kinematics. Therefore both calibrated and predicted RMSE values in Table 2.2 should be considered as measures of the distance between estimates provided by two differently approximated methods;
- *sensor mounting*: it is difficult to firmly affix the accelerometers and the rhomboid rigid plates onto the segments without any relative motion. Unlike the mechanical arm, the soft tissue artifacts and the muscle activation add noise to the accelerometric measures. In particular, respiration represents an undesired effect for the sensor placed on the lateral side of the trunk, upon the rib;
- *propagation errors*: RMSEs are lower in the distal segment and

increase in the thigh and HAT. As shown in Equation (2.8), the accelerations are related to the estimated angles of the lower links, therefore the errors in the angle estimation of the $(i-1)$ -th link propagate to the angle estimation of the i -th link.

Despite these considerations, the results are very encouraging for several reasons. First, it is important to note the effectiveness of the calibration procedure, both for the mechanical arm and the 3-link biomechanical model, which allows the evaluation of the sensor position and misalignment and thus provides a better kinematic estimation. The parameter estimation provides unbiased results, both for description and prediction. Significantly, calibration allows us to reduce the errors from 11.0° - 12.2° to 0.6° - 1.1° . Second, our estimation method provides a simple, accurate and portable joint angle evaluation for postural tasks. The movement analysis laboratory is required only in the calibration phase, after which the clusters of markers are removed and only the three SAAs are used.

Squatting exercises are often performed to characterize the bilateral lower-extremity kinematics after anterior cruciate ligament reconstruction. The main outcome measures are the sagittal plane ankle, knee and hip angles and their maximum excursion [173], in addition to the net joint moments. The procedure presented in this Chapter speeds up the experimental sessions, reducing the computational and economic costs, especially when several subject are involved. The novel method presented in this Chapter overcomes the limitation of the QS model, often used in literature [97, 118, 127, 128, 136, 203], in which the accelerometers are used as inclinometers. Since some authors used more than one sensors per segment [35, 112, 128], we demonstrated one SAA per segment is enough to estimate 2D joint angles accurately in a kinematic chain of any number of link providing errors smaller than those reported in literature.

The methods presented in this Chapter is therefore suitable to be included in different balance assessments tests which includes perturbed postures by applying a direct force to the subject or by tilting or trans-

lating the surface upon which he stands. The presented approach could be able to discriminate among different strategies adopted for recovery balance after external stimuli by the evaluation of sway angles, highlighting how the subject's motor system responds in terms of hip, ankle or combined ankle-hip strategies.

Chapter 3

Dynamics evaluation during the *repeated* *Sit-to-Stand* functional test

In the previous Chapter a novel method was proposed for estimating the kinematics of a multi-link model by using a body-sensor network during squat tasks. The same method is extended in this and in next Chapters for the kinematic description of Sit-to-Stand. In addition, this Chapter proposes a functional subject-specific 2D evaluation tool for estimating body-segment and dynamic parameters which makes use of a simple motor task (repeated Sit-to-Stand, rSTS), recorded with one single-axis accelerometer (SAA) per segment and a Force Plate (FP). After this preliminary estimation, the quasi-real-time prediction of the Ground Reaction Force (anterior/posterior, F_x , and vertical, F_z , components), the Centers of Pressure (CoP) and Mass (CoM), and the Net Joint Moments (NJMs) at the ankle, knee and hip, is performed by the use of accelerometry only during the rSTS functional test in the

sagittal plane. Predicted dynamic variables and those obtained using anthropometric parameters derived from De Leva were compared to the FP outputs, in terms of Root Mean Squared Errors (RMSEs). RMSEs increase, using De Leva’s parameters in place of those estimated, from 12N to 21N (Fx), from 21N to 24N (Fz), from 21.1mm to 55.6mm (CoP), and from 10.3Nm to 17.0Nm (ankle NJM) in rSTS. In addition, a telescopic inverted pendulum was adopted to analyse the balance control in rSTS using only predicted CoP and CoM. Results suggest that one SAA per segment may be used to predict the dynamics of a biomechanical-model of any degrees of freedom [9, 64, 65].

3.1 Introduction

Sit-to-Stand is an important task in daily life, and it has been identified as one of the most mechanically demanding activities, confirming the general acceptance of its use as an indicator of the mobility level. This task requires coordination, balance, adequate mobility and strength. The transfer from sitting to standing and back to sitting requires voluntary movement of the different segments that contribute to the change of posture and balance control during the Center of Mass (CoM) forward and backward displacement. In several studies, repeated Sit-to-Stand (rSTS) performance has been associated with age-related changes in muscular strength in leg extensor [167] and vestibular disorders as well as changes in movement strategies [95]. Consequently, standardized assessment of rSTS postural transitions has been used for multiple purposes, including evaluation of postural control [54, 115], risk of fall [21, 51], lower-extremity strength [26, 37], and impairment after stroke [106, 130].

A comprehensive analysis of kinematics and dynamics performance of the rSTS test requires the knowledge of the trajectories of the body Center of Pressure (CoP) and the body CoM, commonly investigated in studies on human posture and balance control [84, 88, 160, 205] and in many functional tests [62, 148, 151]. In balance-related studies [107], it

is often interesting to quantify the motion of CoP and CoM in order to investigate kinetic quantities such as the moment of the Ground Reaction Force (GRF) with respect to the CoM or the whole body stiffness around the ankles [206]. However, while the CoP can be measured by means of a Force Plate (FP), the whole body CoM location is not directly observed and it should be estimated. Kinematics-based [77, 206] and FP-based methods [25, 176, 217] have been proposed to estimate CoM position, involving the definition of an adequate biomechanical model of the body and the identification of anthropometric properties of body-segments.

Anthropometric parameters and kinematic data have been also used as inputs to the equations of motion, with or without dynamic data depending on the method used [23, 204], to estimate the Net Joint Moments (NJMs) during functional tests. The knowledge of the lower limb joint moments provides information on muscle strength and inter-muscular coordination across the joint. These quantities are then used to determine dynamic stability in human subjects, and may provide an indicator of deterioration in the motor performance of subjects with motor disorders (e.g. Parkinsonian [119]) or to discriminate between fallers and non-fallers [51].

Body-Segment Parameters (BSP) are typically derived from geometric models [75, 78, 92, 202, 213] and/or regression models scaled to the height and the weight of the subject (e.g. cadaver segmentation [27, 43] and imaging methods [29, 56, 174, 175, 196, 216]). The intrinsic limits of the geometric models are the assumption of a common model which neglects individual differences in segment shape and density, and the requirement of a large number of measurements (between 90 [213] and 248 [78]). About regression models, if equations are obtained from cadaver's data, they assume that embalmed and frozen tissue properties are similar to their in vivo state. Regression equations derived from imaging methods provide more accurate anthropometric parameter estimates, but they are invasive and expensive.

Recently, optimization methods combining model-based and exper-

imental approaches were proposed to estimate anthropometric parameters [28, 163]. Riemer *et al.* [163] used a 2D two-step optimization approach to solve a constrained non-linear optimization problem. Three calibration motions were considered: i) a long motion that involved a single cycle of a flexion and hyperextension of the hips, followed by flexion and extension of the knees, ii) a squat motion, and iii) a sway motion. The authors used a stereo-photogrammetric (SP) system and a FP, minimizing the residuals between measured GRF and the one calculated via a top-down inverse dynamics approach. Chen *et al.* [28] developed a 3D non-invasive, radiation-free optimization method, using a SP system and two FPs. The authors evaluated the performance by comparing the predicted GRF and CoP to those directly measured for static postures, squatting and walking. They obtained mean CoP errors less than 5 mm during stationary standing postures, 9.4 mm for squatting and 12.8 mm for walking. These methods need costly laboratory instrumentations and complex experimental protocols. Their implementation requires a fully equipped movement analysis laboratory, with a SP system and skilled personnel (e.g. in [28] each subject wore 54 retro-reflective markers placed by a well-trained physical therapist).

In conclusion, while the current state of the art offers several alternatives for BSP estimation, to the best of our knowledge, there are no published methods based on inertial measurements related to this relevant topic. Even if inertial tracking technologies are becoming widely accepted for the assessment of human movement both in clinical applications and scientific research, there is still a lack of applications of inertial wearable technology for dynamics evaluation of human movement.

Aims of this Chapter are:

- to present a novel, functional, model-based approach to estimate subject-specific BSP using a single-axis accelerometer (SAA) per segment and a FP;

- to predict GRF, CoP, CoM and NJMs at the ankle, knee and hip, using only the SAAs and the estimated anthropometric parameters, during the rSTS functional test.

The predicted dynamic variables are compared to those measured by the FP and those obtained using anthropometric parameters derived from De Leva’s tables [42]. Moreover, an inertial-based quasi-real-time balance monitoring during the rSTS is suggested.

3.2 Methods and Materials

3.2.1 Experimental Set-Up

Three young healthy subjects - two males, Body Mass Index (BMI) = $[25.5, 22.3]kg/m^2$; one female, BMI = $23.6kg/m^2$ - with no previous orthopedic ailment, participated in this study after giving their informed consent. The subjects, standing on a FP (Bertec 4060-08) with the feet supposed rigidly connected to the ground, were asked to perform five trials of ten rSTS on a chair with height $h_c = 0.48m$, with their arms folded and keeping their movement in the anterior/posterior (AP) direction. The first five repetitions of each rSTS trial were performed at the subjects’ maximum speed, and the second five at the subjects’ self-selected speed. Three SAA (Analog Device, ADXL 103) were placed at measured heights h_1, h_2, h_3 , with respect to the ankle, knee, and hip joint, respectively. Each of the three sensors was mounted directly on the skin, in a central position on the lateral side of the thigh and the shank, and on the posterior side of the Head-Arms-Trunk (HAT), in order to minimize skin artifact effects and model errors. In order to measure the sensor position, $h_i (i = 1, \dots, 3)$, and the segment length, $l_i (i = 1, \dots, 3)$, anatomical landmarks of body-segments (lateral malleolus, lateral epicondyle and L5 vertebra) were identified by palpation. FP and accelerometer signals were acquired at a 100Hz sampling rate and low-pass filtered (2nd order zero-phase Butterworth filter) at a cut-off frequency of 3Hz.

3.2.2 N -link Biomechanical Model

In order to describe the new method in the most general way, a N -link biomechanical model (N degrees of freedom) in the sagittal plane is initially analyzed.

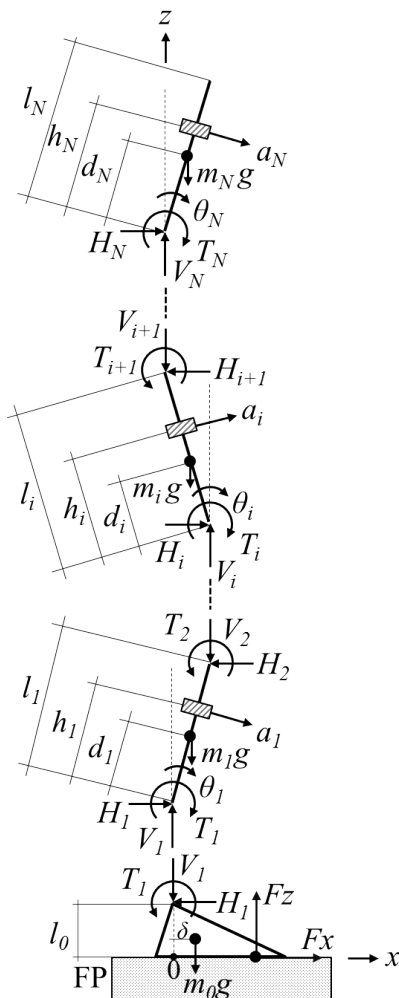


Figure 3.1: N -link free-body diagram in the sagittal plane

The free-body diagram (Figure 3.1) was used to define the dynamic equilibrium equations of the N -link model and the relationships between kinematic and kinetic variables. Feet and other body segments were considered separated from each other and the interaction between adjacent segments was described by horizontal and vertical forces, H_i and V_i , and net joints moments, T_i . The AP and the vertical components of the GRF, F_X and F_Z , and the moment component about the medial/lateral (ML) axis, M_Y , can be expressed, in the discrete-time domain, as follows:

$$\begin{aligned}
F_X(k) &= \tilde{\mathbf{D}}^T \ddot{\mathbf{S}}_\theta(k) \\
F_Z(k) &= Mg + \tilde{\mathbf{D}}^T \ddot{\mathbf{C}}_\theta(k) \\
M_Y(k) &= \tilde{\mathbf{D}}^T [g\mathbf{S}_\theta(k) - l_0 \ddot{\mathbf{S}}_\theta(k) - \mathbf{A}_{\mathbf{IS}}(k)] - \tilde{\mathbf{J}}^T \ddot{\theta}(k) \\
k &= 1, \dots, n
\end{aligned} \tag{3.1}$$

where $\ddot{\theta}(k)$, $\mathbf{S}_\theta(k)$, $\ddot{\mathbf{S}}_\theta(k)$, $\ddot{\mathbf{C}}_\theta(k)$, $\mathbf{A}_{\mathbf{IS}}(k)$, $\tilde{\mathbf{D}}$, $\tilde{\mathbf{J}}$ are $[N \times 1]$ -column vectors and n is the number of samples. The vectors' elements are defined as follows:

$$\begin{aligned}
S_{\theta,i}(k) &= \sin \theta_i(k) \\
C_{\theta,i}(k) &= \cos \theta_i(k) \\
A_{IS,i}(k) &= \sum_{j=1}^{i-1} l_j \{ [\ddot{\theta}_j(k) + \ddot{\theta}_i(k)] \cos[\theta_i(k) - \theta_j(k)] + \\
&\quad [\dot{\theta}(k)_j^2 - \dot{\theta}(k)_i^2] \sin[\theta_i(k) - \theta_j(k)] \} \\
\tilde{D}_i &= m_i d_i + l_i \sum_{j=i+1}^N m_j \\
\tilde{J}_i &= J_i + m_i d_i^2 + l_i^2 \sum_{j=i+1}^N m_j \\
k &= 1, \dots, n \\
i &= 1, \dots, N
\end{aligned}$$

The vector $\boldsymbol{\theta}_i = [\theta_i(1) \dots \theta_i(n)]$ represents the i -th angular deviation from the vertical line, $\dot{\boldsymbol{\theta}}_i$, the i -th angular velocity vector, and $\ddot{\boldsymbol{\theta}}_i$ the i -th angular acceleration vector. The two sensitivity vectors $\tilde{\mathbf{D}}$ and $\tilde{\mathbf{J}}$ are defined as linear combinations of the anthropometric parameters, as segment length, l_i , mass, m_i , distance of CoM from distal joint axis, d_i , and moment of inertia, J_i .

The i -th SAA output vector, $\mathbf{a}_i = [a_i(1) \dots a_i(n)]$, along the sensitive axis directed normally to the segment and oriented anteriorly, can be expressed as the sum of an inertial and a gravitational term plus two contributions, related to the horizontal and vertical accelerations at the lower joint, \mathbf{a}_i^x and \mathbf{a}_i^y , due to the underlying chain kinematics (see Chapter 2):

$$\begin{aligned} a_i(k) &= h_i \ddot{\theta}_i(k) - g \sin \theta_i(k) + a_i^x(k) \cos \theta_i(k) - a_i^y(k) \sin \theta_i(k) \\ & \quad k = 1, \dots, n \\ & \quad i = 1, \dots, N \end{aligned} \quad (3.2)$$

According to the iterative technique presented in the previous Chapter, the i -th sway angle of the N -link model, θ_i , can be evaluated from the accelerometer outputs, using a low-pass bi-directional filter with cut-off frequencies depending on sensor positions. After computing θ_i and its first numerical derivative $\dot{\theta}_i$, its second derivative, $\ddot{\theta}_i$, can be computed by Equation (3.2). Therefore, the dynamic equilibrium equations can be expressed as linear combinations of the i -th angular position, θ_i , the i -th angular velocity, $\dot{\theta}_i$, and the i -th SAA output, \mathbf{a}_i , through the $2N$ unknown anthropometric parameters, $\tilde{\mathbf{D}}$ and $\tilde{\mathbf{J}}$.

3.2.3 Subject-specific Body-Segment Parameters Estimation

Adequate to the trials carried out, a 3-link model is then used for the subject-specific BSPs estimation. The rSTS trials were used to estimate the anthropometric parameters $\tilde{\mathbf{D}}$ and $\tilde{\mathbf{J}}$, for each subject. After computing $\theta_i (i = 1, \dots, N)$, $\tilde{\mathbf{D}}$ and $\tilde{\mathbf{J}}$ can be calculated by a linear regression using the FP outputs, $\mathbf{F}_{X,FP}$, $\mathbf{F}_{Z,FP}$ and $\mathbf{M}_{Y,FP}$, as the dependent variables, and the angular position vector, θ_i , the angular velocity vector, $\dot{\theta}_i$, and the SAA outputs, $\mathbf{a}_i (i = 1, \dots, N)$, as the regressors. Three offset parameters must be also taken into account: two instrumental offsets are related to the forces and the third, M_Y^0 , is related to the distance between the origin of the FP's reference system

and the equilibrium position. Parameters reliability was assessed by calculating the Intra-Class Correlation coefficient (ICC3,1) from the five measurements of the three subjects. The significance level for all tests was set to an uncorrected $\alpha = 5\%$ (two-sided). Additionally, the mean value of each estimated parameter was compared with the one provided by De Leva's anthropometric tables [42].

3.2.4 Dynamics Prediction

The predictive ability of the 3-link model is finally tested on each subject during the rSTS functional test. The estimated parameters, $\tilde{\mathbf{D}}$ and $\tilde{\mathbf{J}}$, were used to predict \mathbf{F}_X , \mathbf{F}_Z , the displacement of the CoP in the AP direction, $\Delta\mathbf{CoP}_X$, the displacements of the CoM in the AP and in the vertical direction, $\Delta\mathbf{CoM}_X$ and $\Delta\mathbf{CoM}_Z$, the NJMs at the ankle, the knee and the hip, $\mathbf{T}_i (i = 1, 2, 3)$, using the three SAAs only and a top-down approach, as follows:

$$\begin{aligned}
F_X(k) &= \tilde{\mathbf{D}}^T \ddot{\mathbf{S}}_\theta(k) \\
F_Z(k) &= Mg + \tilde{\mathbf{D}}^T \ddot{\mathbf{C}}_\theta(k) \\
\Delta CoP_X(k) &= \frac{\Delta M_Y(k) + m_0 g \delta}{F_Z(k)} - CoP_X^0 \\
\Delta CoM_X(k) &= \frac{1}{M} [\tilde{\mathbf{D}}^T \mathbf{S}_\theta(k)] \\
\Delta CoM_Z(k) &= \frac{1}{M} [\tilde{\mathbf{D}}^T \mathbf{C}_\theta(k)] \\
T_i(k) &= T_{i+1}(k) + \tilde{J}_i \ddot{\theta}_i - g \tilde{D}_i \sin \theta_i + \\
&+ \tilde{D}_i \sum_{k=1}^{i-1} l_k [\ddot{\theta}_k \cos(\theta_k - \theta_i) - \dot{\theta}_k^2 \sin(\theta_k - \theta_i)] + \\
&+ l_i \sum_{k=i+1}^3 \tilde{D}_k [\ddot{\theta}_k \cos(\theta_k - \theta_i) - \dot{\theta}_k^2 \sin(\theta_k - \theta_i)] \\
k &= 1, \dots, n
\end{aligned} \tag{3.3}$$

where m_0 is the estimated feet mass, δ is the AP location of the feet CoM with respect to the malleolus (see Figure 3.1), $\Delta M_Y(k) =$

$M_Y(k) - M_Y^0$, and $CoP_X^0 = \frac{M_Y^0}{F_Z^0} = m_0 g \delta$ is the CoP value at the equilibrium position.

For comparison, the NJM at the ankle was also obtained from the FP outputs as follows:

$$T_{1,FP}(k) = F_{Z,FP}(k)CoP_{X,FP}(k) + F_{Z,FP}(k)l_0 - m_0 g \delta \quad (3.4)$$

The effectiveness of the method was evaluated for each subject in terms of Root Mean Square Error (RMSE) between the measured and estimated FP outputs, as follows:

- the mean description error was computed by averaging the RMSEs obtained by using the estimated parameters of the p -th rSTS trial for the evaluation of the dynamic variables of the same p -th trial;
- the mean prediction error was computed by averaging the RMSEs obtained by using the estimated parameters of the p -th rSTS trial ($p = 1, \dots, 5$) for the evaluation of the dynamic variables of the q -th rSTS trial ($q = 1, \dots, 5, q \neq p$);
- the mean De Leva's prediction error was evaluated considering the De Leva's parameters [42] in place of the estimated parameters $\tilde{\mathbf{D}}$ and $\tilde{\mathbf{J}}$;
- the predicted ankle moment \mathbf{T}_1 and that obtained using De Leva's parameters, $\mathbf{T}_{1,DeLeva}$, was compared to that provided by FP outputs, $\mathbf{T}_{1,FP}$, in terms of RMSEs.

For an effective description of the rSTS task by using the accelerometry -based predicted CoP and CoM in the AP direction, the Telescopic Inverted Pendulum (TIP) model, presented by Papa and Capozzo [151], was analyzed. In this study, a minimum measured-input model, which used only information obtained from a six-component FP, a seat uniaxial load-cell and anthropometric data derived from [26], was adopted.

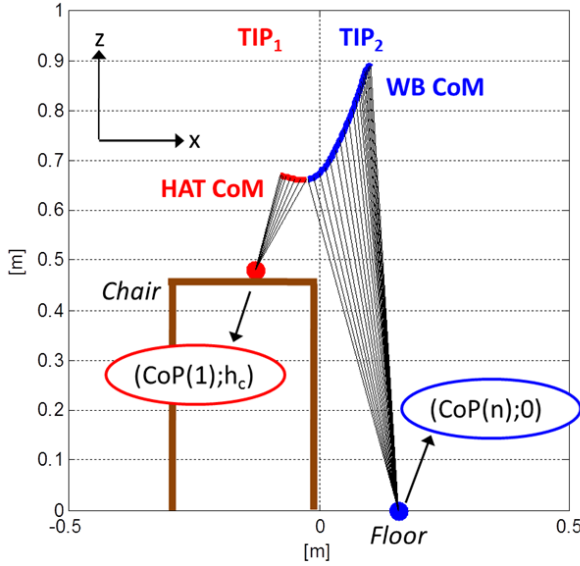


Figure 3.2: Schematic representation of the two TIP models

In the present study, only the information derived from accelerometers were assumed as measured input. According to [151], two TIP models were used in temporal sequence, as shown in Figure 3.2 : the first one (TIP_1) is related to the time preceding seat-off, in which only the HAT system moves, and the second one (TIP_2) to the whole body movement during the interval of time following seat-off. For the TIP_1 model, the vertical projection of the first sample of the predicted $\Delta\mathbf{CoP}_X$ on the seat surface, $P_1 = (\Delta\mathit{CoP}_X(1); h_c)$, was considered in place of the midpoint between the hips. For the TIP_2 model, the last sample of the predicted $\Delta\mathbf{CoP}_X$ under the feet, $P_2 = (\Delta\mathit{CoP}_X(n); 0)$, was considered in place of the midpoint between the ankles. The linear actuator (LA) and the sagittal plane rotational actuator (SA) were taken into account to describe the elongation and the forward and backward rotations of the link. The telescopic link joined P_1 to the predicted HAT CoM position (phase TIP_1), and P_2 to the predicted whole-body CoM position (phase TIP_2). The linear and angular velocity of the SA and

LA actuators were evaluated and compared with those presented in [151].

3.2.5 Quasi-Real-Time Prediction

Prediction of dynamic variables could be extended to real-time applications for balance monitoring during the rSTS functional test. The ΔCoP_X and ΔCoM prediction is based on quasi-real-time estimation of the sway angles $\theta_i (i = 1, \dots, N)$ from the accelerometer outputs. The quasi-real-time technique is derived from the procedure described in Chapter 2 by applying the low-pass bi-directional filter to a sliding time window of the i -th accelerometer outputs $\mathbf{a}_i (i = 1, \dots, N)$. The length of the time window is set to $N_W = 160$ samples ($T_W = 1.6s$). For the sake of clarity, the procedure is reported here for a single segment and the index i is neglected (e.g. $a_i(k)$ becomes $a(k)$). At the k -th instant of time ($k = \frac{N_W}{2}, \dots, \frac{N_W}{2}$) the angle $\theta(k)$ is evaluated as follows:

1. the 1.6s time-window $\mathbf{a}_W = [a(k - \frac{N_W}{2}), \dots, a(k + \frac{N_W}{2})]$ is filtered using the low-pass bidirectional filter-based technique and the vector angle $\theta_W = [\theta_W(1), \dots, \theta_W(N_W)]$ evaluated;
2. the central value $\theta_W(\frac{N_W}{2})$ is considered as $\theta(k)$ estimate.

These two steps are repeated by shifting, sample by sample, the 1.6s time-windows.

The method was evaluated on-line using Matlab R2011a 7.12.0. The time required for the execution of the described two-steps procedure is 2ms only. The kinematic and dynamic variables can be estimated with a delay of 0.8s since $\frac{N_W}{2}$ accelerometer future samples have to be taken into account. The technique provides results consistent with the ones presented in the previous Chapter.

3.3 Results

Test-retest reliability was good for the estimated parameters \tilde{D}_i and $\tilde{J}_i (i = 1, \dots, 3)$, with $ICC_{3,1}$ equal to 0.98, 0.99, 0.99 and 0.91, 0.89, 0.92, respectively. Subjects' characteristics (sex, age and BMI), the mean value (standard deviation) of subject-specific estimated anthropometric parameters and the De Leva's parameters [42] are reported in Table 3.1.

Table 3.1: Characteristics of participants, estimated and De Leva's inertial parameters. The three rows for each subject represent the i -th element ($i = 1, \dots, 3$) of the sensitivity vectors $\tilde{\mathbf{D}}$ and $\tilde{\mathbf{J}}$.

Subject	Sex	Age	BMI [kg/m ²]	$\tilde{\mathbf{D}}$	$\tilde{\mathbf{J}}$	$\tilde{\mathbf{D}}_{\text{DeLeva}}$	$\tilde{\mathbf{J}}_{\text{DeLeva}}$
				mean (std) [Kg m]	mean (std) [Kg m ²]	mean (std) [Kg m]	mean (std) [Kg m ²]
1	M	29	25.5	32.2 (0.6)	10.1 (0.8)	32.4	25.9
				30.8 (0.4)	10.2 (0.9)	16.1	13.9
				15.2 (0.2)	6.5 (0.8)	10.5	7.9
2	M	28	22.3	24.4 (0.5)	9.7 (0.5)	25.1	17.9
				22.9 (0.3)	10.9 (0.3)	12.3	10.2
				12.7 (0.3)	9.3 (0.6)	6.1	5.8
3	F	31	23.6	23.8 (0.8)	10.0 (0.8)	26.4	21.3
				20.8 (0.1)	8.7 (1.0)	13.0	11.1
				9.3 (0.4)	5.9 (1.1)	8.4	6.2

Mean description and prediction RMSEs are shown in Figure 3.3 for the rSTS trials. For each subject the mean prediction error is close to the mean description error: the difference ranges from 0.1N to 0.4N for the forces and from 0.1mm to 1.8mm for $\Delta\text{CoP}_{\mathbf{X}}$. De Leva's parameters provide prediction errors higher than those obtained with the estimated parameters. RMSEs of $\mathbf{F}_{\mathbf{Z}}$, $\mathbf{F}_{\mathbf{Z}}$ and $\Delta\text{CoP}_{\mathbf{X}}$, get worse in all cases. For the three subjects, the mean prediction error of $\Delta\text{CoP}_{\mathbf{X}}$ increases, using De Leva's parameters in place of those estimated, from

21.5mm to 57.9mm, from 17.8mm to 36.0mm, and from 24.0mm to 72.9mm, respectively.

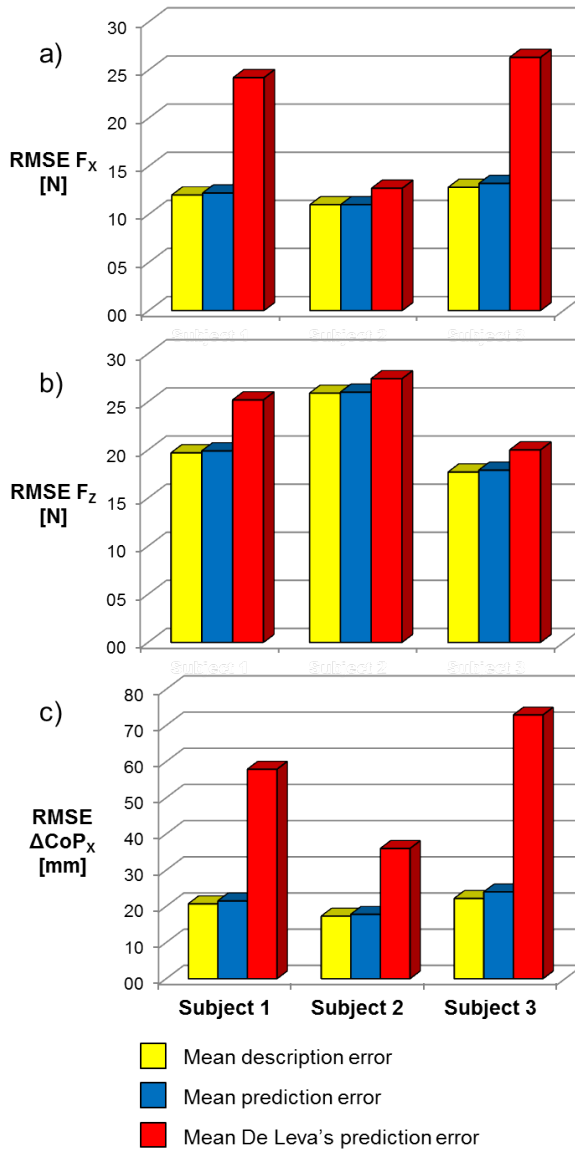


Figure 3.3: RMSEs of: a) F_x , b) F_z , c) ΔCoP_x , for rSTS trials

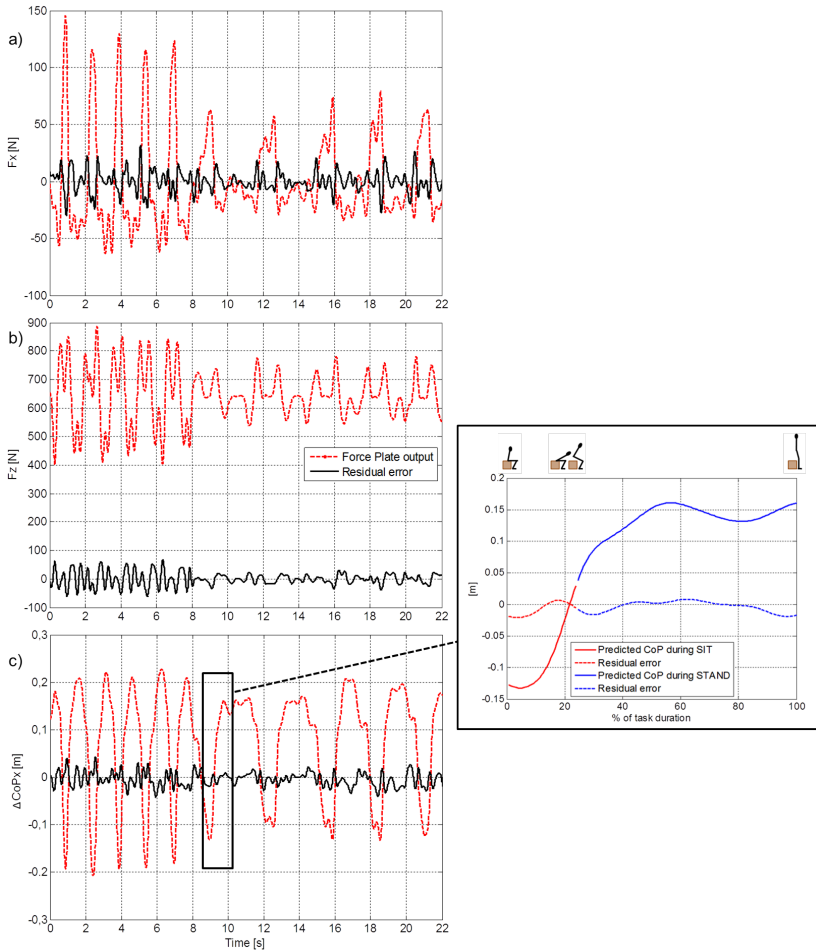


Figure 3.4: Pattern of: a) F_x , b) F_z , c) ΔCoP_x and residual errors during a rSTS trial (Subject 2)

By way of example, FP outputs and residuals between measured signals and signals predicted by SAAs are reported in Figure 3.4 for one rSTS trial of Subject 2. In the box, the CoP displacement and the residual error during a single translation from sitting to standing is shown related to the task duration. The mean prediction RMSE of ΔCoP_x , averaged on the three subjects, is about 21.1mm with mean

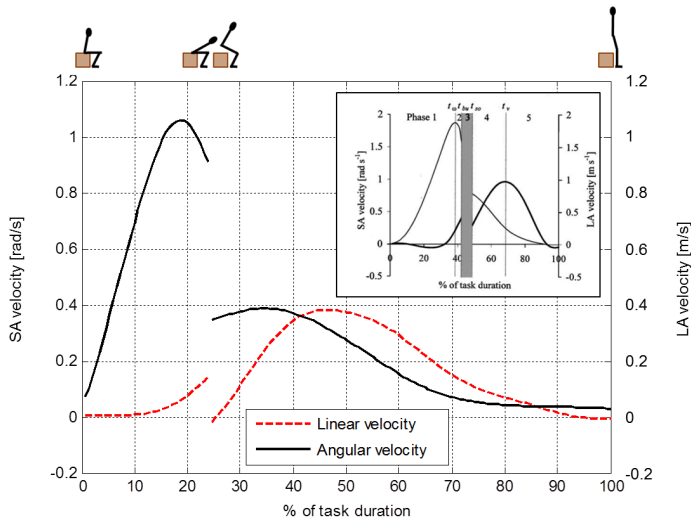


Figure 3.5: Linear and angular velocity of the rotation (SA) and linear (LA) actuator during a rSTS trial (Subject 2). Image in the box is from [151]

peak-to-peak range of 40cm. The percentage ratio between the mean RMSE and the range of the CoP displacement is about 5%.

In Figure 3.5 an example of the predicted ΔCoP_X , ΔCoM_X and ΔCoM_Z analysis during a rSTS trial is shown for Subject 2. This figure helps to identify the functional phases of the rSTS by monitoring the CoM position with respect to the CoP, in terms of linear and angular velocities. These variables were obtained by accelerometer-based prediction. The figure in the box is from Papa and Cappozzo [151].

RMSEs of \mathbf{T}_1 and $\mathbf{T}_{1,\text{DeLeva}}$ with respect to that obtained from FP output, averaged on the three subjects, are 10.3Nm and 17.0Nm, respectively. In Figure 3.6 the predicted NJMs are reported for Subject 2. In Figure 3.7 the ankle moment provided from FP outputs is shown at the top of the picture. The residual errors between: i) measured signal and signal predicted using the SAAs, and ii) measured signal and signal evaluated using the De Leva's parameters are shown at bottom of the picture.

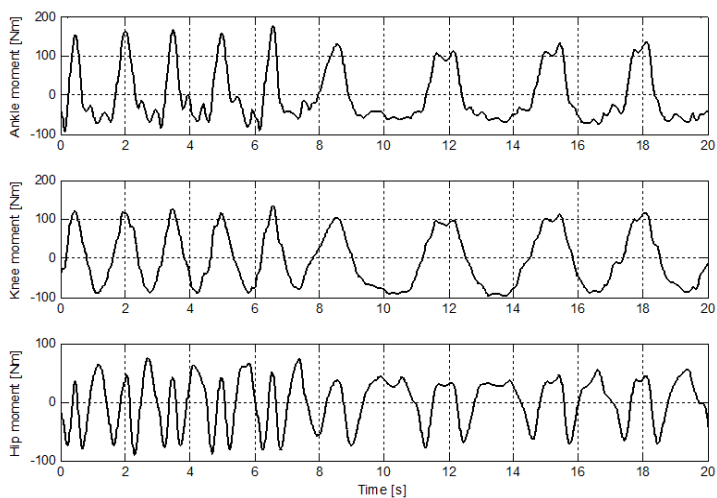


Figure 3.6: Patterns of ankle, knee and hip joint moments during a rSTS trial (Subject 2)

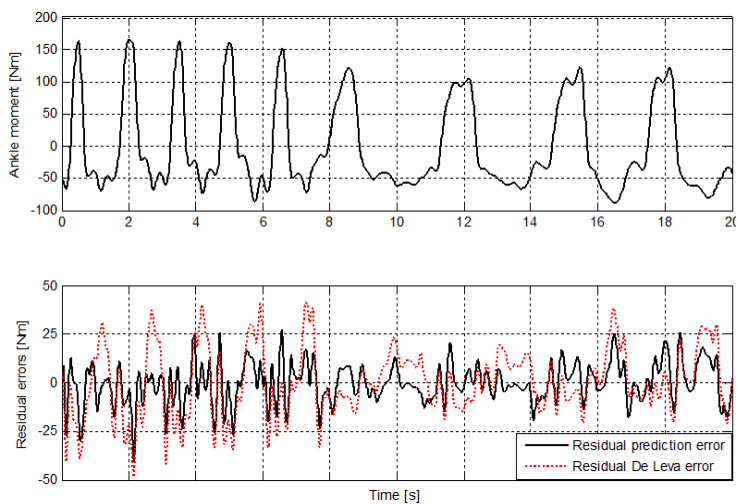


Figure 3.7: Patterns of ankle joint moment provided from FP and residual errors during a rSTS trial (Subject 2)

3.4 Discussion

This Chapter suggests a novel method aimed at estimating subject-specific anthropometric parameters using one SAA per segment and a FP, during a common functional motor task (rSTS) and taking advantage of a model-based approach. Several authors estimated these parameters in different ways, but no study, at our knowledge, evaluates the body-segment properties using inertial tracking technologies. FP and portable and cost-effective inertial sensors represent an easy and non-invasive alternative for anthropometric measurements, compared to previous invasive [27, 29, 43, 56, 174, 175, 196, 216] or expensive [28, 163] setups. The use of a traditional instrument for movement analysis, as the FP, is exclusively required for the subject-specific BSP estimation, after which only the SAA outputs and the estimated parameters allow the GRF, CoP, CoM and NJMs prediction during the rSTS functional test. During this exercise, the above mentioned kinetic variables are often used for balance monitoring [31, 148, 149], and to extract temporal and power-related features [51, 221].

The CoP, CoM and NJMs prediction by using only SAAs and the estimated parameters during sit-to-stand tasks could have several positive feedbacks from clinical applications. As explained in the Introduction of this Chapter, the rSTS exercise is a skill that helps to determine the functional level of a subject. The proposed method allows the kinematics and dynamics prediction by using a simple, accurate and portable setup. Since rSTS tasks is frequently used in clinical routine by taking advantages of quantitative and semi-quantitative techniques [89], the procedure presented in this thesis can speed up the experimental sessions, reducing the computational and the economic costs, especially when several subjects are involved.

The effectiveness of the suggested method was evaluated by comparing the predictive ability of the estimated parameters and those derived from the De Leva's tables [42]. As shown in Table 3.1, the mean values of $\tilde{\mathbf{D}}$ and $\tilde{\mathbf{J}}$ are significantly different from $\tilde{\mathbf{D}}_{DeLeva}$ and $\tilde{\mathbf{J}}_{DeLeva}$. These

differences can be related to the specific morphology of the subjects' segments, not taken into account by the De Leva's parameters, which depend only on mass and height of the subjects. The good reliability of each estimate ($ICC_{3,1}$ always higher than 0.89) and the negligible difference between the mean description and prediction errors for the dynamic variables of the three subjects (see Figure 3.3) suggest that a single rSTS trial is enough to estimate the subject-specific anthropometric parameters. The model-based approach and the integration of FP and SAAs data allow "one-shot" regression estimation. As computational cost is concerned, previously published studies [163, 194], combining model-based and experimental approaches, showed higher complexity and computational requirements.

One of the main aims of the presented study was to predict the GRF, the displacement of the CoP and CoM in the AP direction, and the NJMs at the ankle, the knee and the hip, using only the SAAs and the estimated parameters during the rSTS functional test.

As shown in Figures 3.3 and 3.7, mean prediction RMSEs, averaged on the three subjects, are about 12N, 21N, 21.10mm and 10.3Nm for \mathbf{F}_X , \mathbf{F}_Z , $\Delta\mathbf{CoP}_X$ and \mathbf{T}_1 , with mean peak-to-peak ranges of 203N, 520N, 0.401m and 228.8Nm, respectively. These values are lower than those obtained with the De Leva's parameters, which are about 21N, 24N, 55.60mm and 17.0Nm for \mathbf{F}_X , \mathbf{F}_Z , $\Delta\mathbf{CoP}_X$ and \mathbf{T}_1 . These considerations confirm that the presented experimental protocol provides the best anthropometric parameter estimates.

By comparing $\Delta\mathbf{CoP}_X$ prediction errors with those presented in a previous study [28], the results are very encouraging. Chen *et al.* [28] obtained a mean CoP error (standard deviation) of 9.40(2.95)mm for arm-swing squatting, lower than the proposed prediction method in rSTS (about 21.10mm), the CoP range should be taken into account with relation to the performed task. During squatting, the CoP displacement is confined to few centimeters, whereas during rSTS movement the $\Delta\mathbf{CoP}_X$ range is about 40cm. Therefore, the percentage ratio between $\Delta\mathbf{CoP}_X$ error and its range obtained from our study is

about 5%, significantly lower than that reported in [6], which is around 32%. Moreover, Chen *et al.* [28] assumed 3D geometric shapes for the body segments instead of a rigorous biomechanical model. Despite of these encouraging results, one limitation of the presented study is the 2D model-based approach, which neglects the ML movement during the performed trials.

Since sit-to-stand task requires coordination, balance, adequate mobility and strength, several authors investigated the change of posture and balance control [62, 148, 149] and of muscle strength and intermuscular coordination across the joint [23, 51, 119, 204] during the CoM forward and backward displacement from sitting to standing and back to sitting, using SP systems and FPs. The traditional movement analysis systems, usually considered as a goal standard for the kinematics and dynamics evaluation, show several drawbacks, as lack in portability and usability, costs, and high computing demanding for real-time applications. These drawbacks could be overcome by using inertial sensors. In this study the quasi-real-time CoP and CoM prediction is accomplished by using only SAAs and a set of subject-specific anthropometric parameters. As shown in Figure 3.5, the dynamics accelerometer-based prediction provides results consistent with the relevant study of Papa and Cappozzo [151], related to the TIP model applied to rSTS movements. Linear and angular velocity of LA and SA were evaluated by using only CoP and CoM positions, predicted through SAAs, the inputs of the minimum measured-input model, in place of FP and seat uni-axial load-cell data as suggested by [151]. Therefore, applications of the balance control techniques during rSTS tasks could take advantage of accelerometry, in terms of portability, availability of the setup in either clinical/laboratory settings or free-living environments, both for off-line and real-time monitoring. These benefits are not task-related, since the subject-specific anthropometric parameters, estimated in a single rSTS trial, can be well-applied to different motor tasks sharing the same biomechanical model.

In summary, this Chapter provides a subject-specific evaluation tool

for estimating inertial parameters through a simple motor task (rSTS), involving only few SAAs and a FP. After this preliminary estimation, the quasi-real-time prediction of GRF, CoP, CoM and NJMs at the ankle, knee and hip during rSTS, postural sway, squatting, etc., could be performed by the use of accelerometry only, which compares favorably to commercial SP movement analysis systems in terms of cost, size, weight, convenience, and portability. As a result, data collection is no longer confined to a laboratory environment. One limitation of the study is the 2D model-based approach, which neglects the ML movement during the performed trials. Future developments of the presented work will address the extension of the dynamic analysis to a 3D biomechanical model and the prediction of kinematic and kinetic variables in different motor tasks, extending the model to any number of degrees of freedom.

Chapter 4

Kinematic strategies and dynamics evaluation during the *voluntary* *Postural Sway* functional tests

In the previous Chapters, novel methods were proposed for estimating the kinematics and the dynamics of a multi-link model by using a body sensor network during different dynamic motor tasks. The same methods are applied in this Chapter for the kinematic and dynamic description of the voluntary Postural Sway (PS) functional test. One of the main aim of this Chapter is to evaluate the kinematic strategies performed during a self-imposed perturbed stance, applying the quantitative assessment tool of body sway angles presented in Chapter 2. A body-sensor network, consisting on one single-axis accelerometer (SAA) per segment was used and three different biomechanical mod-

els (from 1- to 3-link) were analyzed in order to describe as well as possible the sway movement. In addition, the anterior/posterior component of the ground reaction force (Fx), and the Centers of Pressure (CoP) and of Mass (CoM) displacements were predicted in this Chapter for the voluntary PS analysis. The prediction technique is based on the use of the SAAs located on the subject and the set of subject-specific body-segment parameters provided by the estimation method presented in Chapter 3. In order to support the usability of SAA for angular kinematics estimation in PS functional tests, results were compared with those previously provided using different and more expensive measurement systems in other published studies. Estimated Fx and CoP, related to the different models and calculated through De Leva's anthropometric parameters [42] scaled on the models order, were compared to the Force Plate (FP) outputs, in terms of Root Mean Square Errors (RMSEs). RMSEs of Fx decrease from 7.3N (1-link) to 4.6N (2-link) and to 3.3N (3-link), and RMSEs of CoP decrease from 27.7mm (1-link) to 11.1mm (2-link) and to 6.6mm (3-link). In addition, the simultaneous existence of an in-phase and an anti-phase behaviors between trunk and leg segments is demonstrated, confirming the unsuitability of the inverted pendulum model to describe PS movements. In order to validate the Fx, CoP and CoM prediction method based on the preliminary body-segment parameters estimation, predicted dynamic variables and those obtained using anthropometric parameters derived from De Leva's tables were compared to the FP outputs, in terms of RMSEs. RMSEs increase, using De Leva's parameters in place of those estimated, from 3.1N to 3.3N (Fx), and from 5.5mm to 6.6mm (CoP). Although at the present moment only GRF, CoP and CoM are predicted using the previously estimated parameters, the positive results suggest that also body kinematic strategies evaluation can take advantages by the use of the subject-specific inertial properties [63, 64].

4.1 Introduction

Bipedal stance is an important prerequisite for human functional movement [158]. The ease with which we maintain our vertical posture is surprisingly considered the open-loop-controlled musculo-skeletal system, unstable under the effect of the gravity [139]. The principal objective of the balance control system is to keep the vertical projection of the body's Center of Mass (CoM) within the area of the base of support [207]. To accomplish this in a biomechanical perspective, models related to ankle stiffness [206, 208] and reactive muscle strategies [138, 139] predict that adjustments in the location of the underfoot Center of Pressure (CoP) are used to guide the trajectory of the CoM towards an equilibrium position. For this reason, during upright stance the body is never perfectly still. An irregular and low amplitude motion, termed Postural Sway (PS), is ever-present and produces a constant flow of information across the sensory systems that are used to maintain postural stability [131, 162]. The disruption of one of these information might lead to change the postural strategies [101] and the responses to different mechanical perturbations [98], due to the failure of the nervous system which does not induce adequate compensatory movements. Analytic methods have been used to quantify the temporal structures of PS [34, 164] as indicators of the individual's performance. In this perspective, the trajectories of the body CoP and CoM are commonly investigated in studies on human posture and balance control [84, 88, 160, 205]. The analyses have revealed that the CoP fluctuations are a blend of deterministic and stochastic dynamics, depending, in part, upon what types of sensory information are available [165].

Several authors investigated human balance control in unperturbed stance considering one-segment inverted pendulum model [91, 113, 114, 139, 155, 206, 208]. In these studies, the human body is represented as rigid segment, the ankle torque acts as the single control input of the link and other joints do not contribute to both postural sway and postural control. However, it has recently become clear that for main-

taining stability the required local stiffness at the ankle joint is much lower than the destabilizing effect of the gravity when a multi-segmental model is assumed [171]. Multi-segmental biomechanical models were introduced for the evaluation of postural responses following platform or visual perturbations, considering the contribution of hip and knee [3, 13, 14, 143] to balance control. Only recently, studies on unperturbed stance bring into focus the importance of rotations at joints other than the ankle that contribute to the minimization of the body CoM movement [1, 5, 36, 66, 87].

The relative balance improvement or deterioration of a subject can be of interest in several case of the clinical setting: neurodegenerative disorder that leads to a progressive decline in motor function (e.g. Parkinson disease [122, 150], diabetic neuropathies [189], cerebellar diseases [49]), risk of falls evaluation that might cause bone fractures [73, 121, 177, 220], sport medicine pathologies [169], rehabilitation programs for the postural training on ankle, knee and hip joint after a traumatic event [83], gerontology studies for the aging and balance relationship [103, 120, 154, 211]. In these studies, the evaluation of the PS temporal structures provides a window into the functional organization of the postural control system [165], and may be used in order to find objective indicators of subject's balance performance [150].

Different balance tests may include evaluation of: i) spontaneous sway in standard condition or following proprioception, vestibular or visual perturbations, and ii) induced sway due to external or self-imposed threats to stability. Voluntary PS movements represent a simple approach to examining deficits in postural control that may contribute to the evaluation of risk of fall in elderly and pathological subjects. In a recent study [188], three categories of voluntary PS tasks, including maximum voluntary leans held statically, continuous steady-state voluntary sway, and rapidly initiated voluntary sway movement, were analyzed in order to differentiate and identify the fall-history status of older adults.

Actually, traditional clinical balance tests are dependent on subjec-

tive scores (e.g. the *Romberg Test* [96], the *Berg Balance Scale* [140], the *Balance Evaluation System Test* [85]), and traditional FP-based [157, 184] or active balance system-based [187] methods, focused on CoP displacement and neglected the biomechanics of the single body segments [188]. Recently, kinematic and dynamic measures have been evaluated for a comprehensive analysis of balance control during PS trials [5, 36, 158], considering the contribution of a several number of joint to postural control. In Pinter *et al.* [158], the authors used a stereo-photogrammetric system and an FP, analyzing the variance of the joint angles in order to verify that the variance of the knee and hip joint angles did not differ from the variance found in the ankle angle during an unperturbed stance. Aramaki *et al.* [5] found the angular displacement at the hip to be significantly greater than the angular displacement at the ankle and further found that angular acceleration of the ankle was compensated by oppositely directed acceleration of the hip joint. The authors used three CDD (charge coupled device) laser-displacement sensors to measure the angular motion of the shank, the thigh and the trunk body-segment, and a FP to measure the CoP excursion, restricting movements at knee and head-neck-trunk with stiff wooden splints. More recently, Creath *et al.* [36] found a simultaneous coexistence of an in-phase and anti-phase patterns between lower and upper body angles. Spectral analysis tasks showed that the body behaves like a multi-link pendulum with two coexisting modes, depending on motion frequency. Experiments were carried out on quiet stance motor tasks, restricting visual information performing an eye-closed condition and using a variable pitch platform and potentiometers located on the subjects.

Complicating factors in comparing published researches concerns the nature of the postural control mechanism in the variety of the experimental conditions and the several technologies used for the test instrumentations, different in terms of economical and computational costs, portability and usability. Their use in clinical practice has been partly limited by the cost and the need of qualified personnel. For these

reasons, wearable inertial technologies increasingly investigated for human movement analysis. Few authors, [94, 136, 137], have used accelerometers to study balance while standing quietly. Kamen *et al.* [94] used two uni-axial accelerometers taped to the back (at S2 level) and forehead of the subject and measured in the anterior–posterior direction. They calculate root mean square and frequency spectrum of the gathered signals as performance parameters. Unfortunately this sensor configuration is affected by the acceleration of gravity, a function of the angle of the accelerometer with respect to the vertical. Moe-Nilssen, in [136] and [137], used a tri-axial accelerometer placed at the small of the back. The average tilt of the sensor is used to subtract the static gravity error and then the data are transformed to a horizontal–vertical orthogonal coordinate system by a trigonometric algorithm. Root mean square is used on the data from each of the three axes as a performance parameter. This system has demonstrated test-retest reliability [137]. Mayagoitia *et al.* [127] distinguished between different standing conditions comparing tri-axial accelerometer and FP measurements. In Chiari *et al.* [30], high correlations were found between the CoP displacement and trunk acceleration in an audio-biofeedback application for balance improvement.

All these methods still lack a rigorous biomechanical analysis. In addition, even if these studies focused on the comprehensive analysis of kinematic and dynamic data, they neglected the CoM evaluation. While the current state of the art offers several alternatives for CoP and Ground Reaction Force (GRF) measures by means of a FP, the whole body CoM location is not directly observed and it should be estimated, considering an adequate biomechanical model of the body. FP-based methods estimate CoM location from CoP by using either an “anthropometric filter” [25] or by double-integration of the horizontal GRF [176, 217]. Since FPs, generally used in a movement analysis laboratory, are typically embedded in the ground, they do not represent a flexible and portable solution for measuring body sway and postural stabilization in different environments.

To the best of our knowledge, there are no published methods based on inertial measurements that provide a comprehensive analysis for kinematics and dynamics evaluation of PS, all-considering the sway angles, the GRF, the CoP and the CoM estimates as indicators of subject's balance performance.

Aims of this Chapter are:

- to evaluate kinematic strategies performed during a self-imposed perturbed stance, applying the iterative technique presented in Chapter 2 for the sway angles estimation and using a body sensor network, consisting of one single-axis accelerometer (SAA) per segment;
- to predict GRF, CoP and CoM during voluntary PS trials, using only the SAAs and a set of subject-specific anthropometric parameters (these parameters are provided by the estimation method presented in Chapter 3, which is based on a SAAs per segment data and a FP measure during a sit-to-stand exercise).

In order to support the usability of SAA for angular kinematics estimation in PS functional tests, the obtained results are compared with those provided by previous researches, which used different and more expensive measurement systems. GRF and CoP are estimated for different biomechanical models in order to define the postural strategies adopted by the subjects, using the anthropometric parameters provided by De Leva's tables [42], consistently scaled on the models order. Finally, in order to validate the GRF, CoP and CoM prediction method, the predicted variables are compared to those measured by the FP and those obtained using anthropometric parameters derived from De Leva's tables [42].

4.2 Methods and Materials

4.2.1 Experimental Set-Up

Three young healthy subjects - two males, Body Mass Index (BMI) = $[25.5, 22.3]kg/m^2$; one female, BMI = $23.6kg/m^2$ - with no previous orthopedic ailment, participated in this study after giving their informed consent. The subjects, standing on a FP (Bertec 4060-08) with the feet supposed rigidly connected to the ground, were asked to perform five trials of self-imposed PS around their ankle joint, with their arms folded, keeping their movement in the anterior/posterior (AP) direction and using as much as possible a pure ankle strategy. In order to obtain a broad frequency spectrum, each oscillatory trial was performed at the subjects' maximum speed in the first part (about 1Hz) and at the subjects' self-selected speed in the second part (about 0.5Hz). Three SAA (Analog Device, ADXL 103) were placed at measured heights h_1, h_2, h_3 , with respect to the ankle, knee, and hip joint, respectively. Each of the three sensors was mounted directly on the skin, in a central position on the lateral side of the thigh and the shank, and on the posterior side of the Head-Arms-Trunk (HAT), in order to minimize skin artefact effects and model errors. In order to measure the sensor position, $h_i (i = 1, \dots, 3)$, and the segment length, $l_i (i = 1, \dots, 3)$, anatomical landmarks of body-segments (lateral malleolus, lateral epicondyle and L5 vertebra) were identified by palpation. FP and accelerometer signals were acquired at a 100Hz sampling rate and low-pass filtered (2nd order zero-phase Butterworth filter) at a cut-off frequency of 3Hz.

4.2.2 Kinematic Strategies Evaluation

According to the analysis of the N -link biomechanical model, presented in the previous Chapter (see Section 3.2.2) and in order to evaluate the strategies performed during the oscillations, three biomechanical models in the sagittal plane, consisting in 1- 2- and 3-link, were analyzed (Figure 4.1).

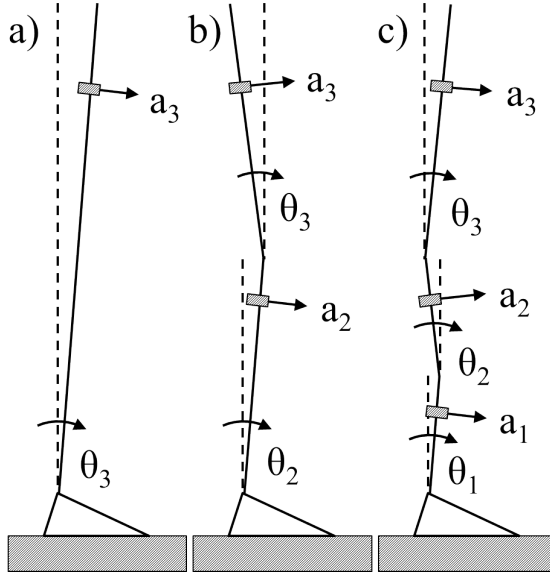


Figure 4.1: Tested models: a) inverted pendulum, b) 2-link model, c) 3-link model

The tested models are listed below:

- *Inverted pendulum model* ($N = 1$): the only accelerometric signal used for the inverted pendulum approximation is the output of the accelerometer \mathbf{a}_3 , mounted on the posterior side of the HAT at a measured height from the ankle joint. Consequently, the angular sway of the inverted pendulum corresponds to θ_3 ;
- *Two-link model* ($N = 2$): the accelerometric signals used are the outputs of the accelerometers \mathbf{a}_2 , mounted on the lateral side of the thigh, and \mathbf{a}_3 ; their positions are assumed at measured heights from the ankle joint and from the hip joint;
- *Three-link model* ($N = 3$): the accelerometric signals used are the outputs of the accelerometers \mathbf{a}_1 , mounted on the lateral side of the shank, \mathbf{a}_2 and \mathbf{a}_3 ; their positions are assumed at measured heights from the ankle, the knee and the hip joint, respectively.

The dynamic equilibrium equations of an N -link model and the relationships between kinematic and kinetic variables, as defined in Equation (3.1), were evaluated for each tested biomechanical model. The AP component of the GRF, F_X , and the moment component about the medium/lateral (ML) axis, M_Y , were expressed as follows:

$$\begin{aligned} F_X(k) &= \tilde{\mathbf{D}}_{DeLeva}^T \ddot{\mathbf{S}}_\theta(k) \\ M_Y(k) &= \tilde{\mathbf{D}}_{DeLeva}^T [g\mathbf{S}_\theta(k) - l_0\ddot{\mathbf{S}}_\theta(k) - \mathbf{A}_{IS}(k)] - \tilde{\mathbf{J}}_{DeLeva}^T \ddot{\theta}(k) \\ k &= 1, \dots, n \end{aligned} \quad (4.1)$$

where $\ddot{\theta}(k)$, $\mathbf{S}_\theta(k)$, $\ddot{\mathbf{S}}_\theta(k)$, $\mathbf{A}_{IS}(k)$, $\tilde{\mathbf{D}}_{DeLeva}$, $\tilde{\mathbf{J}}_{DeLeva}$ are $[N \times 1]$ -column vectors and n is the number of samples. As regards the vectors' element definitions, we refer to Equation (3.1). The vertical force is not reported for the PS functional test since the CoM vertical acceleration is negligible and \mathbf{F}_Z is approximately Mg .

The vector $\boldsymbol{\theta}_i = [\theta_i(1) \dots \theta_i(n)]$ represents the i -th angular deviation from the vertical line, $\dot{\boldsymbol{\theta}}_i$ the i -th angular velocity vector, and $\ddot{\boldsymbol{\theta}}_i$ the i -th angular acceleration vector. The two sensitivity vectors $\tilde{\mathbf{D}}_{DeLeva}$ and $\tilde{\mathbf{J}}_{DeLeva}$ are defined as linear combinations of the anthropometric parameters, as segment length, l_i , mass, m_i , distance of CoM from distal joint axis, d_i , and moment of inertia, J_i . In this part of this Chapter, these parameters are obtained from the De Leva's anthropometric tables [42], scaled on the subjects' mass and height and calculated for an inverted pendulum model, a 2- and a 3-link biomechanical models.

The i -th SAA output vector, $\mathbf{a}_i = [a_i(1) \dots a_i(n)]$, along the sensitive axis directed normally to the segment and oriented anteriorly, can be expressed as the sum of an inertial and a gravitational term plus two contributions, related to the horizontal and vertical accelerations at the lower joint, \mathbf{a}_i^x and \mathbf{a}_i^y , due to the underlying chain kinematics (see Chapter 2):

$$\begin{aligned} a_i(k) &= h_i \ddot{\theta}_i(k) - g \sin \theta_i(k) + a_i^x(k) \cos \theta_i(k) - a_i^y(k) \sin \theta_i(k) \\ k &= 1, \dots, n \\ i &= 1, \dots, N \end{aligned} \quad (4.2)$$

According to the iterative technique presented in Chapter 2, the i -th sway angle of the three models, θ_i , can be evaluated from the accelerometer outputs, using a low-pass bi-directional filter with cut-off frequencies depending on sensor positions. After computing θ_i and its first numerical derivative $\dot{\theta}_i$, its second derivative, $\ddot{\theta}_i$, can be computed by Equation (4.2). Therefore, the dynamic equilibrium equations can be expressed as linear combinations of the i -th angular position, θ_i , the i -th angular velocity, $\dot{\theta}_i$, and the i -th SAA output, \mathbf{a}_i , through the $2N$ De Leva's anthropometric parameters, $\tilde{\mathbf{D}}_{DeLeva}$ and $\tilde{\mathbf{J}}_{DeLeva}$. The dynamic variables in Equation (4.1) can be estimated using the SAA outputs only and the anthropometric parameters.

The effectiveness of the estimation method was evaluated for each subject in terms of Root Mean Square Error (RMSE) between the measured and the estimated FP outputs, \mathbf{F}_X and $\Delta\mathbf{CoP}_X = \frac{\Delta\mathbf{M}_Y + m_0g\delta}{Mg} - CoP_X^0$, where m_0 is the estimated feet mass, δ is the AP location of the feet CoM with respect to the malleolus (see Figure 3.1), $\Delta\mathbf{M}_Y = \mathbf{M}_Y - M_Y^0$, and $CoP_X^0 = \frac{M_Y^0}{F_Z^0} = m_0g\delta$ is the CoP value at the equilibrium position. For an effective description of the kinematic strategies adopted by the subjects during the self-imposed oscillations, RMSEs were calculated for the three biomechanical models.

4.2.3 Dynamics Prediction

In the second part of this Chapter, the predictive ability of the 3-link model presented in Chapter 3 is tested on each subject during the oscillatory trials. The subject-specific body-segment parameters, $\tilde{\mathbf{D}}$ and $\tilde{\mathbf{J}}$, estimated in the previous Chapter, were used to predict \mathbf{F}_X , and the displacement of the CoP and CoM in the AP direction, $\Delta\mathbf{CoP}_X$, $\Delta\mathbf{CoM}_X$, using the three SAAs only and a top-down approach, as

follows:

$$\begin{aligned}
F_X(k) &= \tilde{\mathbf{D}}^T \ddot{\mathbf{S}}_\theta(k) \\
\Delta CoP_X(k) &= \frac{\Delta M_Y(k) + m_0 g \delta}{Mg} - CoP_X^0 \\
\Delta CoM_X(k) &= \frac{1}{M} [\tilde{\mathbf{D}}^T \mathbf{S}_\theta(k)] \\
k &= 1, \dots, n
\end{aligned} \tag{4.3}$$

The effectiveness of the method was evaluated for each subject in terms of RMSE between the measured and estimated FP outputs, as follows:

- the mean prediction error was computed by averaging the RMSEs obtained by using the estimated parameters of the p -th rSTS trial ($p = 1, \dots, 5$) for the evaluation of the dynamic variables of the q -th oscillatory trial ($q = 1, \dots, 5$);
- the mean De Leva's prediction error was evaluated considering the De Leva's parameters [42] in place of the estimated parameters $\tilde{\mathbf{D}}$ and $\tilde{\mathbf{J}}$;

4.3 Results

4.3.1 Kinematic Strategies Evaluation

In order to identify the kinematic strategies performed by the subjects during a voluntary PS exercise, Figure 4.2 shows the RMSEs on estimated \mathbf{F}_X and $\Delta \mathbf{CoP}_X$: the three markers are representative of the RMSE obtained by the 1-, 2- and 3-link biomechanical models for each subject. As it can be seen, both RMSEs and their between-subjects variability are decreasing functions of the model order.

In the 2- and 3-link models the errors and the variability are significantly reduced: mean RMSE of \mathbf{F}_X decreases from 7.3N in the inverted pendulum model to 4.6N in the 2-link model and to 3.3N in the 3-link model, while mean RMSE of $\Delta \mathbf{CoP}_X$ decrease from 27.7mm in the

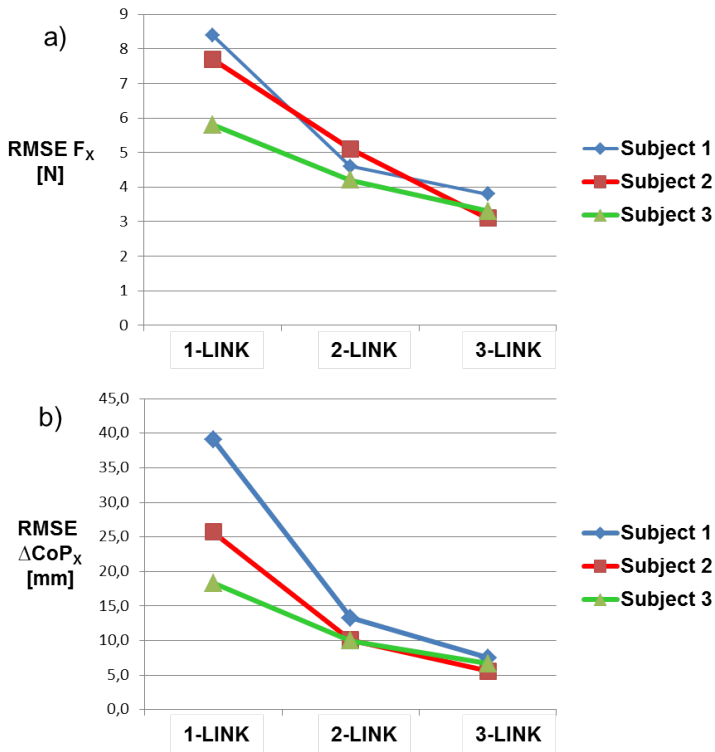


Figure 4.2: RMSEs of: a) F_x , b) ΔCoP_x , for oscillatory trials related to 1-, 2- and 3-link biomechanical models

inverted pendulum model to 11.1mm in the 2-link model and to 6.6mm in the 3-link model. The mean peak-to-peak range, averaged across all trials and all subjects, is $84.2 \pm 12.7N$ for F_x and $0.17 \pm 0.02m$ for ΔCoP_x .

The relationship between the trunk and leg segment angles during quiet stance is shown in the representative plots of ankle-hip angular displacements in Figure 4.3 for low- and high-frequency oscillations. In Figure 4.3a for low sway frequency, the trunk and leg trajectories are primarily moving in unison with large excursion of the trunk, mirrored by those of the legs. In Figure 4.3b a shift from in-phase to anti-phase behavior due to the high frequency is shown.

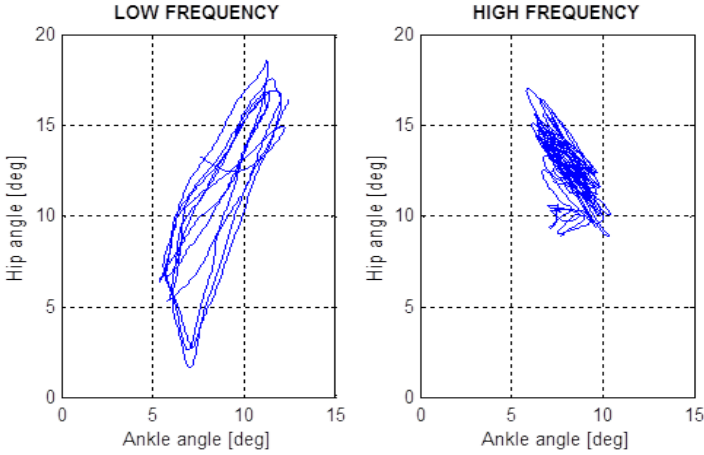


Figure 4.3: Ankle-Hip angular displacements for: a) low-, b) high-frequency oscillations during a PS trial (Subject 2)

4.3.2 Dynamics Prediction

The 3-link biomechanical model defined in the Chapter 3 by the estimation of a set of subject-specific body-segment parameters was used to predict dynamic variable during the voluntary PS functional test. Mean prediction RMSEs are shown in Figure 4.4. For each subject, the mean prediction error of dynamic variables obtained using the rSTS estimated parameters is lower than the one obtained by using De Leva's parameters. For the three subjects, the mean prediction error of ΔCoP_X increases, using De Leva's parameters in place of those estimated, from 6.2mm to 7.5mm, from 4.4mm to 5.6mm, and from 5.9mm to 6.7mm, respectively. By way of example, FP outputs and residuals between measured signals and signals predicted by SAAs are reported in Figure 4.5 for one self-imposed oscillatory trial of Subject 2.

In Figure 4.6 an example of the predicted ΔCoP_X and ΔCoM_X during an oscillatory trial is shown for Subject 2: the predicted ΔCoP_X and the predicted difference $\Delta\text{CoM}_X - \Delta\text{CoP}_X$ are in counter-phase as one would expect in an optimal balance control strategy.

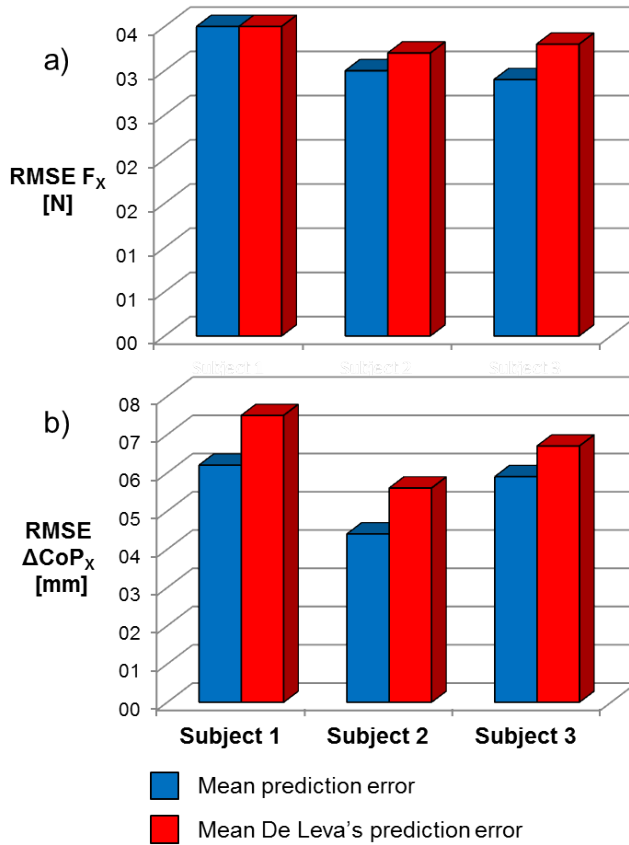


Figure 4.4: RMSEs of: a) F_x , b) ΔCoP_x , for oscillatory trials

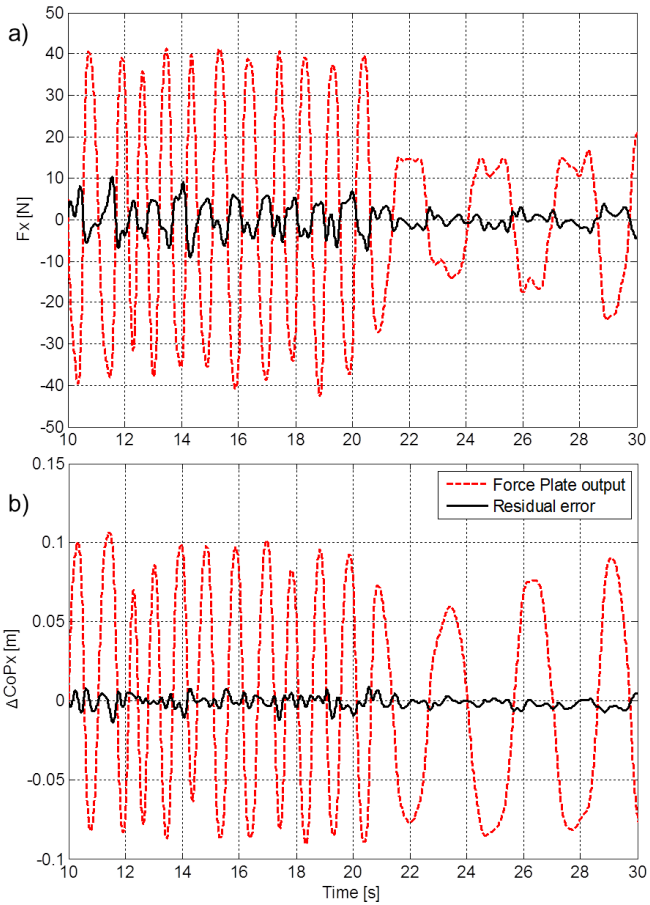


Figure 4.5: Pattern of: a) F_X , b) ΔCoP_X and residual prediction errors during an oscillatory trial (Subject 2)

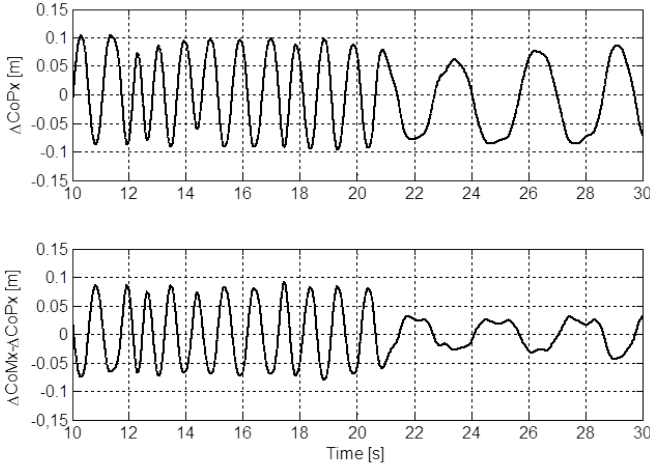


Figure 4.6: Pattern of: a) ΔCoP_X and b) $\Delta\text{CoM}_X - \Delta\text{CoP}_X$ during an oscillatory trial (Subject 2)

4.4 Discussion

This Chapter suggests a novel method aimed at evaluating kinematic strategies performed by a subject during a simple functional motor task (voluntary PS), using one SAA per segment and taking advantage of a model-based approach. Several authors provided significant results in term of quiet and perturbed stance characterization, but no study, at our knowledge, evaluates the kinematic strategies during the sway using inertial tracking technologies. The procedure presented in this Chapter speeds up the experimental sessions, reducing the computational and economic costs, especially when several subjects are involved. Moreover, an innovative method for the voluntary PS dynamics analysis is introduced in the second part of this Chapter. The use of a traditional instrument for movement analysis, as the FP, is exclusively required for a preliminary subject-specific anthropometric parameters estimation during a repeated Sit-to-Stand (rSTS) exercise, after which only the SAA outputs and the estimated parameters allow

the GRF, CoP and CoM prediction during the voluntary PS functional test. These kinetic variables are often used for balance monitoring [84, 88, 160, 205], and to extract temporal and power-related features [150].

Multisegmental posturography [1, 153] allows direct investigation of the kinematics of the segmental movements controlling stance. The first results of this study indicate that, although CoM displacement can accurately be described by ankle angular displacement, a one-segment inverted pendulum model cannot give a comprehensive description of PS data. The knee and the hip joint rotations can be decomposed into both an amplifying and reducing pattern with regard to the position of the body CoM.

As shown in Figure 4.2 during voluntary PS, the postural movement is never characterized by a pure ankle strategy, particularly at high frequencies, but rather by a combined ankle-hip strategy, consistent with the results obtained by Creath *et al.* [36] through a variable pitch platform and a set of potentiometers located on the subject. Mean RMSEs of \mathbf{F}_Z and $\Delta\mathbf{CoP}_X$, averaged on the five trials, show that estimated outputs are highly dependent on the model order: the inverted pendulum model, that should be the most suitable for describing PS, provides the largest errors and between-subjects variability. The improvement taken switching from the inverted pendulum to the 2-link is significant in terms of kinematic strategies descriptive ability.

A concise picture of the coordinative relationship between trunk and leg segments was assessed by analyzing the phase angle between the two links, as shown in Figure 4.3. The in-phase and anti-phase relationship between ankle and hip angular displacements, at low- and high-frequency oscillation respectively, are indicative of the trunk and leg synergies, demonstrating the simultaneous existence of these patterns during voluntary PS, as well Creath *et al.* [36] demonstrated for quiet stance motor tasks. In order to describe the body-kinematics during the movement, both pattern in Figure 4.3 suggest the use of a 2-link biomechanical model. The in-phase behavior during the low-

frequency oscillation suggest that the trunk and leg trajectories are mirrored, with a small excursion of the leg and a large excursion of the trunk. Although the excursion of the two links are similar during the high-frequency oscillation, the anti-phase behavior of ankle and hip angles suggests that trunk and leg move in opposite directions in order to maintain a good margin of stability.

Based on these considerations, the inverted pendulum model is indeed an oversimplification of reality during a PS functional test. A multi-link pendulum, consisting at least of two links, is required for the correct description of the body movement during the posture adjustments used to maintain the CoP and CoM locations in balance positions. In a multi-segmental posturography study, *Acconero et al.* [1] demonstrated that the 2-link biomechanical model represents an economic way to maintain the upright posture. The inverted pendulum, in their study, was used to describe sway only in elderly people, in which the increased postural rigidity is justified by an age-related increase in joint stiffness and a more rigid motor strategy per se.

One of the main aims of the presented study was to predict the GRF, and the displacement of the CoP and CoM in the AP direction, using only the SAAs and the previously estimated parameters (see Chapter 3) during postural oscillation motor tasks.

As show in Figure 4.4, mean prediction RMSEs, averaged on the three subjects, are about 3.1N and 5.5mm for \mathbf{F}_Z and $\Delta\mathbf{CoP}_X$, with mean peak-to-peak ranges of 84.2N and 0.17m, respectively. These values are lower than those obtained with the De Leva's parameters, which are about 3.3N and 6.6mm for \mathbf{F}_Z and $\Delta\mathbf{CoP}_X$. These considerations are confirmed by the results obtained in the previous Chapter, related to the rSTS (see Figure 3.3). Since the differences between mean prediction errors and mean De Leva's prediction errors are less significant than in the rSTS trials, the experimental protocol presented in Chapter 3 provides the best anthropometric parameter estimates.

By comparing $\Delta\mathbf{CoP}_X$ prediction errors with those presented in a previous study [28], the results are very encouraging. *Chen et al.* [28]

obtained mean errors (standard deviations) of about 2.72(1.23)mm, 4.68(1.52)mm and 3.30(1.44)mm during static postures with 30° trunk flexion, 45° hip flexion and 90° shoulder abduction, respectively. As shown in [160], during quiet standing, the range of the CoP displacement is around 14.30mm, as confirmed by experimental evidences. The percentage ratio between the mean CoP error provided by [28] and the CoP range is around 25%. In the oscillatory trials presented in this study, subjects performed voluntary oscillations, with a mean CoP range, averaged on the three subjects, of 170mm in the AP direction and with a mean error of about 5.50mm. The related percentage ratio between $\Delta\text{CoP}_{\mathbf{x}}$ error and the range is hence about 3%, significantly lower than that obtained by [28]. Similar results are obtained from the dynamic trials evaluation, discussed in the previous Chapter. Moreover, Chen *et al.* [28] assumed 3D geometric shapes for the body segments instead of a rigorous biomechanical model. Despite of these encouraging results, one limitation of the presented study is the 2D model-based approach, which neglects the ML movement during the performed trials.

Applications of the balance control techniques during voluntary PS tasks could take advantage of accelerometry, in terms of portability, availability of the setup in either clinical/laboratory settings or free-living environments, both for off-line and real-time monitoring. These benefits are not task-related, since the subject-specific anthropometric parameters, estimated in a single rSTS trial, can be well-applied to different motor tasks sharing the same biomechanical model, which is composed by a 3-link kinematic chain in this and in the previous Chapters. As shown in Figure 4.6, the accelerometry-based predicted CoP and CoM in the AP direction are suitable to quantifying standing balance during postural oscillations. For the sake of simplicity, considering a simple inverted pendulum in place of the correct biomechanical model, the difference $\Delta\text{CoM}_{\mathbf{x}} - \Delta\text{CoP}_{\mathbf{x}}$ is directly proportional to the CoM acceleration. The ankle moment, and consequently the CoP, is then in counter-phase in order to keep balance.

In summary, this Chapter provides a kinematic strategies evaluation tool for estimating angular displacements in an important clinical functional test (voluntary PS), involving only few SAAs. The method is suitable for the evaluation of the response strategy to unexpected perturbation even if it has been evaluated on a self-induced sway only. Obtained results support its possible use in clinical practice as tool for estimating how subject's motor system responds to external stimuli and for estimating balance control quantitative reactions. Moreover, the prediction method for GRF, CoP and CoM evaluation during the voluntary PS is presented. It could be performed during different functional tests in the clinical settings by the use of accelerometry only and considering a set of subject-specific body-segment parameters, previously estimated during a simple motor task (rSTS). Accelerometry compares favorably to commercial and traditional movement analysis systems in terms of cost, size, weight, convenience, and portability. As a result, data collection is no longer confined to a laboratory environment.

Future developments will be address to evaluate the kinematic strategies using the estimated subject-specific body-segment parameters in place of those obtained from anthropometric De Leva's tables [42]. Although at the present moment only GRF, CoP and CoM are predicted using the previously estimated parameters, the positive results suggest that also body kinematic strategies evaluation can take advantages by the use of the subject-specific inertial properties.

Chapter 5

Joint kinematics evaluation during the *Fugl-Meyer Motor* *Assessment* for the upper extremity

A novel inertial sensors-based technique for joint kinematics estimation is provided in this Chapter in order to obtain 3D objective biomechanical measurements of upper extremity kinematics. Aim of this Chapter are: i) to overcome the limitations of clinical scales based on individual judgment, ii) to help clinicians to objectively track changes in motor ability and iii) to provide timely feedback about of the effectiveness of administered rehabilitation interventions. A kinematic chain of 3-link is considered, using one IMU per body-segment during some easy exercises administered by the Fugl-Meyer Motor Assessment, and taking advantage by the use of a sensors fusion algorithm based

on an extended Kalman Filter to estimate segment orientations. A preliminary IMU technical systems of reference alignment procedure, using accelerometers and gyroscopes data only, allows the definition of a common global system of reference, neglecting the use of any magnetometers in the experimental set-up, which are typical affected by disturbances due to the presence of iron in both clinical and domestic environments. To evaluate the method, the technique is tested on a subject during shoulder flexion/extension, abduction/adduction and internal/external rotation movements. Shoulder and elbow joint angles are estimated after a functional calibration of body-segment anatomical axes, and a stereo-photogrammetric system is used for validation taking into account the data provided by the standard anatomical calibration. The results are consistent with those provided by the reference system and those published in previously studies. Mean root mean squared error range from 1.2° to 5.2° , with a mean value equal to 2.7° for shoulder angles and equal to 3.2° for elbow angles. Overlooking the type of task, mean errors are about 3.1° , 2.4° , 2.6° for shoulder angles of flexion/extension, ab/adduction and intra/extra rotation, respectively, and are about 2.9° , 3.2° , 3.6° for elbow angles of flexion/extension, pronation/supination and carrying angle, respectively. These results suggest that, after the alignment procedure and the functional calibration, one IMU per segment, consisting of a tri-axial accelerometer and a tri-axial gyroscope only, is enough to estimate 3D joint kinematics in a kinematic chain modeling upper limb, providing the usability of this instrumented test in the clinical practice.

5.1 Introduction

Stroke is one of the leading causes of death and disability and has been described as a worldwide epidemic [52, 59]. The effects of a stroke may include sensory, motor and cognitive impairment as well as a reduced ability to perform self care and participate in social and community activities [129]. Many stroke survivors report long-term disability

and reduced quality of life [152, 180] and have difficulty moving, thinking and sensing. While most recovery is thought to be made in the first few weeks after stroke, patients may have improvements on functional tasks and experience neural reorganization many months after having a stroke [183].

Stroke rehabilitation is the process realized in order to help post-stroke patients undergo treatment to return to normal life as much as possible by regaining and relearning the skills of everyday living. It also aims to help the survivors to understand and to adapt to difficulties, to prevent secondary complications and to educate family members to play a supporting role. A rehabilitation team is usually multidisciplinary and involves staff with different skills working together to help the patients. For most people with stroke, physical, occupational and speech-language therapies are the cornerstones of the rehabilitation process. Physical therapy focuses on joint range of motion and strength by performing exercises and re-learning functional tasks such as bed mobility, transferring, walking and other general motor functions, improving the awareness and the use of the hemiplegic side and involving constraint-induced movement therapy. Occupational therapy is involved in training to help relearn everyday activities known as the Activities of Daily Living (ADLs) such as eating, drinking, dressing, bathing, cooking, reading and writing, and toileting. Speech and language therapy is appropriate for patients with the speech production disorders: dysarthria and apraxia of speech, aphasia, cognitive-communication impairments and/or dysphagia (problems with swallowing).

A complete functional assessment should be made for the benefit of the stroke survivor which will be used as reference for proper therapeutic management and for the rehabilitation of stroke patients. Also, the advent of new treatments and rehabilitation options for post-stroke therapy has made measuring recovery after a stroke very important. Aside from establishing the plan of treatment for the stroke patient, such assessments can also prepare the stroke survivor, his or her family for any anticipated and expected outcomes.

Up to 85% of the stroke survivors experience hemiparesis, resulting in impairment of one upper extremity immediately after stroke, and between 55% and 75% of survivors continue to experience limitation in upper extremity function, which are associated with diminished health-related quality of life [111]. Defined in terms of the capacity of the patient to perform movements in the same way as age-matched non-disabled subjects, upper extremity sensorimotor recovery of arm function may be slower or more complex than that of the lower limb. Movements of the upper extremity are also far less stereotypical than those of the lower extremity, involving a wider inventory of coordinated trunk and multi-joint movements to manipulate objects in the environment. In order to assess recovery in post-stroke hemiplegic patients, clinical outcomes scales meant to measure improvement mainly focus on task accomplishment and are often not qualitatively sensitive enough to discriminate improvements in how the task is performed. The treatment effects are usually investigated on the following domains:

1. *Upper limb function and activity:*

- arm function and activity: including assessments such as the *Motor Assessment Scale* (upper limb), the *Action Research Arm Test*, the *Wolf Motor Function Test*, the *Fugl-Meyer Motor Assessment* (upper limb);
- hand function and activity: including assessments such as the *Nine Hole Peg Test* and the *Box and Block Test*.

2. *Gait and balance function and activity:*

- lower limb function and activity: including assessments such as the *Walking Distance*, the *Walking Speed*, *Community Walk Test*, the *Functional Ambulation*, the *Fugl-Meyer Motor Assessment* (lower limb), the *Timed Up and Go*;
- standing reach: including assessments such as the *Berg Balance Scale* and laboratory-based force plate measures.

3. *Global motor function*: including assessments such as the *Motor Assessment Scale*.
4. *Cognitive function*: including assessments such as the *Trail making test* and the *Useful Field of View Test*.
5. *Activity limitation*: including assessments such as the *Functional Independence Measure*, the *Barthel Index*, the *Activities-Specific Balance Confidence Scale*, the *On-Road Driving Test*.
6. *Participation restriction and quality of life*: including assessments such as the *SF36*, the *EQ5D*, the *Stroke Impact Scale* or other patient-reported outcomes.
7. *Imaging studies*: including functional magnetic resonance imaging (MRI).
8. *Adverse events*: including motion sickness, pain, injury, falls and death.

This Chapter will focus on the upper limb function evaluation through the *Fugl-Meyer Motor Assessment* (FMA).

Fugl-Meyer Motor Assessment

As shown in the previous Chapters, the main aim of this Thesis is to provide quantitative assessment of traditional functional tests by using inertial sensors. In particular, this Chapter focuses on the instrumentation of some easy exercises administered in the FMA for the upper extremity [61].

The FMA is a stroke-specific and performance-based impairment index. This means that all stroke survivors are considered unique and that a grading system is in place for proper evaluation. Basically, it provides a numeric value to determine the severity of the stroke, describe motor recovery, plan the post-stroke treatment and evaluate these treatments. Evaluation can be done immediately after a stroke and can be repeated while the stroke patient is already undergoing therapy. The

FMA was developed to be used in both clinical and research settings, and is the first numerical evaluation tool based on the chronological stages of motor and sensory return in hemiplegic stroke patients. Although the FM allows the health care team to properly evaluate the motor and sensory recovery of survivors after a stroke, it can also assess balance, joint functions, clear changes in motor impairment following stroke [71], capacity of the stroke survivor to perform ADLs, and pain.

A physical therapist, an occupational therapist or any other rehabilitation professional trained on FMA can administer the evaluation on the stroke patient on a one-on-one basis. The person tasked to administer the test shall guide the stroke victim through demonstrations and by giving out verbal instructions. It can be applied in any setting as a hospital and at the home of stroke survivors and tracks the progress in stroke patients from the initial day that he or she had the stroke to days, weeks, months or even years post-stroke. The traditional FMA does not need any special equipment, at most it requires a mat or a bed and a number of small objects for assessment of sensation, reflexes and range of motion. Sections of the evaluation can be administered separately. The FMA is usually takes about 30-35 minutes to administer the whole test.

Scoring in the FMA is based on direct observation of the performance of stroke survivors and is based on the ability to complete an item. The maximum score that a stroke patient can have is 226 points and items in the FMA are scored on a 3-point scale:

- 0 = cannot perform;
- 1 = performs partially;
- 2 = performs fully.

There are five domains which are evaluated by the occupational or physical therapist during the FMA:

- *Motor function*: this part of the test includes assessing the movement, coordination and reflex action of the shoulder, elbow, fore-

arm, wrist, hand, hip, knee and ankle. The score for this test range from 0 (paralysis) to 100 (normal motor function): 66 is the upper extremity maximum score and 34 is the lower extremity maximum score.

- *Sensory function*: this part evaluates light touch on two surfaces of the arm and leg, and position sense for 8 joints, maximum score is 24.
- *Balance*: this part contains 7 tests, 3 seated and 4 standing, maximum score is 14.
- *Joint range of motion*: this part considers 8 joints, maximum score is 44.
- *Joint pain*: maximum score is 44.

Despite FMA is a commonly used clinical test that has been developed to qualitatively describe complex motor tasks by functional testing, this method depends on individual observation and subjective interpretation, which make the assessment results inconsistent and have limited accuracy in recall [132]. The need for objective, cost-effective and clinically applicable methods, as well as methods that possess a high sensitivity and specificity, is hence clear. Aim of this Chapter is to develop a new motion analysis protocol for the upper extremity FMA instrumentation, by using inertial sensors in order to estimate the body-segment angular displacements of the kinematic chain used to model the upper limb. In this study, 3D joint kinematics is estimated taking advantages from the use of a simple and portable measurement system (inertial sensors) and from the assumption of a rigorous biomechanical model related to the single patient. This new technique for the instrumented upper extremity FMA would enable quantitative assessment of performance on a subject-specific basis, overcoming the limitations due to the lack of objectiveness related to individual judgment, and possibly disclosing subtle alterations that are not clearly visible to the observer.

Upper Limb Motion Analysis Protocol

Quantifying upper extremity dysfunction in neurological and orthopedic disorders is technically complex because of the multi-joint structure, and interpretation is hindered by the variability of possible movements. Increasing interest in upper limb biomechanics has led to closer investigations of both segment movements and detailed joint motion. Unfortunately, conceptual and practical differences in the motion analysis protocols reduce compatibility for post-data and cross validation analysis. For instance, several authors used different kinematic models of the upper limb, different coordinate systems, different motor tasks, and different measurement systems [4, 39, 141, 192, 193]. A new and flexible framework for the definition of standardized protocols for measuring upper extremity kinematics was design in 2008 by Kontaxis *et al.* in [100]. The steps required to build a motion analysis protocol, recommended by the authors, are the following:

1. Joints/segments of interest selection;
2. Mechanical model of joints/segment DoFs definition;
3. Joint/segment coordinate systems and angles definition;
4. Marker setup/ sensors placement identification;
5. Selection of the set of activities to be measured;
6. Kinematics refinements definition.

The protocol developed for the upper limb kinematics estimation presented in this Chapter is based on these recommendations. The used measurement system, as mentioned above, is a body-sensor network consisting on one Inertial Measurement Unit (IMU) per segment, including a tri-axial accelerometer and a tri-axial gyroscope. The use of a traditional movement analysis system, as the Stereo-Photogrammetric (SP) system, is required only in order to validate the method.

Since micro-machined sensors have become generally available on the market, human movement can be continuously measured outside a

specialized laboratory, overcoming the limitation of traditional movement analysis systems. In addition to inertial sensors, some commercial IMUs, often used in motion analysis, include a magnetometer able to measure the earth magnetic field strength. Body-segments orientation can be estimated by combining the sensor signals from accelerometers, gyroscopes and magnetometers, approximating the body-segment anatomical axes to the IMU technical axes and considering the IMUs orientation.

The design of a filter for the IMU orientation estimation (in place of the human body-segments orientation) has been first described by Foxlin *et al.* [60] and Bachmann *et al.* [10]. Foxlin *et al.* [60] described a sensor unit containing a 2D fluid inclinometer, a 2D electronic compass and a 3D gyroscope, with a Kalman Filter (KF) that incorporated a continuous gyroscope offset estimate. Although this method seemed to work for some controlled 2D test movements, applicability of this sensor was limited for general 3D movements, owing to the singularities arising from the 2D instead of 3D sensors and the use of Euler angles. Bachman *et al.* [10] used a filter that relied on accelerometers and magnetometers for low-frequency components of the orientation and used gyroscopes to measure faster changes of orientation. This method seemed to be robust, although the performance of the filter has not been investigated for 3D human movements. In 2005, Luinge and Veltink [116] designed and evaluated a KF that fused tri-axial accelerometer and tri-axial gyroscope signals for ambulatory recording of human body-segments orientation. The method continuously corrected orientation estimates obtained by mathematical integration of the 3D angular velocity measured using the gyroscope. The correction was performed using an inclination estimate continuously obtained using the signal of the 3D accelerometer. The error in rotation around the vertical was not significantly reduced. Zhu and Zhou [219] used also magnetometers in addition to accelerometers and gyroscopes to overcome this problem.

Thanks to their portability and usability, inertial sensors have been largely used for the evaluation of kinematic variables in order to assess neurological disorders by measuring arm movements. By way of example, Beer *et al.* [15] measured the path of the hand in pointing tasks for quantifying hemiparesis, Goldvasser *et al.* [72] for quantifying ataxia and Topka *et al.* [186] for quantifying dyskinesia. Symptoms of Parkinson's disease were measured using accelerometers [55, 82]. Uswatte *et al.* [191] and Bernmark and Wiktorin [17] used an accelerometer attached to the arm in order to obtain a measure of arm function during daily life. More detailed and accurately studies have been published in the last years regarding the use of inertial and magnetic sensors for the upper limb motion tracking. By way of example, Zhou *et al.* [218] presented a new motion tracking system using two IMUs that are placed near the wrist and the elbow joints. Each IMU consisted of a tri-axial accelerometer, a tri-axial gyroscope and a tri-axial magnetometer. The position of the wrist and the elbow joints was obtained from a kinematic model previously designed. The position of the shoulder joint was estimated using a Lagrangian-based optimization technique, which integrated the values of acceleration and the estimated value of rotation measured from both the inertial sensors. Experimental results, compared to an optical motion tracker, provided position error less than 0.01m and angle error ranged from 2.5° and 4.8°.

In these studies, the data supplied by the accelerometer, gyroscope and magnetometer are combined through sensor fusion algorithms to measure the 3D orientation of the IMU technical System of Reference (SoR), defined basing on the sensitive axis of the inertial and magnetic sensors, with respect to a global, earth-based SoR. In order to estimate joints kinematics: i) an IMU has been attached to each body-segment of interest, ii) at least one anatomical SoR has been defined for each body-segment, and iii) the orientation of the anatomical SoR has been expressed in the IMU technical SoR. Joint kinematics are finally obtained from the relative orientation of the anatomical SoRs. The standard procedure for the definition of an anatomical SoR is based on

the measurement of the position of bony landmarks [24, 212]. Obviously, this is not a practical solution when IMUs are being used since it would require the use of an additional measurement system to record bony landmarks position in 3D, relative to the orientation of the IMU technical SoR [156]. There is a need for an anatomical calibration procedure for inertial sensors, to obtain comparable results as in procedures developed for optical recording systems. Only a few studies have investigated the use of IMUs to analyze the joint kinematics of the upper limb, considering the human body-segment SoRs orientation. These studies have mainly focused on determining the kinematics of the humerus [33], the humerothoracic [10], and the elbow [10, 117]. In particular, in order to measure the kinematics between arm and forearm, the method designed by Luinge *et al.* [117] on the basis of the previous study published in 2005 [116] used the adduction constraints in the elbow to measure the orientation of the forearm with respect to the arm. They considered a sensor calibration in order to determine the exact devices orientation with respect to the body-segments. The accuracy of this method was limited by the accuracy of the sensor to segment calibration. Cutti *et al.* [39] developed a protocol to measure scapulothoracic, humerothoracic, and elbow kinematics using four IMU positioned on each body-segment of interest. For each segment, anatomical SoRs were defined and were expressed in the SoR of the IMU placed on the segment. Comparing joint kinematics estimates with those obtained from a SP system, Cutti *et al.* obtained mean errors between 0.2° and 3.2° , demonstrating the considerable accuracy of the sensor-based estimation method. In order to exclude differences in the measurements of the two systems, the clusters of markers were glued on the IMUs to ensure that the same soft tissue artifacts affected both tracking devices. Moreover, the same protocol for the definition of the anatomical SoRs both for SP system and IMU was used: the ones of the thorax, scapula and proximal humerus had a constant orientation with respect to IMU technical SoR of the corresponding segment, while the direction of elbow flexion/extension and pronation/supination axes

were estimated before exercise [179, 210] in order to define the anatomical SoRs for distal humerus and forearm. In another study, De Vries *et al.* [48] developed a functional method in which the anatomical SoRs were constructed from estimations of the functional axes of rotation of a segment. Angular velocity, as measured by the IMUs during some defined exercises, was used as an estimate of the functional axis of rotation (averaged over time and normalized to unit length) [117]. Thorax, arm, forearm and hand kinematics was estimated using four IMUs, considering their above functional procedure for anatomical SoRs, and a SP system for validation, considering the ISB recommendations [212]. In order to determine the difference between methods, the angles of rotation between the bony landmarks-based and the IMU-based SoRs were calculated for each segment, obtaining 6.4° , 8.7° , 17.2° and 15.2° for thorax, arm, forearm and hand respectively. The authors justified the high errors considering the offset between the anatomical SoR definition methods and the soft tissue artifacts, which have different effects on both the involved measurement systems.

Almost all the previously published studies focused on the use of commercial IMU containing inertial and magnetic sensors and there is a lack in the literature of the use of inertial technologies only. By an inboard fusion algorithm, these sensors data are used to estimate IMU orientation under the assumption of homogeneity of the earth magnetic field. Although not always obvious, it is usual that the condition of the earth magnetic field is far from optimal, if not homogeneous at all. These irregularities can be caused by construction iron in floors, walls and ceilings, or other equipment in the environment, and occur in both the horizontal and vertical plane [11]. In the recent past, De Vries *et al.* [47] developed a technique to investigate the distortion of the earth magnetic field in their laboratory and to define the effect of these disturbances on the accuracy of the orientation estimation IMU-based method. Despite their results, the protocol presented in this Chapter neglects the use of magnetometers, considering that the developed measurement system would be used in both clinical and do-

mestic environments: the difficulties related to the mapping of the earth magnetic field are not compatible with the characteristics of portability and usability required in this study. An important issue for the IMU-based joint kinematics estimation method, is the alignment of the different technical SoRs related to the different sensors placed on the body-segments. IMUs which include magnetometers use gravity and heading of the earth magnetic field to obtain the same global SoR.

In this perspective, aims of this Chapter are:

- to develop a new procedure in order to align the technical SoR of each inertial sensor, obtaining a common global SoR, by using only accelerometers and gyroscopes data measured during a preliminary system calibration phase;
- to evaluate 3D upper limb joint kinematics during some easy exercises administered by the FMA: the relative orientation of the anatomical body-segment SoRs will be obtain considering the functional procedure described in [48] for anatomical axes definition, and applying a KF to accelerometer and gyroscope signals in order to obtain 3D IMU orientation.

In order to support the usability and the accuracy of the method presented in this Chapter, a SP system is used during the FMA exercises for validation. The traditional anatomical calibration procedure to define body-segment SoRs [24, 212] is performed in order to evaluate the difference between methods, in terms of angles of rotation between the bony landmarks-based and the IMU-based SoRs for each body-segment. Preliminary results are obtained in 2D, considering a multi-link mechanical arm for experimental sessions and evaluating KF performance in real-time.

5.2 Methods and Materials

5.2.1 2D real-time multi-link model kinematics

A 2D multi-link model was initially analyzed, and the real-time estimation algorithm of the angular displacements was provided. An Extended Kalman Filter (EKF) was developed to estimate the dynamic state of the system, considering accelerometer and gyroscope signals. Next, in order to validate the method in a simple set-up, a mechanical arm equipped with absolute encoders and IMUs was used to estimate the multi-link kinematics.

Multi-link model

In order to describe the new method in the most general way, a 3-link model (3 degrees of freedom, DoFs) in the sagittal plane was initially analyzed (see Figure 5.1)

The multi-link shown in Figure 5.1b models the upper limb kinematic chain in the sagittal plane (see Figure 5.1a). In this first part of the Chapter, the kinematics of arm, forearm and hand was investigated. The angles θ_1 , θ_2 , θ_3 , defined with respect to the vertical lines passing through the rotation centers of shoulder (SH), elbow (E) and wrist (W) joints, respectively, represent the three model's DoF.

Three IMUs are supposed placed at height h_1 , h_2 , h_3 from the rotation centers SH, E and W, respectively. The measured accelerometer and gyroscope outputs for the i -th link can be expressed as follows:

$$\begin{aligned} a_{x,i}(k) &= h_i \ddot{\theta}_i(k) + g \sin \theta_i(k) + a_i^x(k) \cos \theta_i(k) - a_i^z(k) \sin \theta_i(k) \\ a_{z,i}(k) &= h_i \dot{\theta}_i^2(k) + g \cos \theta_i(k) - a_i^x(k) \sin \theta_i(k) - a_i^z(k) \cos \theta_i(k) \\ \omega_{y,i}(k) &= \dot{\theta}_i(k) \end{aligned} \quad (5.1)$$

considering:

$$\begin{aligned} a_i^x(k) &= a_{i-1}^x(k) + l_{i-1} \left. \frac{d^2[\sin \theta_{i-1}(t)]}{dt^2} \right|_{t=kT_s} \\ &\approx a_{i-1}^x(k) + l_{i-1} \frac{[\sin \theta_{i-1}(k+1) - 2 \sin \theta_{i-1}(k) + \sin \theta_{i-1}(k-1)]}{T_s^2} \end{aligned}$$

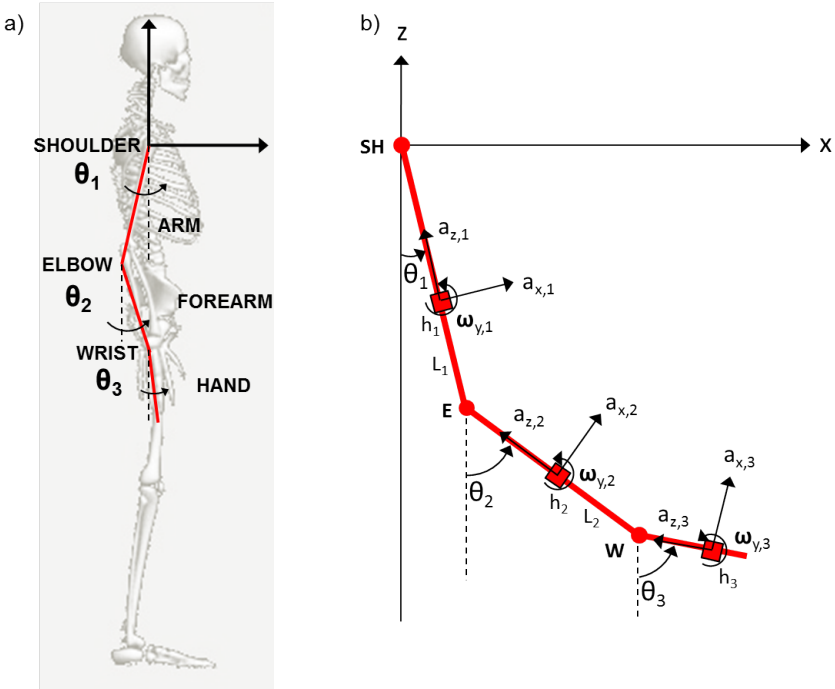


Figure 5.1: a) Upper limb kinematic chain representation in the sagittal plane, b) 2D multi-link model

$$\begin{aligned}
 a_i^z(k) &= a_{i-1}^y(k) + l_{i-1} \left. \frac{d^2[\cos \theta_{i-1}(t)]}{dt^2} \right|_{t=kT_s} \\
 &\approx a_{i-1}^y(k) + l_{i-1} \frac{[\cos \theta_{i-1}(k+1) - 2 \cos \theta_{i-1}(k) + \cos \theta_{i-1}(k-1)]}{T_s^2}
 \end{aligned}$$

for $k = 1, \dots, n$ (n is the number of samples) and $i = 1, \dots, 3$, where T_s is the sample time and l_{i-1} is the length of the $(i-1)$ -th segment (it is assumed that $a_0^{x,y} = 0$, $l_0 = 0$).

In order to describe the dynamic state of the system, an EKF [93, 201] was implemented to accurately estimate the three angles θ_1 , θ_2 , θ_3 , by fusing the accelerometer and gyroscope outputs, calculated by Equation (5.1). The main equations of the EKF are shown in Equation (5.2), where \mathbf{w}_k and \mathbf{v}_k represent the process and measurement noise, assumed to be independent, white and with normal probability distribution, having a process noise covariance \mathbf{Q} and a measurement

noise covariance \mathbf{R} . More details about the algorithm are presented elsewhere [201]. The state-space model of the EKF is described by the process and measurement model equations:

$$\begin{aligned}\mathbf{x}_{k+1} &= \mathbf{A}\mathbf{x}_k + \mathbf{w}_k \\ \mathbf{z}_k &= h(\mathbf{x}_k) + \mathbf{v}_k\end{aligned}\quad (5.2)$$

The state vector of the EKF, $\mathbf{x}(k)_{[9 \times 1]}$, at every sampled instant of time k , was defined considering the angles, θ_1 , θ_2 , θ_3 , their first and second time derivatives as:

$$\mathbf{x}(k) = \begin{bmatrix} \theta_1(k) \\ \omega_1(k) \\ \alpha_1(k) \\ \theta_2(k) \\ \omega_2(k) \\ \alpha_2(k) \\ \theta_3(k) \\ \omega_3(k) \\ \alpha_3(k) \end{bmatrix}\quad (5.3)$$

In the discrete-time domain, the predicted state at the instant $k+1$ was obtained as:

$$\mathbf{x}(k+1) = \underbrace{\begin{bmatrix} \mathbf{A}_{[3 \times 3]} & \mathbf{0}_{[3 \times 3]} & \mathbf{0}_{[3 \times 3]} \\ \mathbf{0}_{[3 \times 3]} & \mathbf{A}_{[3 \times 3]} & \mathbf{0}_{[3 \times 3]} \\ \mathbf{0}_{[3 \times 3]} & \mathbf{0}_{[3 \times 3]} & \mathbf{A}_{[3 \times 3]} \end{bmatrix}}_{\mathbf{A}_{[9 \times 9]}} \mathbf{x}(k)\quad (5.4)$$

where

$$\mathbf{A}_{[3 \times 3]} = \begin{bmatrix} 1 & T_s & \frac{T_s^2}{2} \\ 0 & 1 & T_s \\ 0 & 0 & 1 \end{bmatrix}\quad (5.5)$$

The upper triangular state matrix $\mathbf{A}_{[9 \times 9]}$ was obtained considering the extension of $\mathbf{A}_{[3 \times 3]}$ to the $[9 \times 1]$ -state vector defined in Equation (5.3).

The measurement vector $\mathbf{z}(k)_{[9 \times 1]}$, at every sampled instant of time k , was defined considering the outputs of the sensors, expressed in Equation (5.1), as:

$$\mathbf{z}(k) = \begin{bmatrix} a_{x,1}(k) \\ a_{z,1}(k) \\ \omega_{y,1}(k) \\ a_{x,2}(k) \\ a_{z,2}(k) \\ \omega_{y,2}(k) \\ a_{x,3}(k) \\ a_{z,3}(k) \\ \omega_{y,3}(k) \end{bmatrix} \quad (5.6)$$

According to Equation (5.1), the output vector is related to the state vector through the non-linear relationship $\mathbf{z}_k = h(\mathbf{x}_k)$. The output matrix $\mathbf{H}(k)_{[9 \times 9]}$, which relates the measurements $\mathbf{z}(k)_{[9 \times 1]}$ to the state $\mathbf{x}(k)_{[9 \times 1]}$, was thus obtained evaluating the Jacobian matrix of partial derivatives of $h(\mathbf{x}_k)$ with respect to the state vector.

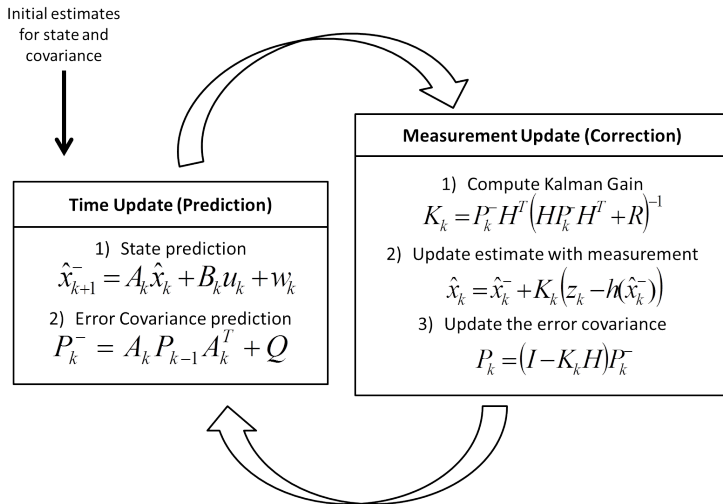


Figure 5.2: Summary scheme of the operations implemented in the Kalman Filter

The process covariance matrix \mathbf{Q} was defined under the assumption that noise affects the jerk only and there are no correlations between the jerk noise sequences. $\mathbf{Q}_{[9 \times 9]}$ has therefore three non-zero elements only ($Q(i, i), i = 3, 6, 9$). The measurement noise covariance matrix \mathbf{R} was defined considering the noise which affects the accelerometer and the gyroscope outputs. Since correlations between noise of the sensors were assumed to be zero, $\mathbf{R}_{[9 \times 9]}$ is diagonal. In order to run the filter procedure (see Figure 5.2), initial estimate of the state vector was zeroed, whereas the initial estimate of the error covariance matrix $\mathbf{P}_{[9 \times 9]}$ was set equal to the identity matrix.

The three angles of rotation $\theta_1, \theta_2, \theta_3$, are the elements $x_1(k), x_4(k), x_7(k)$ of the estimated state vector $\mathbf{x}(k)$, after the filtering procedure.

Multi-link mechanical arm

The method was tested by using an aluminum rectangular 3-link mechanical arm driven by hand. The mechanical arm is equipped with three absolute encoders (Gurley Precision Instrument, mod. 7700, resolution 19 bit) and three IMUs (Microstrain, mod. Inertia-Link, range $\pm 5g, \pm 300^\circ/s$, resolution 16 bit) placed at height $h_1 = 0.20m, h_2 = 0.15m, h_3 = 0.10m$ from the rotation center SH, E and W, respectively (see Figure 5.3). Considering that movement takes place in the sagittal plane, the output signals from accelerometers with sensitive axes placed along orthogonal $a_{x,i}(k)$ and centripetal $a_{z,i}(k)$ direction with respect to the links, and the output signals from gyroscopes with sensitive axes orthogonal to the sagittal plane $\omega_{y,i}(k)$ were considered only ($k = 1, \dots, n$ and $i = 1, \dots, 3$). Signals were acquired at 100Hz sampling rate and five trials were performed, oscillating the multi-link arm at different frequencies and with different angular excursions.

In order to validate the estimation method, the three encoder outputs were compared with the estimated angles $\theta_1, \theta_2, \theta_3$. Root Mean Square Errors (RMSEs) are thus provided.



**Gurley Precision Instrument,
Virtual Absolute Encoder**



**Microstrain,
Inertia-Link**

Figure 5.3: Three-link mechanical arm equipped with encoders and IMUs

The acquisition, the EKF and the output processing were developed in LabVIEW programming environment (see Figure 5.4) in order to guarantee the real-time performance of the system.

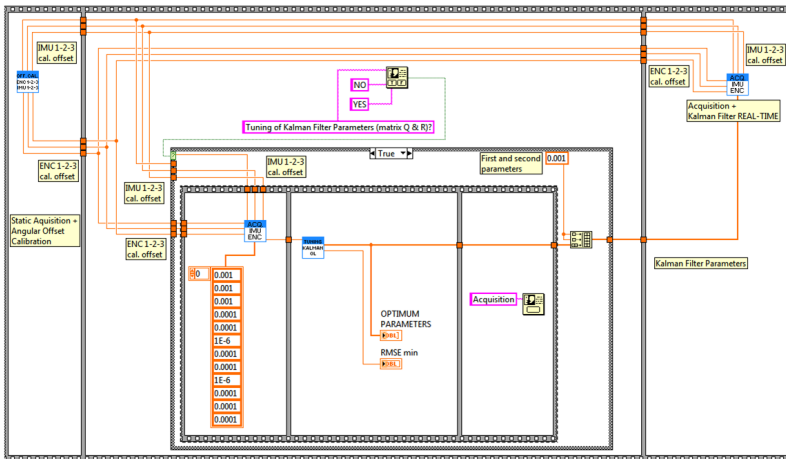


Figure 5.4: Main part of the acquisition and data processing software developed in LabVIEW programming environment

5.2.2 3D upper limb joint kinematics

Starting from the method developed for the 2D multi-link kinematics estimation, the second part of this Chapter focused on the extension of the procedure for a 3D evaluation. In 5.2.1 an EKF was developed considering the upper limb modelled as a 2D 3-link kinematic chain, and sensor outputs were calculated starting from a geometrical perspective of the biomechanical model. In 3D dissertation and in order to extend the EKF procedure to estimate upper limb kinematics, a model of the sensor, positioned on each body-segment of interest, was used in place of a model of the kinematic chain. In addition to rotations, the EKF developed in this Chapter considers the translations in the estimated state vector.

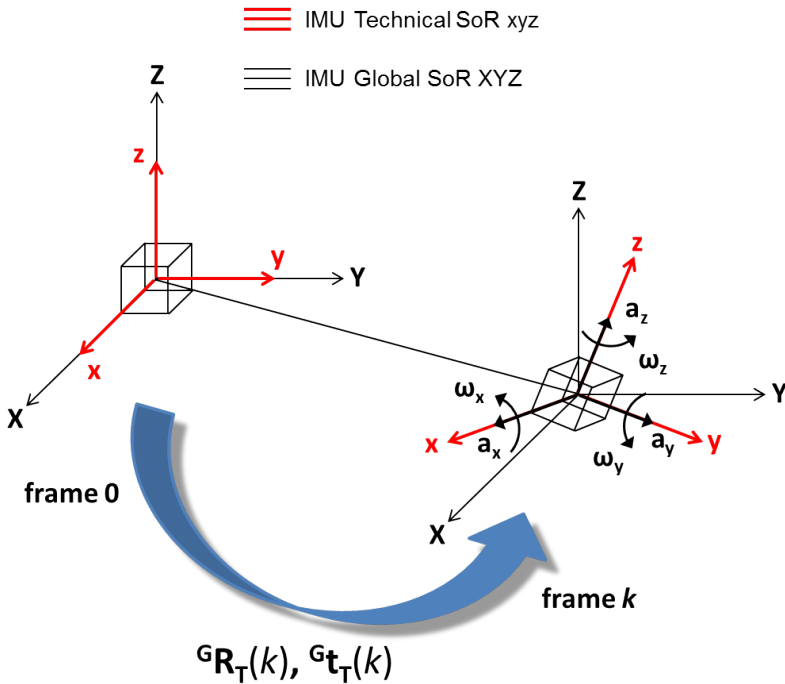


Figure 5.5: Relative rotation and translation between the sensor technical systems of reference (red) and the global systems of reference (black)

All the rotations and translations estimated through the EKF were referred to rotations and translations of the sensor technical SoR xyz with respect to the sensor's technical SoR at the initial condition XYZ (frame 0), which was assumed as global SoR (see Figure 5.5).

For each IMU, the three rotation angles with respect to the global SoR were referred to *roll*, *pitch* and *yaw* angles: at every sampled instant of time k , the *roll* is a counterclockwise rotation of $\alpha(k)$ about the x -axis, the *pitch* is a counterclockwise rotation of $\beta(k)$ about the y -axis, and the *yaw* is a counterclockwise rotation of $\gamma(k)$ about the z -axis. In addition, the three translations with respect to the global SoR were defined as $t_x(k)$, $t_y(k)$ and $t_z(k)$, which correspond to the translation along, the x -, y - and z -axis, respectively.

The rotation matrix and the translation vector from the technical SoR to the global SoR at frame k , were defined as

$$\begin{aligned} {}^G\mathbf{R}_T(k) &= \mathbf{R}_z(\gamma(k)) \cdot \mathbf{R}_y(\beta(k)) \cdot \mathbf{R}_x(\alpha(k)) = \\ &= \begin{bmatrix} C_\beta C_\gamma & S_\alpha S_\beta C_\gamma - C_\alpha S_\gamma & C_\alpha S_\beta C_\gamma + S_\alpha S_\gamma \\ C_\beta S_\gamma & S_\alpha S_\beta S_\gamma + C_\alpha C_\gamma & C_\alpha S_\beta S_\gamma - S_\alpha C_\gamma \\ -S_\beta & S_\alpha C_\beta & C_\alpha C_\beta \end{bmatrix} \\ {}^G\mathbf{t}_T(k) &= \begin{bmatrix} t_x(k) & t_y(k) & t_z(k) \end{bmatrix}^T \end{aligned} \quad (5.7)$$

where, considering the generic angle $\phi(k)$, $S_\phi = \sin \phi(k)$ and $C_\phi = \cos \phi(k)$, respectively.

The state-space model of the EKF is described by the same process and measurement model equations defined in Equation (5.2). The state vector, $\mathbf{x}(k)_{[18 \times 1]}$, at every sampled instant of time k , was defined considering the angles $\alpha(k)$, $\beta(k)$, $\gamma(k)$, with their first and second time derivatives, and the translations $t_x(k)$, $t_y(k)$, $t_z(k)$, with their first and second time derivatives, as:

$$\mathbf{x}(k) = \begin{bmatrix} \Theta_x(k) & \Theta_y(k) & \Theta_z(k) & \mathbf{T}_x(k) & \mathbf{T}_y(k) & \mathbf{T}_z(k) \end{bmatrix}^T \quad (5.8)$$

The vectors expressed in Equation (5.8), for each direction along x -, y -

and z -axis, were defined as:

$$\begin{aligned}
\Theta_x(k) &= [\alpha(k) \quad \dot{\alpha}(k) \quad \ddot{\alpha}(k)]^T \\
\Theta_y(k) &= [\beta(k) \quad \dot{\beta}(k) \quad \ddot{\beta}(k)]^T \\
\Theta_z(k) &= [\gamma(k) \quad \dot{\gamma}(k) \quad \ddot{\gamma}(k)]^T \\
\mathbf{T}_x(k) &= [t_x(k) \quad \dot{t}_x(k) \quad \ddot{t}_x(k)]^T \\
\mathbf{T}_y(k) &= [t_y(k) \quad \dot{t}_y(k) \quad \ddot{t}_y(k)]^T \\
\mathbf{T}_z(k) &= [t_z(k) \quad \dot{t}_z(k) \quad \ddot{t}_z(k)]^T
\end{aligned} \tag{5.9}$$

In the time-discrete domain, the predicted state at the instant $k+1$ was obtained as:

$$\begin{aligned}
\Theta_{x,y,z}(k+1) &= \underbrace{\begin{bmatrix} 1 & T_s & \frac{T_s^2}{2} \\ 0 & 1 & T_s \\ 0 & 0 & 1 \end{bmatrix}}_{\mathbf{A}_{[3 \times 3]}} \Theta_{x,y,z}(k) \\
\mathbf{T}_{x,y,z}(k+1) &= \mathbf{A}_{[3 \times 3]} \mathbf{T}_{x,y,z}(k)
\end{aligned} \tag{5.10}$$

The upper triangular state matrix $\mathbf{A}_{[18 \times 18]}$ was obtained considering the extension of $\mathbf{A}_{[3 \times 3]}$ to the $[18 \times 18]$ -state vector defined in Equation (5.8).

The measurement vector $\mathbf{z}(k)_{[6 \times 1]}$, at every sampled instant of time k , was defined considering the outputs of the sensor, as:

$$\mathbf{z}(k) = [a_x(k) \quad a_y(k) \quad a_z(k) \quad \omega_x(k) \quad \omega_y(k) \quad \omega_z(k)]^T \tag{5.11}$$

The accelerometer and gyroscope outputs measured at the instant k

and defined in the sensor technical SoR were expressed as follows [68]:

$$\begin{bmatrix} a_x \\ a_y \\ a_z \end{bmatrix} = {}^G\mathbf{R}_T^T \cdot ({}^G\mathbf{g} + {}^G\ddot{\mathbf{t}}_T)$$

$$\begin{bmatrix} 0 & -\omega_z & \omega_y \\ \omega_z & 0 & -\omega_x \\ -\omega_y & \omega_x & 0 \end{bmatrix} = {}^G\mathbf{R}_T^T \cdot \frac{d{}^G\mathbf{R}_T}{dt} \quad (5.12)$$

Considering the changes in state and measurement vector definitions, the filtering procedure previously described in 5.2.1 and shown in Figure 5.2, was implemented in order to estimate the three angles of rotation of a single sensor, $\alpha(k)$, $\beta(k)$, $\gamma(k)$, which are the elements $x_1(k)$, $x_4(k)$, $x_7(k)$ of the estimated state vector $\mathbf{x}(k)$.

After the definition of the segments and joints of interest, and their mechanical model description, the first phase of the movement analysis protocol focuses on the application of the filtering procedure to each considered IMU, in order to estimate sensors angular kinematics with respect to the initial condition (global SoR) during the set of activities to be measured, selected in the FMA. Even if commercial IMUs, including magnetometers and considering gravity and heading of the earth magnetic field to define the global SoR, are usually used in this phase, in this Chapter magnetometer data are completely neglected. In this perspective, an alignment procedure is developed in order to obtain a unique global SoR, using accelerometer and gyroscope data, which is used as reference for IMUs angular kinematics.

Then, in a second phase, anatomical SoRs are defined for every body-segments starting from accelerometer and gyroscope data, during some easy exercises defined in a functional calibration procedure. The body-segments angular kinematics with respect to the IMUs global SoR is thus estimated, and the relationship between corresponding anatomical and technical SoRs is known.

The third phase is focused on the joint kinematics estimation, considering the relative orientation between anatomical SoRs related to

adjacent body-segments. In order to validate the method, a SP system is used to compare obtained joint kinematics, considering a cluster of markers glued on each IMU to ensure that the same soft tissue artifacts affected both tracking devices. A standard anatomical calibration is carried on for the body-segment anatomical axes definitions [24], considering the recommendations provided by ISB [212].

Joints/Segments of interest

The 3D kinematic model considered in this part of the Chapter consists of the thorax, the arm and the forearm body-segments, which are assumed to be rigid segment (see Figure 5.6a).

The orientation of the arm was computed with respect to the thorax, defining this as the shoulder kinematics, and the orientation of the forearm was computed with respect to the arm, defining this as the elbow kinematics.

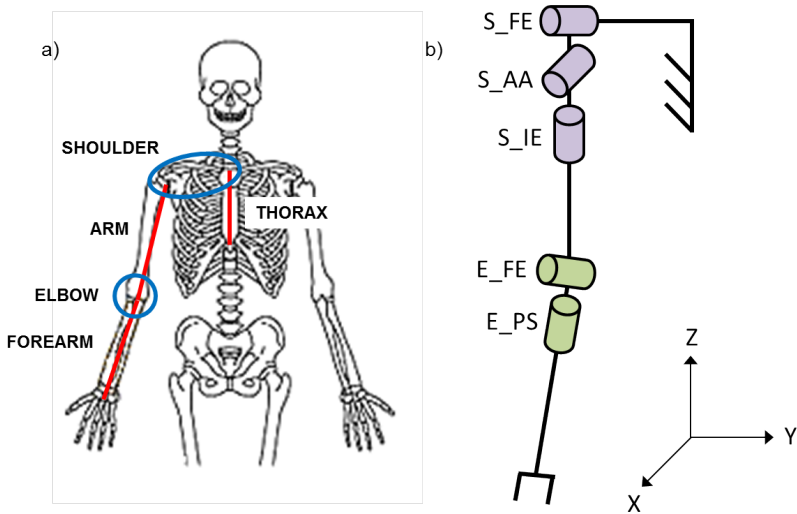


Figure 5.6: a) Kinematic model for the right upper limb, b) representation of the mechanical model of the joints of interest

Joint mechanical models

The shoulder kinematics was modeled with three DoFs (Figure 5.6b), namely Flexion/Extension (S_FE, Figure 5.7a), Abduction/Adduction (S_AA, Figure 5.7b) and Internal/External rotation (S_IE, Figure 5.7c), which are the independent rotation angles around Y -, X - and Z -axis of an IMU global SoR, respectively. Elbow kinematics was described by two DoFs: Flexion/Extension (E_FE, Figure 5.7d) and Pronation/Supination (E_PS, Figure 5.7e), which are the independent rotation angles around Y - and Z -axis of an IMU global SoR, respectively. The Carrying-Angle (E_CA) is a constant parameter of the elbow and measures the relative orientation of the axes of the hinges; it is subject-specific and not necessarily null [38, 198].

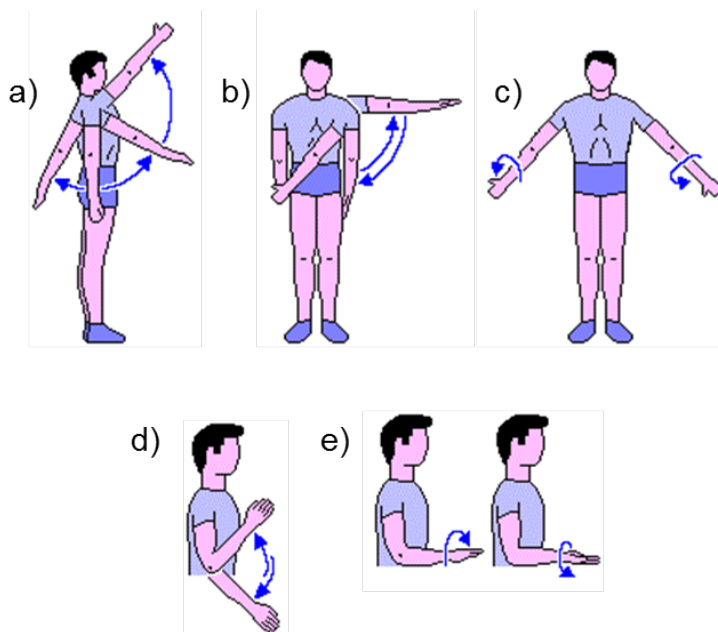


Figure 5.7: DoFs of the joints of interest

Sensors set-up

One healthy subject, without no previous orthopedic ailment, participated in this study after giving his informed consent. Three inertial sensors (Xsens, MTx, range $\pm 50\text{m/s}^2$, $\pm 1200^\circ/\text{s}$) were placed on each body-segment of interest with double sided tape on the right upper limb. For the thorax, the IMU was placed over the flat portion of the sternum. For the arm, the IMU was placed over the central third of the humerus, slightly posterior in order to minimize to soft tissue artifact. For the forearm, the IMU was placed over the distal, flat surface of radius and ulna. Inertial measurements were acquired at $f_s=100\text{Hz}$ sampling rate. The output signals of each sensor are referred to the technical SoR of each IMU.

In order to define a common global SoR XYZ for the three IMUs, using accelerometer and gyroscope data and neglecting magnetometer data, an alignment procedure was carried out. The aim is to obtain a global SoR with the Z -axis pointing vertically as the gravity vector, and with the X - and Y -axes aligned to the technical SoR of IMU placed on the thorax. This configuration was interpreted as the initial condition for the EKF procedure: IMUs angular kinematics are related to a defined global SoR, as inertial and magnetic devices are usually related to the earth magnetic field.

At the beginning of each data collection, the subject was asked to adopt a standard anatomical position (SAP, standing straight, arm hanging along the body, hand palms pointing to the front). In this position, the gravity vector measured by the accelerometers was used as an estimator for the z -axis of the IMU. Afterwards, and starting from the SAP, the subject was asked to perform a rigid movement involving adjacent body-segments, in order to assume that the angular velocities measured by the gyroscopes in a common fixed SoR are equal. The relative angle between the two projected angular velocities in the horizontal plane was then calculated and used in order to estimate the rotation angle between the two IMU technical SoRs [58].

The alignment procedure is described by the following steps:

1. *Static calibration*

The subject is asked to adopt the SAP for five seconds, and the thorax, arm and forearm accelerometer outputs are measured. At every sampled instant of time k , according to Equation (5.12), they are expressed in static condition as:

$$\begin{aligned} a_x(k) &= -g \sin \beta(k) \\ a_y(k) &= g \cos \beta(k) \sin \alpha(k) \\ a_z(k) &= g \cos \beta(k) \cos \alpha(k) \\ k &= 1, \dots, 5 \cdot fs \end{aligned} \quad (5.13)$$

Starting from Equation (5.13) and averaging accelerometer outputs over time, rotation matrices \mathbf{R}_x and \mathbf{R}_y are obtained considering the mean angles, $\bar{\alpha}$ and $\bar{\beta}$, that describe the rotation between the IMU technical SoR xyz and the one with the Z -axis aligned with the gravity vector:

$$\begin{aligned} \bar{\alpha} = \tan^{-1} \frac{\bar{a}_y}{\bar{a}_z} \Rightarrow \mathbf{R}_x &= \begin{bmatrix} 1 & 0 & 0 \\ 0 & \cos \bar{\alpha} & -\sin \bar{\alpha} \\ 0 & \sin \bar{\alpha} & \cos \bar{\alpha} \end{bmatrix} \\ \bar{\beta} = -\sin^{-1} \frac{\bar{a}_x}{g} \Rightarrow \mathbf{R}_y &= \begin{bmatrix} \cos \bar{\beta} & 0 & \sin \bar{\beta} \\ 0 & 1 & 0 \\ -\sin \bar{\beta} & 0 & \cos \bar{\beta} \end{bmatrix} \end{aligned} \quad (5.14)$$

For each body-segment, the resultant rotation matrix $\mathbf{R}_y \cdot \mathbf{R}_x$ allows the alignment of the z -axis of each technical SoR with the gravity vector. After this static calibration, the technical SoR of the IMU placed on the thorax is assumed as the global SoR.

2. *First dynamic calibration*

Starting from the SAP, in order to align the IMU technical SoR of the arm to the the IMU technical SoR of the thorax, the subject is asked to perform five times flexion/extension of the thorax

and the arm body-segments, try to avoid any movement of the shoulder joint to obtain a movement as rigid as possible. After the alignment provided by the static calibration, at every sampled instant of time k , thorax and arm gyroscope outputs, ωT_k and ωA_k , are measured in their technical SoRs, and the angle between the two projected angular velocities in the horizontal plane is calculated using the dot product in Equation (5.15):

$$\theta_k = \text{sign}(\omega A_{x,k} \cdot \omega T_{y,k} - \omega A_{y,k} \cdot \omega T_{x,k}) \cdot \cos^{-1} \left(\frac{\langle [\omega A_{x,k}, \omega A_{y,k}], [\omega T_{x,k}, \omega T_{y,k}] \rangle}{\|\omega A_{x,k}, \omega A_{y,k}\| \cdot \|\omega T_{x,k}, \omega T_{y,k}\|} \right) \quad (5.15)$$

where $\langle \cdot, \cdot \rangle$ denotes the dot product and the sign function expresses the sign (-1 or 1) of its argument, defining the direction of the rotation. Assuming that θ_k is a constant value influenced by the amplitude of angular velocity, $\bar{\gamma}_{A2T}$ is estimated by a weighted averaging of θ_k , using Equation (5.16). Angle $\bar{\gamma}_{A2T}$ describes the rotation between the arm IMU technical SoR and the thorax IMU technical SoR in the horizontal plane:

$$\begin{aligned} \bar{\gamma}_{A2T} &= \frac{\sum_{k=1}^n \|\omega A_{x,k}, \omega A_{y,k}\| \cdot \theta_k}{\sum_{k=1}^n \|\omega A_{x,k}, \omega A_{y,k}\|} \Rightarrow \\ \Rightarrow \mathbf{R}_{z,A2T} &= \begin{bmatrix} \cos \bar{\gamma}_{A2T} & -\sin \bar{\gamma}_{A2T} & 0 \\ \sin \bar{\gamma}_{A2T} & \cos \bar{\gamma}_{A2T} & 0 \\ 0 & 0 & 1 \end{bmatrix} \end{aligned} \quad (5.16)$$

3. Second dynamic calibration

Starting from the SAP, in order to align the IMU technical SoR of the forearm to the the IMU technical SoR of the arm, the subject is asked to perform five times abduction/adduction of the arm and the forearm body-segments, try to avoid any movement of the elbow joint to obtain a movement as rigid as possible. After the alignment provided by the static calibration, at every sampled instant of time k , arm and forearm gyroscope outputs, ωA_k and ωF_k , are measured in their technical SoRs, and the angle between

the two projected angular velocities in the horizontal plane is calculated, modifying the Equation (5.15) in:

$$\theta_k = \text{sign}(\omega F_{x,k} \cdot \omega A_{y,k} - \omega F_{y,k} \cdot \omega A_{x,k}) \cdot \cos^{-1} \left(\frac{\langle [\omega F_{x,k}, \omega F_{y,k}], [\omega A_{x,k}, \omega A_{y,k}] \rangle}{\|\omega F_{x,k}, \omega F_{y,k}\| \cdot \|\omega A_{x,k}, \omega A_{y,k}\|} \right) \quad (5.17)$$

Angle $\bar{\gamma}_{F2A}$ describes the rotation between the forearm IMU technical SoR and the arm IMU technical SoR in the horizontal plane:

$$\bar{\gamma}_{F2A} = \frac{\sum_{k=1}^n \|[\omega F_{x,k}, \omega F_{y,k}]\| \cdot \theta_k}{\sum_{k=1}^n \|[\omega F_{x,k}, \omega F_{y,k}]\|} \Rightarrow \Rightarrow \mathbf{R}_{z,F2A} = \begin{bmatrix} \cos \bar{\gamma}_{F2A} & -\sin \bar{\gamma}_{F2A} & 0 \\ \sin \bar{\gamma}_{F2A} & \cos \bar{\gamma}_{F2A} & 0 \\ 0 & 0 & 1 \end{bmatrix} \quad (5.18)$$

According to the above explained static and dynamic calibrations, the three rotation matrices between the technical SoR xyz of each IMU and the global common SoR XYZ are calculated as follows (see Figure 5.8):

$$\begin{aligned} {}^G \mathbf{R} \mathbf{T}_T &= \mathbf{R} \mathbf{T}_y \cdot \mathbf{R} \mathbf{T}_x \\ {}^G \mathbf{R} \mathbf{A}_T &= \mathbf{R}_{z,A2T} \cdot \mathbf{R} \mathbf{A}_y \cdot \mathbf{R} \mathbf{A}_x \\ {}^G \mathbf{R} \mathbf{F}_T &= \mathbf{R}_{z,A2T} \cdot \mathbf{R}_{z,F2A} \cdot \mathbf{R} \mathbf{F}_y \cdot \mathbf{R} \mathbf{F}_x \end{aligned} \quad (5.19)$$

In order to demonstrate the accuracy of the alignment procedure of the IMU technical SoRs, orientation data were acquired from the three sensors in addition to accelerometer and gyroscope outputs. Orientation data provided by the IMUs are obtained through an embedded EKF with respect to the earth magnetic field SoR, thanks to the use of the internal tri-axial magnetometer. Relative orientation between the IMUs placed on the thorax and the arm were estimated during three trials of flexion/extension, three trials of ab/adduction and three trials of internal/external rotation of the arm, using both the alignment procedure to obtain a common global SoR and the embedded EKF which

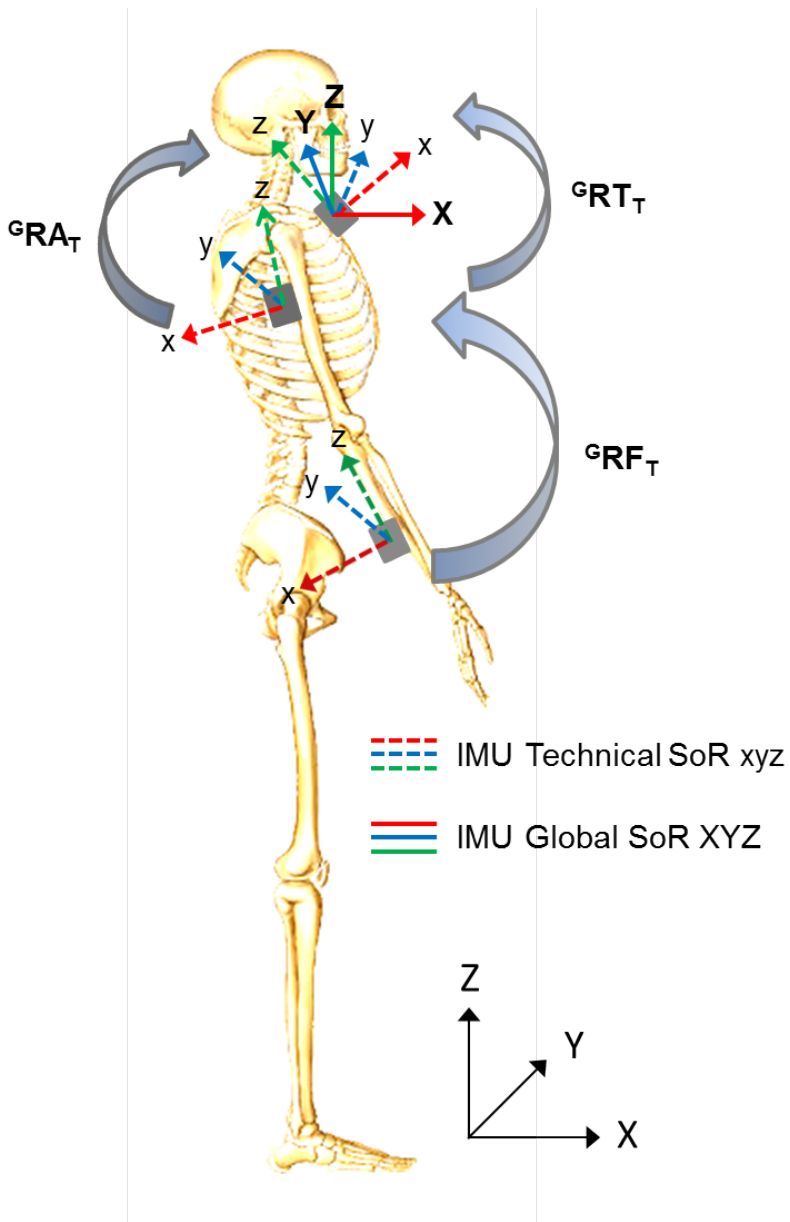


Figure 5.8: Representation of the Thorax (T), arm (A) and forearm (F) system of reference and of the rotation matrices between technical and global frames

works with respect to the earth magnetic field. Relative matrices were calculated at every instant of time k as:

$$\begin{aligned}\mathbf{RS}'(k) &= {}^G\mathbf{RT}_T^T(k) \cdot {}^G\mathbf{RA}_T(k) \\ \mathbf{RS}'_{\text{IMU}}(k) &= {}^E\mathbf{RT}_T^T(k) \cdot {}^E\mathbf{RA}_T(k)\end{aligned}\quad (5.20)$$

where $\mathbf{RS}'(k)$ and $\mathbf{RS}'_{\text{IMU}}(k)$ are the rotation matrices which describe the relative orientation between the technical SoRs of the IMUs placed on the arm and the thorax, provided considering the global SoR, G , and the earth magnetic SoR, E , respectively (\mathbf{S} is about "shoulder").

The relative angles were then obtained by decomposing the relative orientation of the technical SoRs with the following sequences of Euler angles:

- S_FE, S_AA, and S_IE with the sequence $YX'Z''$ for almost sagittal tasks;
- S_AA, S_FE, and S_IE with the sequence $XY'Z''$ for almost frontal tasks;
- S_IE, S_AA, and S_FE with the sequence $ZX'Y''$ for almost transverse tasks;

The effectiveness of the procedure to align the IMU technical SoRs was evaluated for each type of task in terms of RMSEs between the global SoR-based and the earth magnetic field SoR-based estimated angles.

Body-segments anatomical system of reference

In order to define the anatomical SoRs $x_a y_a z_a$ of the thorax, arm and forearm, and to express the orientation of these anatomical SoRs with respect to the IMU technical SoRs xyz , some easy exercises administered in a functional calibration procedure were performed. The body-segments angular kinematics with respect to the IMU global SoR XYZ was thus estimated, and the relationship between corresponding anatomical and technical SoRs was calculated.

The functional calibration of the body-segment anatomical axes is focused on the evaluation of the functional axes of rotation of each segment of interest [48], using accelerometer and gyroscope data. After the static and dynamic calibration for the IMU technical SoRs alignment procedure, subject was asked to perform the following series of well defined, uni-axial rotations, five times each, avoiding the extremes of the range of motion:

Thorax

- perform five times forward flexion of the trunk (0° to 40° flexion), keeping the arms aligned with the thorax and trying to avoid neck flexion, starting and ending adopting the SAP for a few second, in order to estimate the functional axis of thorax flexion/extension, y_a ;
- from standing, adopt SAP for five seconds, in order to estimate the functional axis of thorax lateral flexion, x_a .

Arm

- while seated, with the olecranon supported at a table and the elbow flexed at about 90° , perform five times internal rotation of the humerus, trying to avoid elbow flexion-extension, or forearm prono/supination during the movement, in order to estimate the functional axis of arm axial rotation, z_a ;
- while seated, with both olecranons supported at a table and the elbows at shoulder breadth, holding a stick with both hands at shoulder breadth, with thumbs pointing laterally, perform five times elbow extension (20° to 50° extension), in order to estimate the functional axis of arm flexion/extension, y_a . Since movement of the forearm is used to define the lateral axis of the humerus which is not moving,

data from the IMU on the forearm is expressed in the SoR of the IMU on the humerus.

Forearm

- while seated, with the olecranon supported at a table and the ulna supported and fixated to avoid internal/external rotation of the humerus during the movement, perform five times pronation of the forearm, in order to estimate the functional axis of forearm axial rotation, z_a ;
- perform the same procedure as in obtaining the functional axis of arm flexion/extension, in order to obtain the functional axis of forearm flexion/extension, y_a . Data from the IMU on the forearm is expressed in its SoR.

The definitions of the anatomical SoR $x_a y_a z_a$ of the thorax, arm and forearm body-segments (Table 5.1) are thus applied, considering x_a -axis pointing anteriorly, y_a -axis pointing laterally to the left, and z_a -axis pointing vertically. Angular velocity measured by the IMUs was used as an estimate of the functional axis of rotation (averaged over time, and normalized to unit length) [117]. To enable a clear segmentation, each series of movements was followed by a stop of at least two seconds. To ensure a high signal-to-noise ratio, a cut-off of 30% of the maximal angular velocity amplitude was used.

According to the above explained functional calibration procedure, the three rotation matrices between the anatomical SoR $x_a y_a z_a$ of each body-segment and the IMU global SoR XYZ are calculated as follows:

$${}^G \mathbf{R}(\mathbf{T}, \mathbf{A}, \mathbf{F})_A = \begin{bmatrix} \mathbf{x}_{a,(T,A,F)} \\ \mathbf{y}_{a,(T,A,F)} \\ \mathbf{z}_{a,(T,A,F)} \end{bmatrix}^T \quad (5.21)$$

Table 5.1: Definition of the anatomical SoRs of each body-segment (right upper limb). All vectors are expressed in the IMU global SoR. Symbol \wedge denotes the cross product

Body-segment	Anatomical axes definition
Thorax	$\mathbf{y}_{a,T} = [\bar{\omega}T_x \quad \bar{\omega}T_y \quad \bar{\omega}T_z] / \left\ [\bar{\omega}T_x \quad \bar{\omega}T_y \quad \bar{\omega}T_z] \right\ $ $\mathbf{x}_{a,T} = \mathbf{y}_{a,T} \wedge [\bar{a}T_x \quad \bar{a}T_y \quad \bar{a}T_z] / \left\ \mathbf{y}_{a,T} \wedge [\bar{a}T_x \quad \bar{a}T_y \quad \bar{a}T_z] \right\ $ $\mathbf{z}_{a,T} = \mathbf{x}_{a,T} \wedge \mathbf{y}_{a,T} / \left\ \mathbf{x}_{a,T} \wedge \mathbf{y}_{a,T} \right\ $
Arm	$\mathbf{z}_{a,A} = [\bar{\omega}A_x \quad \bar{\omega}A_y \quad \bar{\omega}A_z] / \left\ [\bar{\omega}A_x \quad \bar{\omega}A_y \quad \bar{\omega}A_z] \right\ $ $\mathbf{y}_{a,A} = [\bar{\omega}F_x \quad \bar{\omega}F_y \quad \bar{\omega}F_z] / \left\ [\bar{\omega}F_x \quad \bar{\omega}F_y \quad \bar{\omega}F_z] \right\ $ $\mathbf{x}_{a,A} = \mathbf{y}_{a,A} \wedge \mathbf{z}_{a,A} / \left\ \mathbf{y}_{a,A} \wedge \mathbf{z}_{a,A} \right\ $
Forearm	$\mathbf{z}_{a,F} = [\bar{\omega}F_x \quad \bar{\omega}F_y \quad \bar{\omega}F_z] / \left\ [\bar{\omega}F_x \quad \bar{\omega}F_y \quad \bar{\omega}F_z] \right\ $ $\mathbf{y}_{a,F} = [\bar{\omega}F_x \quad \bar{\omega}F_y \quad \bar{\omega}F_z] / \left\ [\bar{\omega}F_x \quad \bar{\omega}F_y \quad \bar{\omega}F_z] \right\ $ $\mathbf{x}_{a,F} = \mathbf{y}_{a,F} \wedge \mathbf{z}_{a,F} / \left\ \mathbf{y}_{a,F} \wedge \mathbf{z}_{a,F} \right\ $

The constant relationship between corresponding anatomical and technical SoRs for each body-segment is then calculated according to Equations (5.19) and (5.21) as follows:

$$\begin{aligned}
 {}^A\mathbf{RT}_T &= {}^G\mathbf{RT}_A^T \cdot {}^G\mathbf{RT}_T \\
 {}^A\mathbf{RA}_T &= {}^G\mathbf{RA}_A^T \cdot {}^G\mathbf{RA}_T \\
 {}^A\mathbf{RF}_T &= {}^G\mathbf{RF}_A^T \cdot {}^G\mathbf{RF}_T
 \end{aligned} \tag{5.22}$$

Joint kinematics evaluation

The alignment and the functional calibration procedures require to perform six easy and fast exercises (some exercises can be used for both procedures), schematically represented in Figure 5.9.

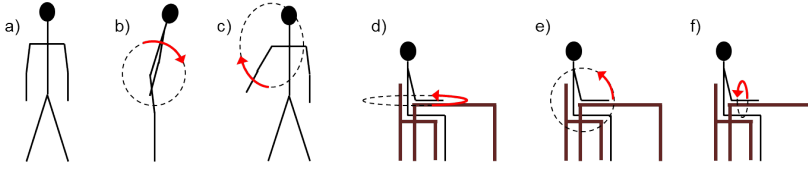


Figure 5.9: Exercises required by the alignment and functional calibration procedures: a) static, b) thorax and arm flexion/extension, c) arm and forearm abduction/adduction, d) arm internal/ external rotation, e) forearm flexion/extension, f) forearm pronation/ supination

After the alignment and functional calibration procedures, subject was asked to perform some similar exercises, administered by the FMA, selected thanks their broad content regarding the kinematic information obtained during the upper limb movements. Starting from the SAP, the subject was asked to perform the following series of exercises, five times each, at a self-selected velocity:

1. arm flexion/extension
2. arm abduction/adduction
3. arm internal/external rotation

During each exercise, the EKF was applied to accelerometer and gyroscope outputs for the thorax, the arm and the forearm body-segments, in order to provide the IMUs angular kinematics with respect to the IMUs global SoR. Estimated rotation angles and rotation matrices were calculated at every instant of time k , for the thorax, the arm and the forearm, following the steps shown in Equation (5.23):

$$\begin{aligned}
 & a(T, A, F)_x(k) \quad \omega(T, A, F)_x(k) \\
 & a(T, A, F)_y(k) \quad \omega(T, A, F)_y(k) \longrightarrow EKF \longrightarrow \\
 & a(T, A, F)_z(k) \quad \omega(T, A, F)_z(k) \\
 & \quad \text{roll}(T, A, F)(k) \\
 & \longrightarrow \text{pitch}(T, A, F)(k) \Rightarrow {}^G\mathbf{R}(\mathbf{T}, \mathbf{A}, \mathbf{F})_T(k) \quad (5.23) \\
 & \quad \text{yaw}(T, A, F)(k)
 \end{aligned}$$

Considering the result of (5.22), the rotation matrices related to the body-segment anatomical SoRs with respect to the IMUs global SoR during the exercises were provided by:

$${}^G\mathbf{R}(\mathbf{T}, \mathbf{A}, \mathbf{F})_A(k) = {}^G\mathbf{R}(\mathbf{T}, \mathbf{A}, \mathbf{F})_T(k) \cdot {}^A\mathbf{R}(\mathbf{T}, \mathbf{A}, \mathbf{F})_A^T \quad (5.24)$$

Joint kinematics were obtained considering the relative orientation between the anatomical SoRs related to adjacent body-segments:

$$\begin{aligned} \mathbf{RS}(k) &= {}^G\mathbf{RT}_A^T(k) \cdot {}^G\mathbf{RA}_A(k) \\ \mathbf{RE}(k) &= {}^G\mathbf{RA}_A^T(k) \cdot {}^G\mathbf{RF}_A(k) \end{aligned} \quad (5.25)$$

where $\mathbf{RS}(k)$ is the rotation matrix which describes the relative orientation between arm and thorax anatomical SoRs, where \mathbf{S} is about "shoulder", and $\mathbf{RE}(k)$ is the rotation matrix which describe the relative orientation between forearm and arm anatomical SoRs, where \mathbf{E} is about "elbow".

The shoulder and elbow angles (see Figure 5.6) were then obtained, at every instant of time k , by decomposing the relative orientation of the anatomical SoRs with the following sequences of Euler angles:

- S_FE, S_AA, S_IE and E_FE, E_CA, E_PS with the sequence $YX'Z''$ for almost sagittal tasks;
- S_AA, S_FE, S_IE and E_CA, E_FE, E_PS with the sequence $XY'Z''$ for almost frontal tasks;
- S_IE, S_AA, S_FE and E_PS, E_CA, E_FE with the sequence $ZX'Y''$ for almost transverse tasks.

In order to validate the method presented in this Chapter for the estimation of upper limb joints kinematics using inertial sensors, a SP system was used (Vicon, mod. Bonita). A cluster of markers glued on each IMU was used as the motion tracking device, and a standard anatomical calibration was carried on for the body-segment anatomical axes definitions [24]. Considering the recommendations provided by

ISB [212] (see Figure 5.10), the bony-landmarks which were measured are shown in the following list:

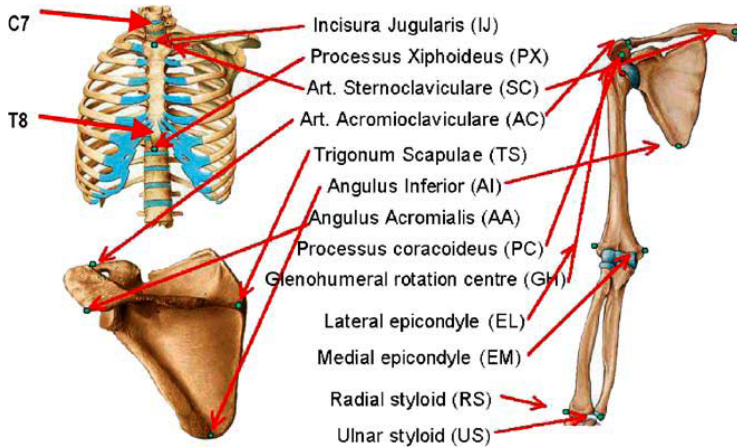


Figure 5.10: Bony-landmarks of the upper limb body-segments. Image is from [212]

Thorax

- C7: processus spinosus of the 7th cervical vertebra
- T8: processus spinosus of the 8th thoracic vertebra
- IJ: deepest point of incisura jagularis
- PX: processus xiphoideus, the most caudal point of the sternum

Arm

- GH: glenohumeral joint rotation center, estimated by the regression model described in [134], which used the following scapula bony-landmarks:
 - AC: Most dorsal point on the acromioclavicular joint (shared with the scapula)

- TS: Trigonum Spinae Scapulae, the midpoint of the triangular surface on the medial border of the scapula in line with the scapular spine
- AI: Angulus Inferior of the scapula, the most caudal point
- AA: Angulus Acromialis of the scapula, the most latero-dorsal point
- PC: Most ventral point of processus coracoideus
- EL: Most caudal point on lateral epicondyle
- EM: Most caudal point on medial epicondyle
- RS: Most caudal–lateral point on the radial styloid
- US: Most caudal–medial point on the ulnar styloid

Forearm

- EL: Most caudal point on lateral epicondyle
- EM: Most caudal point on medial epicondyle
- RS: Most caudal–lateral point on the radial styloid
- US: Most caudal–medial point on the ulnar styloid

5.3 Results

5.3.1 2D real-time multi-link kinematics

First results were obtained evaluating the performance of the EKF procedure using a 2D mechanical arm, consisting in three links which model the upper limb kinematic chain in the sagittal plane. By way of example, estimated angles for shoulder, arm and forearm and residuals obtained from comparison between IMU-based and encoders angles are shown in Figure 5.11 for one trial.

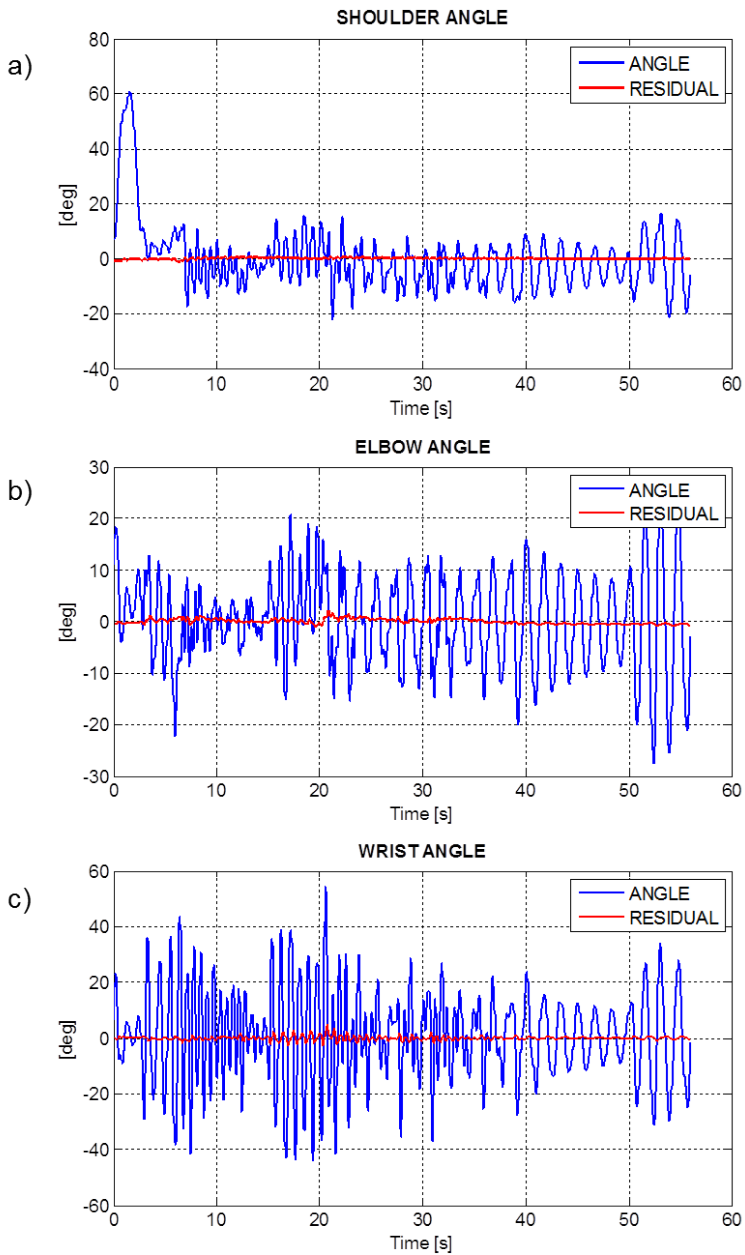


Figure 5.11: Pattern of: a) shoulder angle, b) elbow angle, c) wrist angle (blue line) and residual errors (red line) during a trial

RMSEs and percentages of the ratio RMSE/peak-to-peak range (P-P), averaged on the five trials, are 0.31° (0.4%), 0.49° (0.7%), 0.74° (0.8%) for arm, forearm and hand angles, respectively. Angular excursions performed are about 81.26° , 65.58° , 97.32° , for the three links. Real-Time performance are guaranteed. In order to accurately run the EKF procedure, the values $Q(i, i)$, $i = (3, 6, 9)$ and the elements of the diagonal of \mathbf{R} were set after an optimization procedure, in which the encoders were assumed as validation instruments.

5.3.2 3D upper limb kinematics

In order to develop an innovative technique for the upper limb kinematics evaluation, which could be applied to instrument functional test as FMA, first results concern the usability and the accuracy of the procedure for the alignment of the IMU technical SoRs, to provide a common global SoR and neglecting the use of any magnetometers in the sensors set-up. Then, results in terms of joint kinematics are then provided, considering the comparison between a functional procedure and the traditional anatomical procedure to estimate body-segments anatomical axes, starting from inertial sensors and bony-landmarks data, respectively.

IMU relative kinematics evaluation

For each performed task (three arm flexion/extension, three arm ab/ adduction, three arm internal/external rotation), relative angles between the technical SoRs of the IMUs placed on the arm and the thorax are calculated applying the EKF to the accelerometer and gyroscope outputs of each body-segment, and carrying on the alignment procedure of the IMU technical SoRs in order to describe the kinematics with respect to a common global SoR. The relative angles obtained from the orientation data provided by the IMU with respect to the earth magnetic field SoR (thanks to the use of a magnetometer) are used for validation.

RMSEs and Standard Deviations (STDs), related to each single relative-angle and averaged on the three trials performed for each type of task, are reported in Table 5.2. Mean errors range from 0.4° to 5.3° , with a mean value equal to 1.7° . Overlooking the type of exercise, mean errors are about 1.3° , 0.7° , 3.1° for relative angles of flexion/extension, ab/adduction and intra/extra rotation, respectively.

Table 5.2: RMSEs and STDs related to the relative angles between the technical SoRs of the IMUs placed on the arm and the thorax, averaged on three trials for each task

TASK	SHOULDER	
	Relative angle	RMSE [°] Mean±STD
Arm flexion/extension	S_FE	1.3±0.2
	S_AA	0.5±0.1
	S_IE	0.5±0.1
Arm abduction/adduction	S_AA	1.2±0.2
	S_FE	1.8±0.2
	S_IE	3.4±0.3
Arm internal/external rotation	S_IE	5.3±0.3
	S_AA	0.4±0.1
	S-FE	0.7±0.1

By way of example, estimated relative angles and residuals between global SoR-based and earth magnetic field SoR-based results are reported in Figures 5.12, 5.13, and 5.14 for one task of arm flexion/extension, arm ab/adduction, and arm internal/external rotation, respectively.

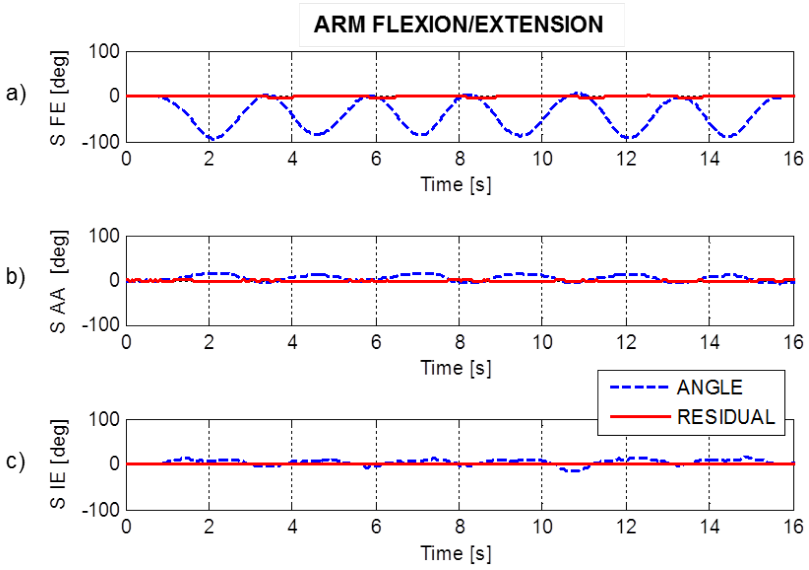


Figure 5.12: Relative angles between technical SoRs of the IMUs placed on the thorax and the arm (blue dashed line) and residual errors (red solid line) for an arm flexion/extension task: a) shoulder flexion/extension, b) shoulder ab/adduction, c) shoulder internal/external rotation, d) elbow flexion/extension

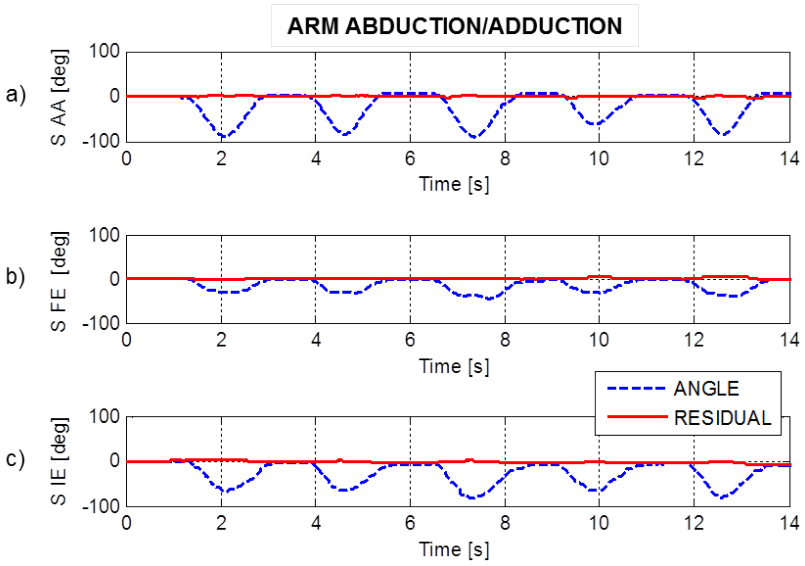


Figure 5.13: Relative angles between technical SoRs of the IMUs placed on the thorax and the arm (blue dashed line) and residual errors (red solid line) for an arm ab/adduction task: a) shoulder ab/adduction, b) shoulder flexion/extension, c) shoulder internal/external rotation

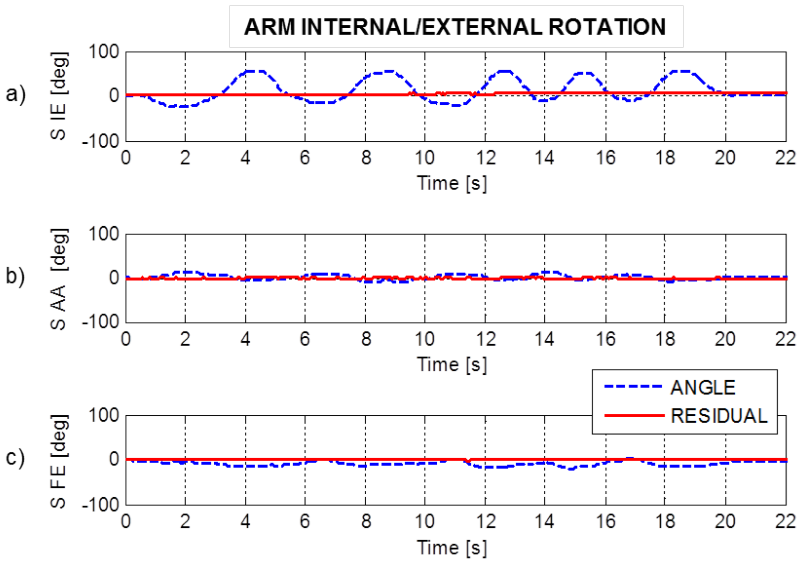


Figure 5.14: Relative angles between technical SoRs of the IMUs placed on the thorax and the arm (blue dashed line) and residual errors (red solid line) for an arm intra/extra rotation task: a) shoulder internal/external rotation, b) shoulder ab/adduction, c) shoulder flexion/extension

Joint kinematics evaluation

Relative angles between arm and thorax, and forearm and arm, anatomical SoRs are calculated applying the EKF to the IMU outputs, carrying on the alignment procedure of the IMU technical SoRs and the functional calibration of the anatomical axes. The relative angles obtained from the data provided by the SP system are used for validation, applying the standard anatomical calibration [24].

RMSEs and STDs, related to each single-joint-angle and averaged on the three trials performed for each type of task, are reported in Table 5.3. Mean errors range from 1.2° to 5.2° , with a mean value equal to 2.7° for shoulder angles and equal to 3.2° for elbow angles. Overlooking the type of task, mean errors are about 3.1° , 2.4° , 2.6° for shoulder angles of flexion/extension, ab/adduction and intra/extra rotation, respectively, and are about 2.9° , 3.2° , 3.6° for elbow angles of flexion/extension, pronosupination and carrying angle, respectively. Joint angles estimated by IMU data and measured by SP system are reported in Figures 5.15, 5.16, and 5.17 for one task of arm flexion/extension, arm ab/adduction, and arm intra/extra rotation, respectively.

Table 5.3: RMSEs and STDs related to the joint angles of shoulder and elbow, averaged on three trials for each task

TASK	SHOULDER		ELBOW	
	Joint angle	RMSE [°] Mean±STD	Joint angle	RMSE [°] Mean±STD
Arm flexion/extension	S_FE	1.9±0.3	E_FE	2.2±0.4
	S_AA	2.3±0.4	E_CA	3.1±0.5
	S_IE	3.1±0.4	E_PS	3.1±0.5
Arm abduction/adduction	S_AA	2.6±0.4	E_CA	4.1±0.6
	S_FE	3.5±0.6	E_FE	4.6±0.7
	S_IE	1.4±0.3	E_PS	5.2±0.7
Arm internal/external rotation	S_IE	3.4±0.6	E_PS	1.2±0.2
	S_AA	2.4±0.4	E_CA	3.6±0.4
	S-FE	3.9±0.6	E_FE	1.8±0.3

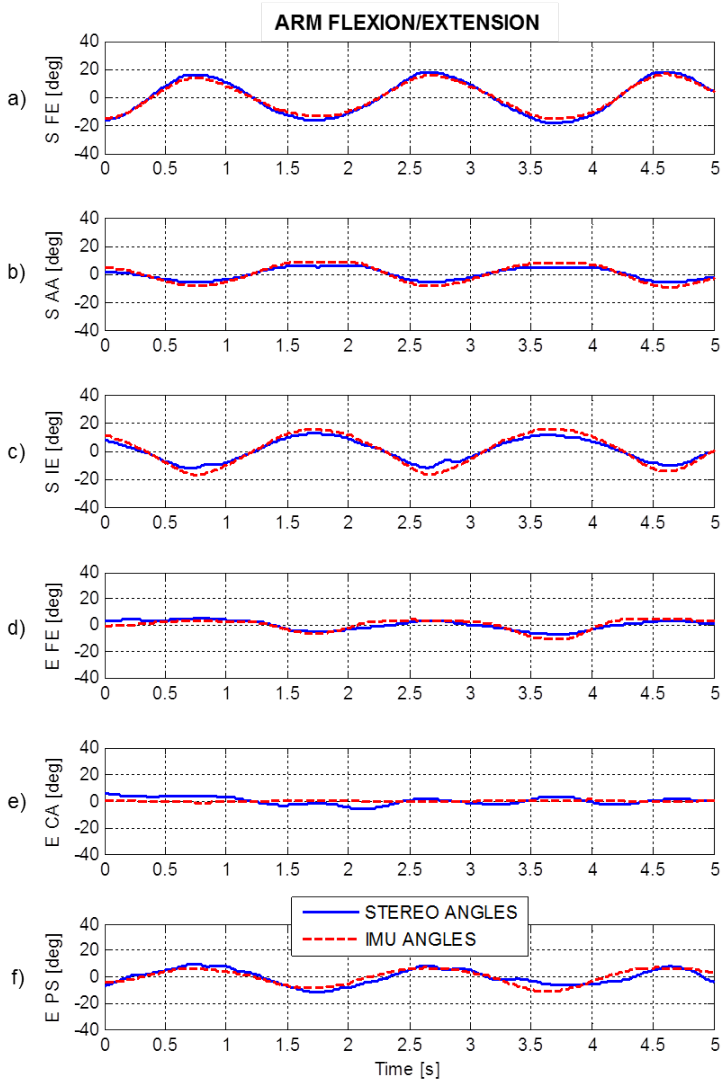


Figure 5.15: Joint angles measured by SP system (blue solid line) and estimated by IMU data (red dashed line) for an arm flexion/extension task: a) shoulder flexion/extension, b) shoulder ab/adduction, c) shoulder internal/external rotation, d) elbow flexion/extension, e) carrying angle, f) elbow pronation/supination

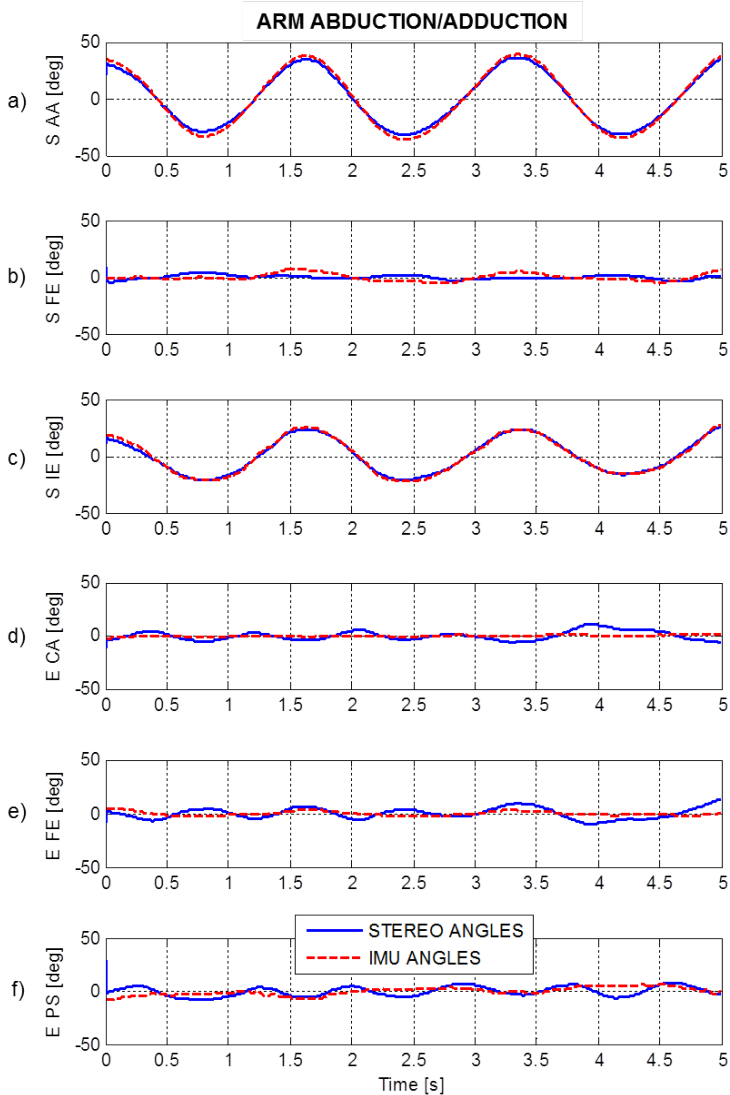


Figure 5.16: Joint angles measured by SP system (blue solid line) and estimated by IMU data (red dashed line) for an arm ab/adduction task: a) shoulder ab/adduction, b) shoulder flexion/extension, c) shoulder internal/external rotation, d) carrying angle, e) elbow flexion/extension, f) elbow pronation/supination

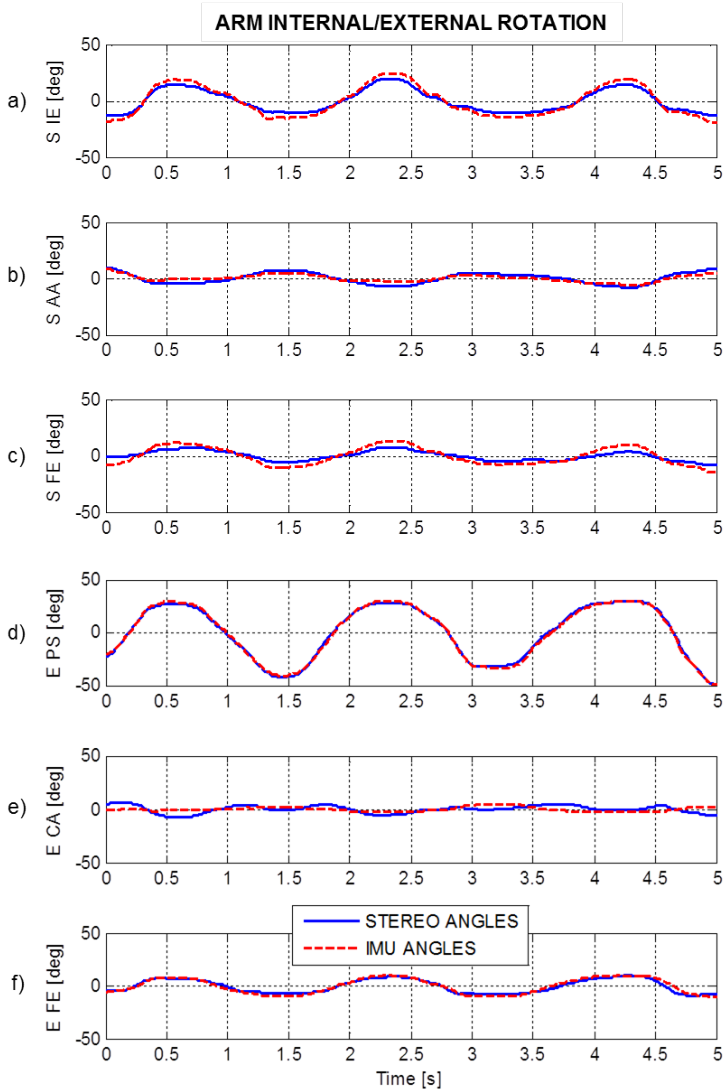


Figure 5.17: Joint angles measured by SP system (blue solid line) and estimated by IMU data (red dashed line) for an arm intra/extra rotation task: a) shoulder internal/external rotation, b) shoulder ab/adduction, c) shoulder flexion/extension, d) elbow pronation/supination, e) carrying angle, f) elbow flexion/extension

5.4 Discussion

This Chapter suggests a novel method aimed at estimating upper extremity joint kinematics, using one IMU per body-segment during some easy exercises administered by the FMA, taking advantage by the use of a sensor fusion algorithm based on an extended KF, and considering the upper limb as a kinematic chain of 3-link (thorax, arm and forearm, respectively). This approach allows to instrument a functional test such as the FMA, enabling quantitative assessment of motor performance on a subject-specific basis, overcoming the limitations due to the lack of objectiveness related to individual judgment, and possibly disclosing subtle alterations that are not clearly visible to the observer.

The method was based on the extension of the 2D approach validated on a mechanical arm instrumented with encoders. Results obtained during that controlled experiment confirm the usability of the extended KF for kinematics estimation.

Several authors in recent published studies have underlined the lack of an unambiguous distinction between *recovery* (the reacquisition of such elemental motor patterns) and *compensation* (the adaptation of remaining motor elements) in stroke rehabilitation, showing that motor scales that assess impairments (Body Functions/Structure level) rather than disability (Activity level) cannot reliably make this distinction and cannot provide an appreciation of the movement quality [99, 111] (see Figure 1.5). This lack concerns about the extent to which rehabilitative interventions provide improvements in reduction of impairment among the patients. Indeed, motor compensation in the upper limb can include the use of movement patterns that incorporate trunk displacement and rotation, scapular elevation, shoulder abduction and internal/external rotation [109, 166]. The use of increased trunk movement to assist arm and hand transport [32, 190], and to aid in hand positioning/orientation for grasping [135], are example of adaptive compensatory strategies. The degree of motor compensations is also related to the severity of the hemiparesis, conditioning the appropriate interventions.

At the Body Function/Structure level, the emphasis is on the quality of movement regardless of movement outcome or task accomplishment. Recovery at this level would be characterized by the reappearance of movement patterns and by a decrease in spasticity or by a reduction in trunk displacement during a reaching or pointing movement. Adaptive compensation at this level would be characterized by the appearance of alternative movement patterns during the accomplishment of a task. Numerous valid and reliable clinical scales measure impairments at this level [19, 61, 74, 108, 110]. Although these scales may offer the clinicians an appreciation of impairments, more detailed kinematic analysis of motor patterns during the performance of functional tasks would provide even more relevant information about movement patterns and motor compensation. At the Activity level, recovery requires that the task is performed using the same end effectors and joints of the movement patterns typically used by non-disabled individuals. Compensation often takes the form of substitution and would be noted if the patients were able to accomplish the task using alternative joints or end effectors. Typical clinical scales [44, 86, 90, 126, 195, 197, 214] neither specify how the task is accomplished nor which compensatory movements were used in place of typical motor patterns.

In this perspective, the method for the upper limb joint kinematics estimation presented in this Chapter, which uses only a tri-axial accelerometer and a tri-axial gyroscope per segment, and an extended KF to estimate body-segment orientations, could have several positive feedbacks from clinical applications and may help overcoming the above described drawbacks. Portable and cost-effective inertial sensors represent an easy non-invasive alternative for the qualitative and subjective evaluation of motor performance during functional tests.

One of the main aims of the present study was to develop a new procedure in order to align the technical SoR of each IMU, obtaining a common global SoR through the use of accelerometers and gyroscopes data recording during three easy exercises. Previously published studies focused on the use of commercial IMU containing inertial and magnetic

sensors, using gravity and heading of the earth magnetic field, assumed homogeneous at all, to define a common global SoR. These sensors are able to estimate IMU orientation through the use of an inboard sensors fusion algorithm. The probably no optimal conditions of the earth magnetic field represent the main limit of these sensors, both in clinical and domestic environments, where it is usual the presence of iron in floors, walls and ceilings or other equipments, which produce disturbances in the earth magnetic field.

In order to demonstrate the effectiveness of the suggested alignment procedure, estimated global SoR-based relative angles were compared with those provided by the orientation data recorded from the IMU, i.e. the earth magnetic field SoR-based relative angles (see Figures 5.12, 5.13, and 5.14 for one task of arm flexion/extension, arm ab/adduction, and arm internal/external rotation, respectively). As shown in Table 5.2, mean errors, averaged on the three trials performed for each motor tasks, range from 0.4° to 5.3° , with a mean value equal to 1.7° . Overlooking the type of exercise, mean errors are about 1.3° , 0.7° , 3.1° for relative angles of shoulder flexion/extension, ab/adduction and intra/extra rotation, respectively. These considerations confirm the accuracy of the alignment procedure presented in this Chapter, which allow to neglect the use of any magnetometers in the experimental set-up and to obtain a common global SoR useful for relative angles estimation.

Several authors in previously published studies used relative angles between IMUs to describe 3D arm movements, taking no notice of the real bone movements [191, 17, 218]. In order to obtain the joint kinematics the relative orientation between adjacent anatomical SoRs is necessary. A practical solution is suggested in this Chapter in order to define anatomical body-segment axes through the application of a functional calibration of the axes of rotation of the body-segments. This procedure, initially defined by De Vries *et al.* [48], takes into account the angular velocity (averaged over time and normalized to unit length) measured by the IMUs during some defined exercises, using it as an estimate of the functional axis of rotation [117].

In order to support the usability and the accuracy of the method, the results obtained by a SP system were compared with those obtained by the technique presented in this Chapter, evaluating the distances affecting joint angles between the functional calibration results and the standard anatomical calibration results, based on bony-landmarks recordings [24, 212] (see Figures 5.15, 5.16, and 5.17 for one task of arm flexion/extension, arm ab/adduction, and arm internal/external rotation, respectively). As shown in Table 5.3, mean errors, averaged on the three trials performed for each motor tasks, range from 1.2° to 5.2° , with a mean value equal to 2.7° for shoulder angles and equal to 3.2° for elbow angles. Overlooking the type of task, mean errors are about 3.1° , 2.4° , 2.6° for shoulder angles of flexion/extension, ab/adduction and intra/extra rotation, respectively, and are about 2.9° , 3.2° , 3.6° for elbow angles of flexion/extension, prono/supination and carrying angle, respectively. These results are affected by errors provided by both IMU-based system and SP system, and the distances between each couple of single-joint-angles is the sum of two contributions. The first is related to the errors committed during the functional calibration for the anatomical axes definition: angular velocities measured by IMUs during this procedure are strongly related to the goodness of the movements. On the other side, the second contribution is due to the errors committed during the anatomical calibration (accuracy in bony-landmarks palpation, assumption of a regression model [134] to estimate the glenohumeral joint rotation center, soft tissue artifacts). These considerations support the obtained results, which are almost always lower than 4° . Considering the type of the performed motor tasks, that principally involved the shoulder joint and the arm body-segment, and in minor measure the elbow and the forearm body-segment, estimated shoulder joint angles are more accurate than estimated elbow joint angles, which show a smaller range of motion than the one related to shoulder.

Joint angles estimation errors are consistent with those presented in previously published studies [39, 48, 117], which used the orientation

data provided by inboard sensors fusion algorithm of commercial IMUs, and are based on magnetometer outputs.

The motion analysis protocol presented in this Chapter, overcoming the limitations and the lacks in objectivity of the clinical scales, could be applied in different scenarios of the upper limb functional evaluation and rehabilitation post-stroke. A recent and promising approach is the use of virtual reality systems, that may enable simulated practice of functional tasks at a higher dosage than traditional therapies [102, 133]. Virtual reality has been defined as the “use of interactive simulations created with computer hardware and software to present users with opportunities to engage in environments that appear and feel similar to real-world objects and events” [199]. In virtual rehabilitation, virtual environments and objects provide the user with visual feedback which may be presented through a head-mounted device, projection system or flat screen. Feedback may also be provided through the senses, for example, hearing, touch, movement, balance and smell [199], and the user interacts with the environment by a variety of mechanisms (simple devices, mouse, joystick, cameras, sensors or haptic feedback devices, etc.). Key concepts related to virtual reality are immersion and presence.

Virtual reality may be advantageous as it offers several features, such as goal-oriented tasks and repetitions, shown to be important in neurological rehabilitation [50] to improve upper [81] and lower extremity functions, gait [46], cognition, perception, and functional tasks such as crossing a street, driving, preparing food and shopping [170]. Virtual reality may have the potential to provide an enriched environment in which people with stroke can solve problems and master new skills. Researches with animals and humans have shown that intensive task-specific practice is able to induce cortical reorganisation [145, 146] and behavioral change [40]. Virtual reality programs capitalize on this by offering simulated real-life functional activities, and grading of tasks and immediate feedback have been shown to optimize motor learning [181].

Although its research in rehabilitation is becoming more prevalent as technology becomes more accessible and affordable [22], the use of virtual reality is not yet commonplace in clinical rehabilitation settings. However, gaming consoles are ubiquitous and so researchers and clinicians are turning to low-cost commercial gaming systems as an alternative way of delivering virtual reality [45, 161]. These systems, which were originally designed for recreation, are being adapted by clinicians for therapeutic purposes. In addition, interactive video games are specifically being designed for rehabilitation [104]. Considering these perspectives, the authors of the last Cochrane review [105] suggest that virtual reality is a promising new rehabilitation approach for stroke recovery, with reasonable effect sizes (that is a moderate effect on arm function and large effect on ADL functions). However, at present, they remind that the studies are too few and too small to draw conclusions. Laver *et al.* [105], underline that as virtual reality interventions may vary greatly (from inexpensive commercial gaming consoles to expensive customized programs), it is unclear what characteristics of the intervention are most important, which type of patients is most likely to benefit, and at what point in their rehabilitation it should be used.

In this perspective, the use of objective biomechanical measurements provided by the inertial sensor-based technique presented in this Chapter, may help clinicians to objectively track changes in motor ability following neurological injury, providing timely feedback about the effectiveness of administered rehabilitation interventions and enabling intervention strategies to be modified or changed if found to be ineffective. Moreover, objective biomechanical measurements related to upper extremity joint kinematics may be used as input data of several virtual reality systems, supporting the rehabilitative exercises, such as goal-oriented tasks and repetitions, with a clear numeric feedback representative of subjects motor performance.

Future developments will address to: i) improve functional calibration procedure mainly for pathological patients, whose movements may

differ from healthy subjects, ii) involve more subjects and increase the number of exercises in order to further validate the usability of the technique.

Epilogue

The aims of this Thesis were to suggest novel methods for the quantitative description of several motor task during some functional tests, typical of the clinical practice. The use of a body-sensors network and the application of a biomechanical approach allowed evaluating kinematic and dynamic variables of human movement, which are usually neglected in widespread clinical tests for the assessment of motor performances. The need for objective, cost-effective and clinically applicable methods, has inspired this Thesis, knowing that instrumented tests would enable quantitative assessment of performance on a subject-specific basis, overcoming the limitations due to the lack of objectiveness related to individual judgment, and possibly disclosing subtle alterations that are not clearly visible to the observer.

In **Chapter 1** a brief introduction about the human movement assessment and the inertial sensor- and model-based instrumentation of functional tests was provided.

In **Chapter 2** a quantitative assessment tool was provided in order to estimate body sway angles of a 2D multi-link kinematic chain, using a single-axis accelerometer (SAA) per segment. To evaluate the method, the algorithm for angular displacement estimation was tested on a subject performing a squat task, considering a 3-link biomechanical model and applying a bi-directional low pass filter to the SAA outputs. Results demonstrated the usability of the method, showing errors lower than 1° for the considered body-segments and suggesting the opportunity to evaluate compensatory postural strategies in a easy

and portable way in different functional tasks, considering a generic kinematic chains of any number of link.

In **Chapter 3** a functional subject-specific 2D evaluation tool was proposed in order to estimate body-segment anthropometric parameters during a repeated sit-to-stand motor task, using a SAA per segment and a force plate. After this preliminary estimation, a quantitative assessment tool was provided in order to predict the ground reaction forces, the centers of pressure and mass, and the net joint moments of a subject performing a repeated sit-to-stand task, considering a 2D 3-link biomechanical model and using a SAA per segment only. Results confirmed the accuracy of the technique, showing errors on predicted center of pressure and on ankle joint moment equal to about 2cm and 10Nm, respectively, demonstrating the usability of this instrumented test in the clinical practice.

In **Chapter 4** the quantitative assessment tool to estimate body sway angles (presented in Chapter 2) was applied to the voluntary postural sway functional test, in order to provide information about the kinematic strategies adopted by a subject during a self-imposed perturbed stance. A SAA per segment was used and three biomechanical models, from 1- to 3-link, were evaluated in order to describe as well as possible the sway movement. In addition, the quantitative assessment tool to predict kinematic and dynamic variables (presented in Chapter 3) was applied to the voluntary postural sway functional test in order to predict the ground reaction forces and the centers of pressure and mass of the subject, considering a 2D 3-link biomechanical model and using a SAA per segment. Results confirmed the accuracy of the technique, showing errors on predicted center of pressure equal to 6mm, suggesting the suitability of this method for the response strategy evaluation to unexpected perturbation, providing objective information to evaluate the balance control in several application of the clinical practice.

In addition to the accelerometers, in **Chapter 5** gyroscopes were used for the estimation of the upper limb kinematics, considering a 3D 3-link biomechanical model. A sensor consisting of a tri-axes accelerom-

eters and a tri-axes gyroscope was placed to each body-segment, and a Kalman Filter-based algorithm was applied. A preliminary sensor technical systems of reference alignment procedure, using accelerometers and gyroscopes data only, allows the definition of a common global system of reference, neglecting the use of any magnetometers in the experimental set-up, which are typical affected by disturbances due to the presence of iron in both clinical and domestic environments. Shoulder and elbow joint angles are estimated during some easy exercise of the Fugl-Meyer Motor Assessment after a functional calibration of the body-segment anatomical axes, showing mean errors lower than 4° and confirming the accuracy of the technique. The instrumentation of these functional tasks will provide an objective evaluation of motor performance in patients following a stroke, and may be considered also for functional evaluation and rehabilitation after different neurological and orthopedic injuries.

Future works

In agreement with the line of reasoning presented in this Thesis, it seems that a logical next step would be to start prospective studies involving pathological and elderly subjects, whose biomechanical measurements will be evaluated through the algorithms presented in this Thesis. In this perspective, the use of objective biomechanical measurements in the context of the rehabilitation, provided by inertial sensor-based technique, may help clinicians to: i) objectively track changes in motor ability, ii) provide timely feedback about the effectiveness of administered rehabilitation interventions, iii) enable intervention strategies to be modified or changed if found to be ineffective, and iv) speed up the experimental sessions when several subjects are asked to perform different functional tests.

Acknowledgements

This thesis would not have been possible without the support of Prof. Angelo Cappello, who introduced me to the rehabilitation bio-engineering research field and supervised my work. I wish to take the opportunity to thank also Prof. Lorenzo Chiari and Prof. Guido Avanzolini for their smart suggestions, and Prof. Kamiar Amian for letting me the chance to work in his laboratory at the École Polytechnique Fédérale de Lausanne for several months.

A special thanks is dedicated to my colleagues, for the hours and hours shared with them, inside and outside the laboratory, learning from each other to face our troubles: Elena, Chiara, Federico, Giacomo, Gonzalo, Luca, Pierpaolo, Sabato... and all the new and the old entry in our group.

I cannot forget to mention my family, mum, dad and Marco, and all my friends, Cristina first of all, for their support and company during the whole PhD course, during the all my life: thank you all!

Finally, I want to reserve one of the last sentence of this page to my lovely partner Fabio: you are my best result, and I want to thank you for having stayed at my side during recent years, come rain or come shine...

...and thanks to me, for having granted my wish. Good luck!

List of Figures

1.1	Schematic representation of the circular path describing contemporary medicine	2
1.2	Classification of the common motion capture systems	3
1.3	A single-axis accelerometer consisting of a mass suspended by a spring	5
1.4	a) A conventional spinning wheel gyroscope, b) a vibrating mass gyroscope consisting in a mass subjected to the Coriolis effect	6
1.5	Integrated model of the rehabilitation cycle incorporating the World Health Organization’s International Classification of Functioning, Disability and Health (WHO-ICF) model. Image is adapted from [172]	12
2.1	a) Inverted Pendulum Model, b) Mechanical Inverted Pendulum	21
2.2	Linear array of SAAs	25
2.3	Experimental testing set-up	27
2.4	Three-link biomechanical model	28
2.5	Snake-like profile for a 40-link kinematic chain	31
2.6	Shank, thigh, HAT angular patterns in prediction	33
3.1	N -link free-body diagram in the sagittal plane	42
3.2	Schematic representation of the two TIP models	47
3.3	RMSEs of: a) \mathbf{F}_X , b) \mathbf{F}_Z , c) $\Delta\mathbf{CoP}_X$, for rSTS trials	50

3.4	Pattern of: a) \mathbf{F}_X , b) \mathbf{F}_Z , c) $\Delta\mathbf{CoP}_X$ and residual errors during a rSTS trial (Subject 2)	51
3.5	Linear and angular velocity of the rotation (SA) and linear (LA) actuator during a rSTS trial (Subject 2). Image in the box is from [151]	52
3.6	Patterns of ankle, knee and hip joint moments during a rSTS trial (Subject 2)	53
3.7	Patterns of ankle joint moment provided from FP and residual errors during a rSTS trial (Subject 2)	53
4.1	Tested models: a) inverted pendulum, b) 2-link model, c) 3-link model	67
4.2	RMSEs of: a) \mathbf{F}_X , b) $\Delta\mathbf{CoP}_X$, for oscillatory trials related to 1-, 2- and 3-link biomechanical models	71
4.3	Ankle-Hip angular displacements for: a) low-, b) high-frequency oscillations during a PS trial (Subject 2)	72
4.4	RMSEs of: a) \mathbf{F}_X , b) $\Delta\mathbf{CoP}_X$, for oscillatory trials	73
4.5	Pattern of: a) \mathbf{F}_X , b) $\Delta\mathbf{CoP}_X$ and residual prediction errors during an oscillatory trial (Subject 2)	74
4.6	Pattern of: a) $\Delta\mathbf{CoP}_X$ and b) $\Delta\mathbf{CoM}_X - \Delta\mathbf{CoP}_X$ during an oscillatory trial (Subject 2)	75
5.1	a) Upper limb kinematic chain representation in the sagittal plane, b) 2D multi-link model	95
5.2	Summary scheme of the operations implemented in the Kalman Filter	97
5.3	Three-link mechanical arm equipped with encoders and IMUs	99
5.4	Main part of the acquisition and data processing software developed in LabVIEW programming environment	99
5.5	Relative rotation and translation between the sensor technical systems of reference (red) and the global systems of reference (black)	100
5.6	a) Kinematic model for the right upper limb, b) representation of the mechanical model of the joints of interest	104

5.7	DoFs of the joints of interest	105
5.8	Representation of the Thorax (T), arm (A) and forearm (F) system of reference and of the rotation matrices between technical and global frames	110
5.9	Exercises required by the alignment and functional calibration procedures: a) static, b) thorax and arm flexion/extension, c) arm and forearm abduction/adduction, d) arm internal/external rotation, e) forearm flexion/extension, f) forearm pronation/ supination	115
5.10	Bony-landmarks of the upper limb body-segments. Image is from [212]	117
5.11	Pattern of: a) shoulder angle, b) elbow angle, c) wrist angle (blue line) and residual errors (red line) during a trial	119
5.12	Relative angles between technical SoRs of the IMUs placed on the thorax and the arm (blue dashed line) and residual errors (red solid line) for an arm flexion/extension task: a) shoulder flexion/extension, b) shoulder ab/adduction, c) shoulder internal/external rotation, d) elbow flexion/extension	122
5.13	Relative angles between technical SoRs of the IMUs placed on the thorax and the arm (blue dashed line) and residual errors (red solid line) for an arm ab/adduction task: a) shoulder ab/adduction, b) shoulder flexion/extension, c) shoulder internal/external rotation	123
5.14	Relative angles between technical SoRs of the IMUs placed on the thorax and the arm (blue dashed line) and residual errors (red solid line) for an arm intra/extra rotation task: a) shoulder internal/external rotation, b) shoulder ab/adduction, c) shoulder flexion/extension	124

5.15	Joint angles measured by SP system (blue solid line) and estimated by IMU data (red dashed line) for an arm flexion/extension task: a) shoulder flexion/extension, b) shoulder ab/adduction, c) shoulder internal/external rotation, d) elbow flexion/extension, e) carrying angle, f) elbow pronation/supination	126
5.16	Joint angles measured by SP system (blue solid line) and estimated by IMU data (red dashed line) for an arm ab/adduction task: a) shoulder ab/adduction, b) shoulder flexion/extension, c) shoulder internal/external rotation, d) carrying angle, e) elbow flexion/extension, f) elbow pronation/supination . . .	127
5.17	Joint angles measured by SP system (blue solid line) and estimated by IMU data (red dashed line) for an arm intra/extra rotation task: a) shoulder internal/external rotation, b) shoulder ab/adduction, c) shoulder flexion/extension, d) elbow pronation/supination, e) carrying angle, f) elbow flexion/extension	128

List of Tables

2.1	RMSEs and P-P range for the mechanical inverted pendulum	30
2.2	RMSEs and P-P range for the subject during squat tests . .	32
3.1	Characteristics of participants, estimated and De Leva’s inertial parameters. The three rows for each subject represent the i -th element ($i = 1, \dots, 3$) of the sensitivity vectors $\tilde{\mathbf{D}}$ and $\tilde{\mathbf{J}}$	49
5.1	Definition of the anatomical SoRs of each body-segment (right upper limb). All vectors are expressed in the IMU global SoR. Symbol \wedge denotes the cross product	114
5.2	RMSEs and STDs related to the relative angles between the technical SoRs of the IMUs placed on the arm and the thorax, averaged on three trials for each task	121
5.3	RMSEs and STDs related to the joint angles of shoulder and elbow, averaged on three trials for each task	125

Bibliography

- [1] ACCONERO N, CAPOZZA M, RINALDUZZI S, MANFREDI GW (1997) *Clinical multisegmental posturography: age-related changes in stance control*, Electroencephalography and Clinical Neurophysiology, 105: 213-219.
- [2] ANDRIACCHI TP, ALEXANDER J (2000) *Studies of human locomotion: past, present and future*, Journal of Biomechanics, 33(10): 1217-1224.
- [3] ALEXANDROV AV, FROLOV AA, HORAK FB, CARLSON-KUHTA P, PARK S (2005) *Feedback equilibrium control during human standing*, Biological Cybernetics, 93: 309-322.
- [4] ANGLIN C, WYSS UP (2000) *Arm motion and load analysis of sit-to-stand, stand-to-sit, cane walking and lifting*, Clinical Biomechanics, 15(6): 441-448.
- [5] ARAMAKI Y, NOZAKI D, MASANI K, SATO T, NAKAZAWA K, YANO H (2001) *Reciprocal angular acceleration of the ankle and hip joints during quiet standing in humans*, Experimental Brain Research, 136: 463-473.
- [6] ARUN K, HUANG T, BLOSTEIN S (1987) *Least-squares fitting of two 3-D point sets*, IEEE Transactions on Pattern Analysis and Machine Intelligence, 9: 698-700.
- [7] AURIEL E, HAUSDORFF JM, HERMAN T, SIMON ES, GILADI N (2006) *Effects of methylphenidate on cognitive function and gait in patients with Parkinson's disease: a pilot study*, Clinical Neuropharmacology, 29: 15-17.
- [8] BAGALÀ F, FUSCHILLO VL, CHIARI L, CAPPELLO F (2012) *Calibrated 2D angular kinematics by single-axis accelerometers: from inverted pendulum to N-link chain*, Naval Post graduate School, Monterey, USA.
- [9] BAGALÀ F, FUSCHILLO VL, CHIARI L, CAPPELLO F (2012) *Accelerometers-based telescopic inverted pendulum model for the analysis of sit-to-stand*, Proceedings of GNB 2012, June 26-29, Roma, Italy (in press).

- [10] BACHMANN ER (2000) *Inertial and magnetic tracking of limb segment orientation for inserting humans in synthetic environment*, Proceedings of IEEE International Conference Robotics Automation, 2: 1115-1122.
- [11] BACHMANN ER, XIAOPING Y, PETERSON CW (2004) *An investigation of the effects of magnetic variations on inertial/magnetic orientation sensors*, Proceedings of IEEE International Conference Robotics Automation, 2: 1115-1122.
- [12] BALASH Y, PERETZ C, LEBOVICH G, HERMAN T, HAUSDORFF JM, GILADI N (2005) *Falls in outpatients with Parkinson's disease: frequency, impact and identifying factors*, Journal of Neurology, 252:1310-1315.
- [13] BARDY BG, MARIN L, STOFFREGEN TA, BOOTSMA RJ (1999) *Postural coordination modes considered as emergent phenomena*, Journal of Experimental Psychology: Human Perception and Performance, 25:1284-1301.
- [14] BARDY BG, OULLIER O, BOOTSMA RJ, STOFFREGEN TA (2002) *Dynamics of human postural transitions*, Journal of Experimental Psychology: Human Perception and Performance, 28:499-514.
- [15] BEER RF, DEWALD JPA, RYMER WZ (2000) *Deficits in the coordination of multijoint arm movements in patients with hemiparesis: evidence for disturbed control of limb dynamics*, Experimental Brain Research, 131: 305-319.
- [16] BEN-ITZHAK R, GILADI N, GRUENDLINGER L, HAUSDORFF JM (2008) *Can methylphenidate reduce fall risk in community-living older adults? A double-blind, single-dose cross-over study*, Journal of the American Geriatrics Society, 56: 695-700.
- [17] BERNMARK E, WIKTORIN C (2002) *A triaxial accelerometer for measuring arm movements*, Applied Ergonomics, 33(6): 541-547.
- [18] BIDARGADDI N, KLINGBEIL L, SARELA A, BOYLE J, CHEUNG V, YELLAND C, GRAY L (2007) *Wavelet based approach for posture transition estimation using a waist worn accelerometer*, Proceedings of the 29th Annual International Conference of IEEE Engineering in Medicine & Biology Society, August 22-26, Lyon, France, pp 1884-1887.
- [19] BOHANNON RW, SMITH MB (1987) *Interrater reliability of a modified Ashworth scale of muscle spasticity*, Physical Therapy, 67: 206-267.
- [20] BORELLI AG (1989) *On the movement of animals. Rome 1680 (1st part) and 1681 (2nd)*, In: Cappozzo A, Marchetti M, Tosi (Eds.), Biocomotion: A Century of Research Using Moving Pictures. Promograph, Rome.

- [21] BUATOIS S, MILJKOVIC D, MANCKOUNDIA P, GUEGUEN R, MIGET P, VANCON G, PERRIN P, BENETOS A (2008) *Five times sit-to-stand test is a predictor of recurrent falls in healthy community-living subjects aged 65 and older*, Journal of the American Geriatrics Society, 56(8): 1575-1577.
- [22] BURDEA G (2003) *Virtual rehabilitation - benefits and challenges*, Methods of Information in Medicine, 5: 519-23.
- [23] CAHOUE T V, MARTIN L, AMARANTINI D (2002) *Static optimal estimation of joint accelerations for inverse dynamics problem solution*, Journal of Biomechanics, 35: 1507-1513.
- [24] CAPPOZZO A, CATANI F, DELLA CROCE U, LEARDINI A (1995) *Position and orientation of bones during movement: anatomical frame definition and determination*, Clinical Biomechanics, 21: S13-S19.
- [25] CARON O, FAURE B, BRENIÈRE Y (1997) *Estimating the center of gravity of the body on the basis of the center of pressure in standing posture*, Journal of Biomechanics, 30: 1169-1171.
- [26] CHANDLER J, DUNCAN P, KOCHERSBERGER G, STUDENSKI S (1998) *Is lower extremity strength gain associated with improvement in physical performance and disability in frail, community-dwelling elders?*, Archives of Physical Medicine and Rehabilitation, 79: 24-30.
- [27] CHANDLER RF, CLAUSER CE, MCCONVILLE JT, REYNOLDS HM, YOUNG JW (1975) *Investigation of inertia properties of the human body*, AMRL Technical Report: 74-137, Wright-Patterson Air Force Base, OH
- [28] CHEN SC, HSIEH HJ, LU TW, TSENG CH (2011) *A method for estimating subject-specific body segment inertial parameters in human movement analysis*, Gait & Posture, 33(4): 695-700.
- [29] CHENG CK, CHEN HH, CHEN CS, CHEN CL, CHEN CY (2000) *Segment inertial properties of Chinese adults determined from magnetic resonance imaging*, Clinical Biomechanics, 15: 559-566.
- [30] CHIARI L, DOZZA M, CAPPELLO A, HORAK FB, MACELLA V, GIANANTI D (2005) *Audio-Biofeedback for balance improvements: an accelerometry-based system*, IEEE Transactions Biomedical Engineering, 52(12): 2108-2111.
- [31] CHIARI L (2011) *Wearable systems with minimal set-up for monitoring and training of balance and mobility*, Proceedings of the 33rd Annual International Conference of IEEE Engineering in Medicine & Biology Society, August 30 - September 3, Boston, pp 5828-5832.

- [32] CIRSTEA MC, LEVIN MF (2000) *Compensatory strategies for reaching in stroke*, Brain, 123: 940-953.
- [33] COLEY B, JOLLES BM, FARRON A, BOURGEOIS A, NUSSBAUMER F, PICHONNAZ C, AMINIAN K (2007) *Outcome evaluation in shoulder surgery using 3D kinematics sensors*, Gait & Posture, 25: 523-532.
- [34] COLLINS JJ, DE LUCA CJ (1995) *The effects of visual input on open-loop and closed-loop postural control mechanisms*, Experimental Brain Research, 103: 151-163.
- [35] COOPER G, SHERET I, McMILLIAN L, SILIVERDIS K, SHA N, HODGINS D, KENNEY L, HOWARD D (2009) *Inertial sensor-based knee flexion/extension angle estimation*, Journal of Biomechanics, 42: 2678-2685.
- [36] CREATH R, KIEMEL T, HORAK FB, PETERKA R, JEKA J (2005) *A unified view of quiet and perturbed stance: simultaneous co-existing excitable modes*, Neuroscience Letters, 377: 75-80.
- [37] CSUKA M, MCCARTY D (1985) *Simple method for measurement of lower-extremity muscle strength*, American Journal of Medicine, 78: 77-81.
- [38] CUTTI AG, RAGGI M, DAVALLI A, CAPPELLO A (2006) *Definition of two reference elbow models from cadaver data*, Gait & Posture, S224-S225.
- [39] CUTTI AG, GIOVANARDI A, ROCCHI L, DAVALLI A, SACCHETTI R (2008) *Ambulatory measurement of shoulder and elbow kinematics through inertial and magnetic sensors*, Medical & Biological Engineering & Computing, 46(2): 169-178.
- [40] DEAN C, SHEPHERD R (1997) *Task-related training improves performance of seated reaching tasks following stroke: a randomized clinical trial*, Stroke, 28: 722-728.
- [41] DEJNABADI H, JOLLE BM, CASANOVA E, FUA P, AMINIAN K (2006) *Estimation and visualization of sagittal kinematics of lower limbs orientation using body-fixed sensors*, IEEE Transactions on Biomedical Engineering, 53: 1385-1393.
- [42] DE LEVA P (1996) *Adjustments to Zatsiorsky-Seluyanov's segment inertial parameters*, Journal of Biomechanics, 29(9): 1223-1230.
- [43] DEMPSTER WT (1955) *Space requirements for the seated operator*, WADC Technical Report: 55-219, Wright-Patterson Air Force Base, OH.

- [44] DESROSIERS J, HEBERT R, BRAVO G, DUTIL E (1995) *Upper extremity performance test for the elderly (TEMPA): normative data and correlates with sensorimotor parameters*, Archives of Physical Medicine and Rehabilitation, 76: 1125-1129.
- [45] DEUTSCH JE, BORBELY M, FILLER J, HUHN K, GUARRERA-BOWLBY P (2008) *Use of a low-cost commercially available gaming console (Wii) for rehabilitation of an adolescent with cerebral palsy*, Physical Therapy, 88(10): 1196-207.
- [46] DEUTSCH JE (2011) *Using virtual reality to improve walking post-stroke: translation to individuals with diabetes*, Journal of Diabetes Science and Technology, 5(2): 309-314.
- [47] DE VRIES WHK, VEEGER HEJ, BATEN CTM, VAN DER HELM FCT (2009) *Magnetic distortion in motion labs, implications for validating inertial magnetic sensors*, Gait & Posture, 29: 535-541.
- [48] DE VRIES WHK, VEEGER HEJ, CUTTI AG, BATEN CTM, VAN DER HELM FCT (2010) *Functionally interpretable local coordinate systems for the upper extremity using inertial & magnetic measurement systems*, Journal of Biomechanics, 43: 1983-1988.
- [49] DIENER HC, DICHGANS J, BACHER M, GOMPF B (1984) *Quantification of postural sway in normals and patients with cerebellar diseases*, Electroencephalography and Clinical Neurophysiology, 57(2): 134-142.
- [50] DOBKIN D (2004) *Strategies for stroke rehabilitation*, Lancet Neurology, 3: 528-536.
- [51] DONHEY EP, FAN CW, FORAN T, GREEN BR, CUNNINGHAM C, KENNY A (2011) *An instrumented sit-to-stand test used to examine differences between older fallers and non-fallers*, Proceedings of the 33rd Annual International Conference of IEEE Engineering in Medicine & Biology Society, August 30 - September 3, Boston, USA, pp 3063-3066.
- [52] DONNAN G, FISHER M, MACLEOD M, DAVIS S (2008) *Stroke*, Lancet Neurology, 371: 1612-1623.
- [53] O'DONOVAN KJ, KAMNIK R, O'KEEFFE DT, LYONS GM (2007) *An inertial and magnetic sensor based technique for joint angle measurement*, Journal of Biomechanics, 40: 2604-2611.
- [54] DUNCAN RP, LEDDY AL, EARHART GM (2011) *Five Times Sit-to-Stand Test performance in Parkinson's disease*, Archives of Physical Medicine and Rehabilitation, 92: 1431-1436.

- [55] DUNNEWOLD RJW, JACOBI CE, VAN HILTEN JJ (1997) *Quantitative assessment of bradykinesia in patients with Parkinson's disease*, Journal of Neuroscience Methods, 74: 107-112.
- [56] DURKIN JL, DOWLING JJ (2003) *Analysis of body segment parameter differences between four human populations and the estimation errors of four popular mathematical models*, Journal of Biomechanical Engineering, 125: 515-522.
- [57] ELBLE RJ (2005) *Gravitational artifact in accelerometric measurements of tremor*, Clinical of Neurophysiology, 116: 1638-1643.
- [58] FAVRE J, JOLLES M, AISSAOUI R, AMINIAN K (2008) *Ambulatory measurement of 3D knee joint angle*, Journal of Biomechanics, 41: 1029-1035.
- [59] GEIGIN V, LAWES C, BENNETT D, BARKER-COLL S, PARAG V (2009) *Worldwide stroke incidence and early case fatality reported in 56 population-based studies: a systematic review*, Lancet Neurology, 8: 355-369.
- [60] FOXLIN E (1996) *Inertial head-tracker sensor fusion by a complementary separate-bias Kalman Filter*, Proceedings of VRAIS 1996, 185-195.
- [61] FUGL-MEYER AR, JAASKO L, LEYMAN I, OLSSON S, STEGLIND S (1975) *The post-stroke hemiplegic patient*, Scandinavian Journal of Rehabilitation Medicine, 7: 13-31.
- [62] FUJIMOTO M, CHOU LS (2012) *Dynamic balance control during sit-to-stand movement: an examination with the center of mass acceleration*, Journal of Biomechanics, 45: 543-548.
- [63] FUSCHILLO VL, CHIARI L, CAPPELLO A (2011) *Kinematic strategy evaluation by single-axis accelerometers during voluntary oscillations*, Proceedings of SIAMOC 2011, September 28 - October 1, Bosisio Parini, Italy, Gait & Posture, 35(1): S19-S20.
- [64] FUSCHILLO VL, BAGALÀ F, CHIARI L, CAPPELLO A (2012) *Accelerometry-based dynamics prediction for balance monitoring*, Medical & Biological Engineering and Computing, 50(9): 925-936.
- [65] FUSCHILLO VL, BAGALÀ F, CHIARI L, CAPPELLO A (2012) *Net joint moments accelerometers-based prediction during sit-to-stand*, Proceedings of GNB 2012, June 26-29, Roma, Italy (in press).
- [66] GAGE WH, WINTER DA, FRANK JS, ADKIN AL (2004) *Kinematic and kinetic validity of the inverted pendulum model in quiet standing*, Gait & Posture, 19: 124-132.

- [67] GANEA R, PARASCHIV-IONESCU A, SALARIAN A, BULA C, MARTIN E, ROCHAT S, HOSKOVEC C, PIOT-ZIEGLER C (2007) *Kinematics and dynamic complexity of postural transitions in frail elderly subjects*, Proceedings of the 29th Annual International Conference of IEEE Engineering in Medicine & Biology Society, August 22-26, Lyon, France, pp 6117-6120.
- [68] GIANSANTI D, MACCIONI G, MACELLARI V (2005) *The development and test of a device for the reconstruction of 3-D position and orientation by means of a kinematic sensor assembly with rate gyroscopes and accelerometers*, IEEE Transactions on Biomedical Engineering, 52(7): 1271-1277.
- [69] GIANSANTI D, MACCIONI G, MACELLARI V, COSTANTINI G, CAROTA M (2006) *Towards the investigation of kinematic parameters from an integrated measurement unit for the classification of the rising from the chair*, Proceedings of the 28th Annual International Conference of IEEE Engineering in Medicine & Biology Society, August 30 - September 3, New York, USA, pp 1742-1745.
- [70] GILLAIN S, WARZEE E, LEKEU F, WOJTASIK V, MAQUET D, CROISIER JL, SALMON E, PETERMANS J (2009) *The value of instrumental gait analysis in elderly healthy, MCI or Alzheimer's disease subjects and a comparison with other clinical tests used in single and dual-task conditions*, Archives of Physical Medicine and Rehabilitation, 52(6): 453-74.
- [71] GLADSTONE DJ, DANELLS CJ, BLACK SE (2002) *The Fugl-Meyer Assessment of motor recovery after stroke: a critical review of its measurement properties*, Neurorehabilitation and Neural Repair, 16(3): 232-240.
- [72] GOLDVASSER D, MCGIBBON C, KREBS D (2001) *High curvature and jerk analysis of arm ataxia*, Biological Cybernetics, 14: 745-752.
- [73] GOULDING A, JONES IE, TAYLOR RW, PIGGOT JM, TAYLOR D (2003) *Dynamic and static tests of balance and postural sway in boys: effects of previous wrist bone fractures and high adiposity*, Gait & Posture, 17(2): 136-141.
- [74] GOWLAND C, STRATFORD P, WARD M, MORELAND J, TORRESIN W, VAN HULLENAAR S, SANFORD J, BARRECA S, VANSPALL B, PLEWS N (1993) *Measuring physical impairment and disability with the Chedoke-McMaster Stroke Assessment*, Stroke, 24: 58-63.
- [75] HANAVAN EP (1964) *A mathematical model of the human body*, AMRL Technical Report: 64-102, Wright-Patterson Air Force Base, OH.

- [76] HANSON R, NORRIS M (1981) *Analysis of measurements based on the singular value decomposition*, SIAM Journal on Scientific Computing, 2: 363-373.
- [77] HASAN SS, ROBIN DW, SZURKUS DC, ASHMEAD DH, PETERSON SW, SHIABI RG (1996) *Simultaneous measurement of body center of pressure and center of gravity during upright stance. Part I: methods*, Gait & Posture, 4: 1-10.
- [78] HATZE H (1980) *A mathematical model for the computational determination of parameter values of anthropomorphic segments*, Journal of Biomechanics, 13: 833-843.
- [79] HATZE H (2000) *The inverse dynamics problem of neuromuscular control*, Biological Cybernetics, 82: 133-141.
- [80] HAYES WC, GRAN JD, NAGURKA ML, FIELDMAN JM, OATIS C (1983) *Leg motion analysis during gait by multi-axial accelerometry: Theoretical foundations and preliminary validations*, Journal of Biomechanics, 105: 283-289.
- [81] HENDERSON A, KORNER-BITENSKY N, LEVIN M (2007) *Virtual reality in stroke rehabilitation: a systematic review of its effectiveness for upper limb motor recovery*, Topics in Stroke Rehabilitation, 14(2): 52-61.
- [82] HOFF JI, HILTEN BJV (1999) *A review of the assessment of dyskinesias*, Movement Disorders, 15: 737-743.
- [83] HOLME E, MAGNUSSON SP, BECHER K, BIELER T, AGAARD P, KJÆR M (1999) *The effect of supervised rehabilitation on strength, postural sway, position sense and re-injury risk after acute ankle ligament sprain*, Scandinavian Journal of Medicine & Science in Sports, 9(2): 104-109.
- [84] HORAK FB (1997) *Clinical assessment of balance disorders*, Gait & Posture, 6(1): 76-84.
- [85] HORAK FB, WRISLEY DM, FRANK J (2009) *The Balance Evaluation System Test (BESTest) to differentiate balance deficits*, Physical Therapy, 89(5): 484-498.
- [86] HSIEH YW, WANG CH, WU SC, CHEN PC, SHEU CF, HSIEH CL (2007) *Establishing the minimal clinically important difference of the Bartel Index in stroke patients*, Neurorehabilitation and Neural Repair, 21: 233-238.
- [87] HSU WL, SCHOLZ JP, SCHONER G, JEKA J, KIEMEL T (2007) *Control and estimation of posture during quiet stance depends on multijoint coordination*, Journal of Neurophysiology, 97: 3024-3035.

- [88] IQBAL K (2011) *Mechanisms and models of postural stability and control*, Proceedings of the 33rd Annual International Conference of IEEE Engineering in Medicine & Biology Society, August 30 - September 3, Boston, USA, pp 7837-7840.
- [89] JANSSEN WGM, BUSSMANN HBJ, STAM HJ (2002) *Determinants of the sit-to-stand movement: a review*, Physical Therapy, 82: 866-879.
- [90] JEBSEN RH, TAYLOR N, TRIESCHMANN RB, TROTTER MJ, HOWARD LA (1969) *An objective and standardized test of hand function*, Archives of Physical Medicine and Rehabilitation, 50: 311-319.
- [91] JEKA J, KIEMEL T, CREATH R, HORAK FB, PETERKA R (2004) *Controlling human upright posture: velocity information is more accurate than position or acceleration*, Journal of Neurophysiology, 92:2368-2379.
- [92] JENSEN RK (1978) *Estimation of biomechanical properties of three body types using a photogrammetry method*, Journal of Biomechanics, 11: 349-358.
- [93] KALMAN R (1960) *A new approach to linear filtering and prediction problems*, Transactions of the ASME – Journal of Basic Engineering, 82(D): 35-45.
- [94] KAMEN G, PATTEN C, DUKE D, SISON S (1998) *An accelerometry-based system for the assessment of balance and postural sway*, Gerontology, 44(1): 40-45.
- [95] KAYA BK, KREBS DE, RILEY PO (1998) *Dynamic stability in elders: momentum control in locomotor ADL*, Journal of Gerontology Series A: Biological Science and Medical Science, 53 A(2): M126-M134.
- [96] KHASNIS A, GOKULA RM (2003) *Romberg's test*, Journal of Postgraduate Medicine, 49(2): 169-72.
- [97] KEMP B, JANSSEN JMW, VAN DER KAMP B (1998) *Body position can be monitored in 3D using miniature accelerometers and earth-magnetic field sensors*, Electroencephalography and Clinical Neurophysiology, 109: 484-488.
- [98] KIM S, HORAK FB, CARLSON-KUHTA P, PARK S (2009) *Postural feedback scaling deficits in Parkinson's disease*, Journal of Neurophysiology, 102(5): 2910-2920.
- [99] KITAGO T, LIANG J, HUANG VS, HAYES S, SIMON P, TENTEROMANO L, LAZAR RM, MARSHALL RS, MAZZONI P, LENNIHAN L (2013) *Improvement after constraint-induced movement therapy: recovery of normal motor control or task-specific compensation?*, Neurorehabilitation and Neural Repair, 27(2): 99-109.

- [100] KONTAXIS A, CUTTI AG, JOHNSON GR, VEEGER HEJ (2008) *A framework for the definition of standardized protocols for measuring upper-extremity kinematics*, *Clinical Biomechanics*, 24: 246-253.
- [101] KUO D, SPEERS RA, PETERKA RJ (1998) *Effect of altered sensory conditions on multivariate description of human postural sway*, *Experimental Brain Research*, 122(2): 185-95.
- [102] KWAKKEL G, VAN PEPPEN R, WAGENAAR R, WOOD DAUPHINEE S, RICHARDS C, ASHBURN A (2004) *Effects of augmented exercise therapy time after stroke. A meta-analysis*, *Stroke*, 35: 1-11.
- [103] LAJOIE Y, TEASDALE N, BARD C, FLEURY M (1993) *Attentional demands for static and dynamic equilibrium*, *Experimental Brain Research*, 97: 139-144.
- [104] LANGE B, FLYNN S, PROFFITT R, CHANG C, RIZZO A (2010) *Development of an interactive game-based rehabilitation tool for dynamic balance training*, *Topics in Stroke Rehabilitation*, 17(5): 345-352.
- [105] LAVER KE, GEORGE S, THOMAS S, DEUTSCH JE, CROTTY M (2011) *Virtual reality for stroke rehabilitation (Review)*, The Cochrane Collaboration. Published by John Wiley & Sons, Ltd.
- [106] LECOURS J, NADEAU S, GRAVEL D, TEIXERA-SALMELA L (2008) *Interactions between foot placement, trunk frontal position, weight-bearing and knee moment asymmetry at seat-off during rising from a chair in healthy controls and persons with hemiparesis*, *Journal of Rehabilitation Medicine*, 40: 200-207.
- [107] LENZI D, CAPPELLO A, CHIARI L (2003) *Influence of body segment parameters and modeling assumptions on the estimate of center of mass trajectory*, *Journal of Biomechanics*, 36: 1335-1341.
- [108] LEVIN MF, HUI-CHAN CW (1992) *Relief of hemiparetic spasticity by TENS is associated with improvement in reflex and voluntary motor functions*, *Electroencephalography and Clinical Neurophysiology*, 85: 131-142.
- [109] LEVIN MF, MICHAEESEN S, CIRSTEA CM, ROBY-BRAMI A (2002) *Use of the trunk for reaching targets placed within and beyond the reach in adult hemiparesis*, *Experimental Brain Research*, 143: 171-180.
- [110] LEVIN MF, DESROSIERS J, BEAUCHEMIN D, BERGERON N, ROCHETTE A (2004) *Development and validation of a scale for rating compensation used for reaching in patients with hemiparesis: the Reaching Performance Scale*, *Physical Therapy*, 84: 8-22.

- [111] LEVIN MF, KLEIM JA, WOLF SL (2009) *What do motor "recovery" and "compensation" mean in patients following stroke?*, *Neurorehabilitation and Neural Repair*, 23(4): 313-319.
- [112] LIU K, LIU T, SHIBATA K, INOUE Y, ZHENG R (2009) *Novel approach to ambulatory assessment of human segmental orientation on a wearable sensor system*, *Journal of Biomechanics*, 42: 2747-2752.
- [113] LORAM ID, LAKIE M (2002) *Direct measurement of human ankle stiffness during quiet standing: the intrinsic mechanical stiffness is insufficient for stability*, *Journal of Physiology*, 545: 1041-1053.
- [114] LORAM ID, MAGANARIS CN, LAKIE M (2005) *Human postural sway results from frequent, ballistic bias impulses by soleus and gastrocnemius*, *Journal of Physiology*, 564: 295-311.
- [115] LORD SR, MURRAY SM, CHAPMAN K, MUNRO B, TIEDEMANN A (2002) *Sit-to-stand performance depends on sensation, speed, balance and psychological status in addition to strength in older people*, *Journal of Gerontology Series A: Biological Science and Medical Science*, 57: M539-M543.
- [116] LUINGE HJ, VELTINK PH (2005) *Measuring orientation of human body segments using miniature gyroscopes and accelerometers*, *Medical & Biological Engineering & Computing*, 43: 273-282.
- [117] LUINGE HJ, VELTINK PH, BATEN CTM (2007) *Ambulatory measurement of arm orientation*, *Journal of Biomechanics*, 40: 78-85.
- [118] LYONS GM, CULHANE KM, HILTON D, GRACE PA, LYONS D (2005) *A description of an accelerometer-based mobility technique*, *Medical Engineering and Physics*, 27: 497-504.
- [119] MAK MKY, LEVIN O, MIZRAHI J, HUI-CHAN CWY (2003) *Joint torques during sit-to-stand in healthy subjects and people with Parkinson's disease*, *Clinical Biomechanics*, 18: 197-206.
- [120] MAKI BE, HOLLIDAY PJ, FERNIE GR (1990) *Aging and postural control. A comparison of spontaneous- and induced-sway balance tests*, *Journal of the American Geriatrics Society*, 38(1): 1-9.
- [121] MAKI BE, HOLLIDAY PJ, TOPPER AK (1994) *A prospective study of postural balance and risk of falling in an ambulatory and independent elderly population*, *Journal of Gerontology*, 49: M72-M84.

- [122] MANCINI M, ROCCHI L, HORAK FB, CHIARI L (2008) *Effects of Parkinson's disease and levodopa on functional limits of stability*, *Clinical Biomechanics*, 23: 450-458.
- [123] MANCINI M, ZAMPIERI C, CARLSON-KUHTA P, CHIARI L, HORAK FB (2009) *Anticipatory postural adjustments prior to step initiation are hypometric in untreated Parkinson's disease: An accelerometer-based approach*, *European Journal of Neurology*, 16(9): 1028-1034.
- [124] MARSCHOLLEK M, NEMITZ G, GIETZELT M, WOLF KH, MEYER ZU SH, HAUX R (2009) *Predicting in-patient falls in a geriatric clinic: a clinical study combining assessment data and simple sensory gait measurements*, *Zeitschrift fur Gerontologie und Geriatrie*, 42: 317-322.
- [125] MATHIAS S, NAYAK US, ISAACS B (1986) *Balance in elderly patients: the "get-up and go" test*, *Archives of Physical Medicine and Rehabilitation*, 67: 387-389.
- [126] MATHIOWETZ V, WEBER K, KASHMAN N, VOLLAND G (1985) *Adult norms for the nine-hole peg test of finger dexterity*, *Occupational Therapy Journal of Research*, 5: 24-37.
- [127] MAYAGOITIA RE, LÖTTERS JC, VELTINK PH, HERMENS H (2002) *Standing balance evaluation using a tri-axial accelerometer*, *Gait&Posture*, 6(1): 55-59.
- [128] MAYAGOITIA RE, NENE AV, VELTINK PH (2002) *Accelerometer and rate gyroscope measurement of kinematics: an inexpensive alternative to optical motion analysis systems*, *Journal of Biomechanics*, 35: 537-542.
- [129] MAYO N, WOOD-DAUPHINEE S, AHMED S, GORDON C, HIGGINS J, McEWEN S (1999) *Disablement following stroke*, *Disability and Rehabilitation*, 21(5/6): 258-268.
- [130] MAZZÀ C, STANHOPE SJ, TAVIANI A, CAPPOZZO A (2006) *Biomechanical modeling of sit-to-stand to upright posture for mobility assessment of persons with chronic stroke*, *Archives of Physical Medicine and Rehabilitation*, 91(2): 288-297.
- [131] MCCOLLUM G, SHUPERT CL, NASHNER LM (1996) *Organizing sensory information for postural control in altered sensory environments*, *Journal of Theoretical Biology*, 180: 257-270.
- [132] MEIJER GA, WESTERTERP KR, VERHOEVEN FM, KOPER HB, HOOR F (1991) *Methods to assess physical activity with special reference to motion sensors and accelerometers*, *IEEE Transactions on Biomedical Engineering*, 38(3): 221-229.

- [133] MERIANS A, JACK D, BOIAN R, TREMAINE M, BURDEA G, ADAMOVICH S (2002) *Virtual reality augmented rehabilitation for patients following stroke*, Physical Therapy, 82(9): 898-915.
- [134] MESKERS CGM, VAN DER HELM FCT, ROZENDAAL LA, ROZING PM (1998) *In vivo estimation of the glenohumeral joint center from scapular bony-landmarks by linear regression*, Journal of Biomechanics,30: 647-652.
- [135] MICHAELSEN SM, JACOBS S, ROBY-BRAMI A, LEVIN MF (2004) *Compensation for distal impairments of grasping in adults with hemiparesis*, Experimental Brain Research, 157: 162-173.
- [136] MOE-NILSSEN R (1998) *A new method for evaluating motor control in gait under real-life environmental conditions. Part 1: The Instrument*, Clinical Biomechanics, 13(4-5): 320-327.
- [137] MOE-NILSSEN R (1998) *Test-retest reliability of trunk accelerometry during standing and walking*, Archives of Physical Medicine and Rehabilitation, 79: 1377-1385.
- [138] MORASSO PG, SCHIEPPATI M (1999) *Can muscle stiffness alone cannot stabilize upright standing?*, Journal of Neurophysiology, 83: 1622-1626.
- [139] MORASSO PG, SANGUINETI V (2002) *Ankle muscle stiffness alone cannot stabilize balance during quiet standing*, Journal of Neurophysiology, 88: 2157-2162.
- [140] MUIR SW, BERG K, CHESWORTH B, SPEECHLEY M (2008) *Use of the Berg Balance Scale for predicting multiple falls in community-dwelling elderly people: a prospective study*, Physical Therapy, 88(4): 449-459.
- [141] MURRAY IA, JOHNSON GR (2004) *A study of the external forces and moments at the shoulder and elbow while performing every day tasks*, Clinical Biomechanics, 19(6): 586-594.
- [142] NAJAFI B, AMINIAN K, LOEW F, BLANC Y, ROBERT PA (2002) *Measurement of stand-sit and sit-stand transitions using a miniature gyroscope and its application in fall risk evaluation in the elderly*, IEEE Transaction on Biomedical Engineering, 49: 843-851.
IEEE Trans Biomed Eng,
- [143] NASHNER LM, MCCOLLUM G (1985) *The organization of human postural movements: a formal basis and experimental synthesis*, Behavioral and Brain Sciences, 8: 135-150.

- [144] NEVELL KM (1991) *Motor skill acquisition*, Annual Review of Psychology, 42: 213-237.
- [145] NUDO R, WISE B, SIFUENTES F, MILLIKEN G (1996) *Neural substrates for the effects of rehabilitative training on motor recovery after ischemic infarct*, Science, 272: 791-794.
- [146] NUDO R (2001) *Role of cortical plasticity in motor recovery after stroke*, Neurology Report, 22: 61-67.
- [147] PADGAONKAR AJ, KRIEGER KW, KING AI (1975) *Measurement of angular acceleration of a rigid body using linear accelerometers*, Journal of Applied Mechanics (Transactions ASME), 42: 552-556.
- [148] PAI YC, NAUGHTON BJ, CHANG RW, ROGERS MW (1994) *Control of body center of mass momentum during sit-to-stand among young and elderly adults*, Gait & Posture, 2: 109-116.
- [149] PAI YC, PATTON J (1997) *Center of mass velocity-position predictions for balance control*, Journal of Biomechanics, 30(4): 347-354.
- [150] PALMERINI L, ROCCHI L, MELLONE S, VALZANIA F, CHIARI L (2011) *Feature selection for accelerometer-based posture analysis in Parkinson's disease*, IEEE Transactions on Information Technology in Biomedicine, 15(3): 481-490.
- [151] PAPA E, CAPPOZZO A (1999) *A telescopic inverted-pendulum model of the musculo-skeletal system and its use for the analysis of the sit-to-stand motor task*, Journal of Biomechanics, 32: 1205-1212.
- [152] PATEL M, TILLING K, LAWRENCE E, RUDD A, WOLFE C, McKEVITT C (2006) *Relationship between long-term stroke disability, handicap and health-related quality of life*, Age and Ageing, 35: 273-279.
- [153] PEDOTTI A, CRENNNA P, DEAT A, FRIGO C, MASSION J (1989) *Postural synergies in axial movement: short and long-term adaptation*, Experimental Brain Research, 74: 3-10.
- [154] PETERKA RJ, BLACK FO (1990) *Age-related changes in human posture control: sensory organization tests*, Journal of Vestibular Research, 1: 73-85.
- [155] PETERKA RJ (2002) *Sensorymotor integration in human postural control*, Journal of Neurophysiology, 88: 1097:1118.
- [156] PICERNO P, CEREATTI A, CAPPOZZO A (2008) *Joint kinematics estimate using wearable inertial and magnetic sensing modules*, Gait & Posture, 28: 588-595.

- [157] PIIRTOLA M, ERA P (2006) *Force platform measurements as predictors of falls among older people: a review*, *Gerontology*, 52(1): 1-16.
- [158] PINTER IJ, VAN SWIGCHEM R, VAN SOEST AJK, ROZENDAAL LA (2008) *The dynamics of postural sway cannot be captured using a one-segment inverted pendulum model: a PCA on segment rotation during unperturbed stance*, *Journal of Neurophysiology*, 100: 3197-3280.
- [159] PODSIADLO, RICHARDSON S (1991) *The timed "Up & Go": a test of basic functional mobility for frail elderly persons*, *Journal of the American Geriatrics Society*, 39: 142-148.
- [160] PRIETO TE, MYKLEBUST JB, HOFFMAN RG, LOVETT EG, MYKLEBUST BM (1996) *Measures of postural steadiness: differences between healthy young and elderly adults*, *IEEE Transaction on Biomedical Engineering*, 43: 956-966.
- [161] RAND D, KIZONY R, WEISS P (2008) *The Sony PlayStation II Eye Toy: low-cost virtual reality for use in rehabilitation*, *Journal of Neurologic Physical Therapy*, 32(4): 155-163.
- [162] RICCIO GE, STOFFREGEN TA (1991) *An ecological theory of motion sickness and postural instability*, *Ecological Psychology*, 3: 195-240.
- [163] RIEMER R, HSIAO-WECKSLER ET (2009) *Improving net joint torque calculations through a two-step optimization method for estimating body segment parameters*, *ASME Journal of Biomechanical Engineering*, 131(1): 011007.
- [164] RILEY MA (2001) *The temporal structure of spontaneous postural sway*, in: Van der Burg JCE, Fong BF, Hijl MIJ, Huys R, Pijnappels M, Riley MA, Clark S, A.A. Post (Eds.), *Balance at All Times: Proceedings of the fifth Symposium of the Institute for Fundamental and Clinical Human Movement Sciences*, Digital Printing Partners, Utrecht, 93-109.
- [165] RILEY MA, CLARK S (2003) *Recurrence analysis of human postural sway during the sensory organization test*, *Neuroscience Letters* 342: 45-48.
- [166] ROBY-BRAMI A, JACOBS S, BENNIS N, LEVIN MF (2003) *Hand orientation for grasping and arm joint rotation patterns in healthy subjects and hemiparetic stroke patients*, *Brain Research*, 969: 217-229.
- [167] ROEBROECK M, DOORENBOSCH C, HARLAAR J, JACOBS R, LANKHORST G (1994) *Biomechanics and muscular activity during sit-to-stand transfer*, *Clinical Biomechanics*, 9: 235-244.

- [168] ROETENBERG D, SLYCKE PJ, VELTINK PH (2007) *Ambulatory position and orientation tracking fusing magnetic and inertial sensing*, IEEE Transactions on Biomedical Engineering, 54: 883-890.
- [169] ROGIND H, SIMONSEN H, ERA P, BLIDDAL H (2003) *Comparison of Kistler 9861A force platform and Chattecx Balance System® for measurement of postural sway: correlation and test-retest reliability*, Scandinavian Journal of Medicine & Science in Sports, 13(2): 106-114.
- [170] ROSE F, BROOKS B, RIZZO A (2005) *Virtual reality in brain damage rehabilitation: review*, CyberPsychology & Behavior, 8(3): 241-262.
- [171] ROXENDAAL LA, VAN SOEST AJ (2005) *Joint stiffness requirements in a multi-segment stance model*, Proceedings of the XXth Congress of the International Society of Biomechanics, Cleveland, OH.
- [172] RUNDELL SD, DAVENPORT TE, WAGNER T (2009) *Physical therapist Management of acute and chronic low back pain using the World Health Organization's International Classification of Functioning, Disability and Health*, Physical Therapy, 89(1): 82-90.
- [173] SALEM GJ, SALINAS R, HARDING FV (2003) *Bilateral kinematic and kinetic analysis of the squat exercise after anterior cruciate ligament reconstruction*, Archives of Physical Medicine and Rehabilitation, 84: 1211-1216.
- [174] SANDOZ B, LAPORTE S, SKALLI W, MITTON D (2010) *Subject-specific body segment parameters' estimation using biplanar X-rays: a feasibility study*, Computer Methods in Biomechanics and Biomedical Engineering, 13(6): 649-654.
- [175] SHEETS AL, CORAZZA S, ANDRIACCHI TP (2010) *An automated image-based method of 3D subject-specific body segment parameter estimation for kinetic analysis of rapid movements*, Journal of Biomechanical Engineering, 132(1), Article (011004).
- [176] SHIMBA T (1984) *An estimation of center of gravity from force platform data*, Journal of Biomechanics, 7: 53-60.
- [177] SHUMWAY-COOK A, WOOLLACOTT M (2000) *Attentional demands and postural control: the effect of sensory context*, Journal of Gerontology, Series A, Biological Sciences and Medical Sciences, 55: M10-M16.
- [178] SMITH G (1989) *Padding point extrapolation techniques for the digital Butterworth filter*, Journal of Biomechanics, 22(8-9): 967-971.

- [179] STOKDIJK M, NAGELS J, GARLING EH, ROZING PM (2000) *The kinematic elbow axis to evaluate total elbow replacement: a cadaver study of the iBP elbow system*, Journal of Shoulder & Elbow Surgery, 12:63-68.
- [180] STURM J, DONNAN G, DEWEY H, McDONNELL R, GILLIGAN A, SRIKANTH A (2004) *Quality of life after stroke: The North East Melbourne stroke incidence study (NEMESIS)*, Stroke, 35: 2340-2345.
- [181] SVEISTRUP H (2004) *Motor rehabilitation using virtual reality*, Journal of Neuroengineering and Rehabilitation, 1(10): 1-10.
- [182] TANAKA S, MOTOI K, NOGAWA M, YAMAKOSHI K (2004) *A new portable device for ambulatory monitoring of human posture and walking velocity using miniature accelerometers and gyroscopes*, Proceedings of 26th Annual International Conference of IEEE Engineering in Medicine & Biology Society, September 1-5, San Francisco, USA, pp. 2283-2286.
- [183] TEASELL R, BAYONA N, BITENSKY J (2005) *Plasticity and reorganization of the brain post stroke*, Topics in Stroke Rehabilitation, 12(3): 11-26.
- [184] THAPA PB, GIDEON P, BROCKMAN KG, FOUGHT RL, RAY WA (1996) *Clinical and biomechanical measures of balance as fall predictors in ambulatory nursing home residents*, The Journal of Gerontology, Series A, Biological sciences and medical sciences, 51(5): M239-M246.
- [185] TINETTI ME, SPEECHLEY M, GINTER SF (1988) *Risk factors for falls among elderly persons living in the community*, New England Journal of Medicine, 319: 1701-1707.
- [186] TOPKA H, KONCZAK J, DICHGANS J (1998) *Coordination of multijoint arm movements in cerebellar ataxia: analysis of hand and angular kinematics*, Experimental Brain Research, 119: 483-492.
- [187] TRUEBLOOD PR, HODSON-CHENNAULT N, McCUBBIN A, YOUNGCLARKE D (2003) *Performance and impairment-based assessments among community dwelling elderly: Sensitivity and specificity*, Issues Aging, 24(1): 2-6.
- [188] TUCKER MG, KAVANAGH JJ, MORRISON S, BARRETT RS (2010) *What are the relations between voluntary postural sway measures and falls-history status in community-dwelling older adults?*, Archives of Physical Medicine and Rehabilitation, 91(5): 750-758.
- [189] TURCOT K, ALLET L, GOLAY A, HOFFMEYER P, ARMAND S (2012) *Postural strategies in diabetes patients with peripheral neuropathy determined using cross-correlation functions*, Diabetes Technology & Therapeutics, 14(5): 403-410.

- [190] USTINOVA KI, GOUSSEV VM, BALASUBRAMANIAM R, LEVIN MF (2004) *Disruption of co-ordination between arm, trunk and center of pressure displacement in patients with hemiparesis*, Motor Control, 8: 139-159.
- [191] USWATTE G, MILTNER WH, FOO B, VARNA M, MORAN S, TAUB E (2000) *Objective measurement of functional upper extremity movements using accelerometer recordings transformed with a threshold filter*, Stroke, 31: 662-667.
- [192] VAN ANDEL CJ, WOLTERBEEK N, DOORENBOSCH CA, VEEGER DH, HARLAAR J (2008) *Complete 3D kinematics of upper extremity functional tasks*, Gait & Posture, 27(1): 120-127.
- [193] VAN DER HELM FC (1994) *Analysis of the kinematic and dynamic behavior of the shoulder mechanism*, Journal of Biomechanics, 27(5): 527-550.
- [194] VAUGHAN CL, ANDREWS JG, HAY JG (1982) *Selection of body segment parameters by optimization methods*, ASME Journal of Biomechanical Engineering, 104(1): 38-44.
- [195] VERHEYDEN G, NIEUWBOER A, DE WIT L, THIJS V, DOBBELAERE J, DEVOS H, SEVERIJNS D, VANBEVEREN S, DE WEERDT W (2008) *Time course of trunk, arm, leg, and functional recovery after ischemic stroke*, Neurorehabilitation and Neural Repair, 22: 173-179.
- [196] VETTE AH, YOSHIDA T, THRASHER TA, MASANI K, POPOVIC MR (2011) *A complete, non-lumped, and verifiable set of upper body segment parameters for three-dimensional dynamic modeling*, Medical Engineering & Physics, 33: 70-79.
- [197] WADE DT (1992) *Measurement in stroke rehabilitation*, Oxford University Press.
- [198] VEEGER HE, YU B, AN KN, ROZENDAL RH (1997) *Parameters for modelling the upper extremity*, Journal of Biomechanics, 30: 647-652.
- [199] WEISS P, KIZONY R, FEINTUCH U, KATZ N (2006) *Virtual reality in neurorhabilitation*, in: Selzer M, Cohen L, Gage F, Clarke S, Duncan P editors, Textbook of Neural Repair and Rehabilitation, Cambridge University Press, 182-197.
- [200] WEISSA A, HERMANA T, PLOTNIKA M, BROZGOLA M, MAIDANA I, GILADIA N, GUREVICH T, HAUSDORFF JM (2010) *Can an accelerometer enhance the utility of the Timed Up & Go Test when evaluating patients with Parkinson's disease?*, Medical Engineering & Physics, 32(2): 119-125.

- [201] WELCH G, BISHOP G (1995) *An introduction to the Kalman Filter*, University of North Carolina at Chapel Hill.
- [202] WICKE J, DUMAS GA (2008) *Estimating segment inertial parameters using fan-beam DEXA*, Journal of Applied Biomechanics, 24: 180-184.
- [203] WILLIAMSON R, ANDREWS BJ (2001) *Detecting absolute human knee angle and angular velocity using accelerometers and rate gyroscopes*, Medical & Biological Engineering & Computing, 39: 1-9.
- [204] WINTER DA (1990) *Biomechanics and motor control of human movement*.
- [205] WINTER DA (1995) *Human balance and posture control during standing and walking*, Gait & Posture, 3: 193-214.
- [206] WINTER DA, PATLA AE, PRINCE F, ISHAC M, GIELO-PERCZAK K (1998) *Stiffness control of balance in quiet standing*, Journal of Neurophysiology, 80: 1211-1221.
- [207] WINTER DA (2009) *Biomechanics and motor control of human movement*, 4th edition, John Wiley & Sons Canada Ltd., Mississauga, Ontario, Canada.
- [208] WINTER DA, PATLA AE, RIETDYK S, ISHAC M (2001) *Ankle muscle stiffness in the control of balance during quiet standing*, Journal of Neurophysiology, 85: 2630-2633.
- [209] WOLF SL, CATLIN PA, ELLIS M, ARCHER AL, MORGAN B, PIACENTINO A (2001) *Assessing Wolf Motor Function Test as an outcome measure for research in patients after stroke*, Stroke, 32: 1635-1639.
- [210] WOLTRING HJ (1990) *Data processing and error analysis*, in: Cappozzo A, Berme N (eds), Biomechanics of human movement, Bertec Corporation, Worthington, Ohio, Usa, 203:237 .
- [211] WOOLLACOTT M, SHUMWAY-COOK A (2002) *Attention and the control of posture and gait: a review of an emerging area of research*, Gait & Posture, 16: 1-14.
- [212] WU G, VAN DER HELM FC, VEEGER HEJ, MAKHSOUS M, VAN ROY P, ANGLIN C, NAGELS J, KARDUNA A, MCQUADE K, WANG X, WERNER FW, BUCHHOLZ B (2005) *ISB recommendation on definitions of joint coordinate systems of various joints for the reporting of human joint motion - Part II*, Journal of Biomechanics, 38: 981-992.
- [213] YEADON MR (1990) *The simulation of aerial movement-II. A mathematical inertia model of the human body*, Journal of Biomechanics, 23(1): 67-74.

- [214] YOZBATIRAN N, DER-YEGHIAIAN L, CRAMER SC (2008) *A standardized approach to performing the Action Research Arm Test*, Neurorehabilitation and Neural Repair, 22: 78-90.
- [215] ZAMPIERI C, SALARIAN A, CARLSON-KUHTA P, AMINIAN K, NUTT JG, HORAK FB (2010) *The instrumented timed up and go test: Potential outcome measure for disease modifying therapies in Parkinson's disease*, Journal of Neurology Neurosurgery and Psychiatry, 81(2): 171-176.
- [216] ZATSIORSKY VM, SELUYANOV VN, CHUGUNOVA LG (1990) *Methods of determining mass-inertial characteristics of human body segments*, Chernyi GG, Regirer SA (eds), Contemporary Problems of Biomechanics, CRC Press, Boston, pp 272-291.
- [217] ZATSIORSKY VM, KING DL (1998) *An algorithm for determining gravity line location from posturographic recordings*, Journal of Biomechanics, 31: 161-164.
- [218] ZHOU H, STONE T, HUOSHENG H, HARRIS N (2008) *Use of multiple wearable inertial sensors in upper limb motion tracking*, Medical Engineering & Physics, 30: 123-133.
- [219] ZHU R, ZHOU Z (2004) *A real-time articulated human motion tracking using tri-axial inertial/magnetic sensors package*, IEEE Transactions of Neural Systems Rehabilitation Engineering, 12(2): 295-302.
- [220] ZIJLSTRA A, UFKES T, SKELTON DA, LUNDIN-OLSSON L, ZIJLSTRA W (2008) *Do dual tasks have an added value oversingle tasks for balance assessment in fall prevention programs? A mini-review*, Gerontology, 54(1): 40-49.
- [221] ZIJLSTRA W, BISSELING RW, SCHLUMBOHM S, BALDUS H (2010) *A body-fixed-sensor-based analysis of power during sit-to-stand movements*, Gait & Posture, 31: 272:278.